A Novel Role for the *Ostm1* Osteopetrotic Gene in Neuronal Homeostasis

By
Adam Griffiths

Faculty of Graduate Studies
Division of Experimental Medicine

McGill University
Montreal, Quebec, Canada

October 2009

A thesis submitted to McGill University in partial fulfillment of the requirements of the degree of Master of Science

ABSTRACT

Osteopetrosis is a genetic disease characterized by an excess of bone resulting from a defect in the bone resorbing osteoclasts. The discovery by our lab of the Osteopetrosis associated transmembrane protein 1 (*Ostm1*) gene responsible for the most severe recessive osteopetrosis in both grey-lethal (*gl/gl*) mice and humans provides us with the unique opportunity to decipher the role of this novel protein in a normal and pathological context. Functional rescue was undertaken by directing *Ostm1* expression in multiple hematopoietic lineages including osteoclasts with a PU1-*Ostm1*-BAC transgene. These mice show complete rescue of the standard bone and hematopoietic osteopetrotic phenotypes however they still die prematurely. Knowing *Ostm1* is highly expressed in brain tissue, we hypothesized that death was associated with CNS defects. These mice consistently display a severe neurodegenerative phenotype with stimulation of autophagy. To demonstrate the functional link of *Ostm1* with the CNS we developed mouse models targeting *Ostm1* to neuronal cells and astrocytes by using the specific Synapsin and GFAP promoters respectively. By rescue of neurodegeneration in these *gl/gl* transgenic mice using the Synapsin promoter, we established a major role for *Ostm1* in neuronal cells independent of the hematopoietic and osteoclast defects.

RÉSUMÉ

L'ostéopétrose est une maladie génétique qui se caractérise par un défaut des ostéoclastes responsables de la résorption osseuse. Il en résulte une accumulation anormale de tissu osseux entraînant des défauts hématopoïétiques et une mort prématurée. Les travaux antérieurs du laboratoire ont permis la découverte et la caractérisation du gène *gl (Ostm1*) qui est responsable de la plus sévère forme d'ostéopétrose récessive chez la souris *gl/gl* et l'humain. Cette découverte constitue une occasion unique de décrypter le rôle de cette protéine peu connue dans un contexte normal et pathologique.

Lors d'un essai de complémentation des phénotypes hématopoïétiques dans la souris *gl/gl,* l'expression du gène *Ostm1* a été ciblée dans des souris transgéniques en utilisant les séquences régulatrices du gène PU.1. Ce facteur transcriptionnel est exprimé très tôt au cours de l'hématopoïèse dans plusieurs lignées incluant l'ostéoclaste. Ces souris transgéniques ont été caractérisées et ensuite croisées successivement pour générer les souris PU.1-*Ostm1-gl/gl*. Ces souris n'étaient plus ostéopetrotiques, ne présentaient plus de défauts hématopoïétiques affectant les cellules B et T mais cependant mourraient prématurément.

Sachant qu'*Ostm1* est fortement exprimé dans le cerveau, nous avons émis l'hypothèse selon laquelle cette mort prématurée pouvait être reliée à un defaut du systéme nerveux. En effet, ces souris démontrent une neurodégénération progressive associée à une stimulation de l'autophagie. Afin de prouver le lien fonctionnel entre *Ostm1* et le phénotype neuronal, nous avons générer deux modèles de souris ciblant l'expression d'*Ostm1* respectivement dans les neurones et les astrocytes en utilisant les promoteurs spécifiques Synapsin et GFAP. En complémentant cette neurodégénérescence dans les souris transgéniques *gl/gl* avec le promoteur Synapsin, nous avons réussi à établir un rôle majeur pour *Ostm1* spécifique aux cellules neuronales indépendamment des défauts hématopoïétiques et des ostéoclastes.

TABLE OF CONTENTS

LIST OF FIGURES

LIST OF TABLES

ABBREVIATIONS

ADO:	Autosomal Dominant Osteopetrosis
ALS:	Amyotrophic Lateral Sclerosis
APP:	Amyloid Precursor Protein
ARO:	Autosomal Recessive Osteopetrosis
BAC:	Bacterial Artificial Chromosome
BMD:	Bone Mineral Density
BSA:	Bovine Serum Albumin
CA-II:	Carbonic Anhydrase II
CNS:	Central Nervous System
CSF:	Cerebrospinal Fluid
CT:	Computed Tomography
FACS:	Fluorescent Activated Cell Sorting
FISP:	Fast Imaging with Steady State Precession
GCL:	Ganglion Cell Layer
GFAP:	Glial Fibrillary Acidic Protein
gl:	Grey-lethal
INL:	Inner Nuclear Layer
IPL:	Inner Plexiform Layer
IRO:	Intermediate Recessive Osteopetrosis
IS:	Inner Segment
LC3:	Microtubule associated protein I Light Chain 3
MCSF:	Macrophage Colony Stimulating Factor
MIPAV:	Medical Image Processing, Analysis and Visualization
MRI:	Magnetic Resonance Imaging
mTOR:	Mammalian Target of Rapamycin
NCL:	Nuclear Cell Layer
Nrf2:	Nuclear Factor Erythroid 2-Related Factor 2
ONL:	Outer Nuclear Layer

OPL:	Outer Plexiform Layer
OS:	Outer Segment
Ostm1:	Osteopetrosis Associated Transmembrane Protein 1
PBS:	Phosphate-Buffered Saline
PCR:	Polymerase Chain Reaction
PIC:	Protease Inhibitor Cocktail
PI3K:	Phosphoinositide 3-Kinase
PMSF:	Phenylmethylsulphonyl Fluoride
PS-1:	Presenilin-1
PVDF:	Polyvinylidene Fluoride
qPCR:	Quantitative Polymerase Chain Reaction
RANK:	Receptor Activator of NFκB
RANKL:	Receptor Activator of NFκB Ligand
RPE:	Retinal Pigment Epithelium
RT PCR:	Reverse Transcriptase Polymerase Chain Reaction
SAIL:	Small Animal Imaging Lab
SOD1:	Superoxide Dismutase
SYN:	Synapsin
S6K:	ribosomal protein S6 Kinase
TRAP:	Tartrate Resistant Acid Phosphatase
TYR:	Tyrosinase
V-ATPase:	Vacuolar type H+-ATPase

ACKNOWLEDGEMENTS

I would like to acknowledge and thank my supervisor Dr. Jean Vacher. He provided me a wonderful opportunity in an excellent lab at a first rate institution. Dr. Vacher's attention to detail, breadth of knowledge, and his patience, supported and helped me achieve success in all areas of my degree. His excellent suggestions, his challenging discussions, as well as financial support, were all very much appreciated.

I would also like to acknowledge the members of the lab both past and present: Dr. Céline Heraud for her help in developing the synapsin transgene and for giving me good ideas and great habits; Janie Beauregard, Michel Arsenault, Dr. Mohamed Rashed, Marie Solange and Oliver Côté for their support and willingness to listen along the way; and last but certainly not least, Monica Pata. who taught me a great deal including the "RT Dance". I am very grateful to her for her constant encouragement.

I recognize the CIHR Training Program in Skeletal Health Research for financial support.

Finally I would like to thank my family and friends for all their love and support: my parents for their warmth, patience and understanding; my aunt for spoiling me; and my wonderful girlfriend who fills my life with joy and made this second year fly by.

Chapter 1

Literature Review

1.1 Bone

While generally omitted from the list, bone is in fact one of the largest organs in the human body. Taken together, the over 206 individual bones in the body make up the skeleton that plays an important role in every day life. Notably, the skeleton handles the support required for the significant load bearing of the body, provides attachments for muscle that allows for movement and helps protect the rest of the vital organs. In addition, bones also serve as a reservoir for minerals such as calcium and phosphorous. Bones in the skeleton are formed and maintained throughout life through bone homeostasis.

1.1.2. Bone Homeostasis

Bone homeostasis is a complex and dynamic process that involves the constant balance of formation and resorption of bone.

The development of bone can be divided into two main processes: that of intramembranous ossification and that of endochondral ossification.

Intramembranous ossification is the mechanism by which the craniofacial flat bones in the mammalian skeleton are formed (Shapiro, 2008). Mesenchymal stem cells condense, replicate and begin to differentiate into bone forming osteoblasts. Osteoblasts deposit the organic part of the matrix that is cross-linked type-I collagen. This is then mineralized with hydroxyapatite by the osteoblasts

(Blair et al. 2002). This is a unique process that involves no cartilage or other cell type.

Endochondral ossification is the mechanism used for bone development in the rest of the skeleton, particularly the long bones. The initial stage of endochondral ossification is the same as seen in intramembranous ossification in that mesenchymal cells once again condense; however, in this situation they then differentiate into cartilage forming cells known as chondrocytes. Chondrocytes are very different from osteoblasts in that they do not produce collagen type-I but rather another important ECM protein, collagen type-II (Ortega et al., 2004). Collagen type-II does not become calcified but still prevents the matrix from being pulled apart. Endochondral ossification proceeds at two distinct sites. The primary site of ossification occurs at the diaphysis and a secondary site of ossification occurs a while later in development at the epiphysis of the long bone. Between these two centers a growth plate is formed. Along the growth plate some chondrocytes undergo proliferation and some then undergo hypertrophy. These hypertrophic chondrocytes secrete a different collagen matrix of collagen type-X. During the early stages of endochondral ossification the cartilage lacks any trace of vasculature. With the increase in collagen-X deposition, blood vessels, starting from outside in, begin to invade the bone. With the highly vascularized bone comes an influx of other cell types. One set of cells differentiates into osteoblasts and begins to produce collagen type-I matrix that then becomes calcified (Ortega et al., 2004). At the same time, hypertrophic

chondrocytes undergo apoptosis and the blood vessels continuing their incursion take over the space left vacant. Finally, pluripotent monocytes fuse to form multinucleated cells that mature and differentiate into osteoclasts (Piper et al., 1992). These cells, capable of resorbing bone, remove cartilage and remodel matrix in order to develop the bone marrow cavity (Chambers et al., 2000) (Figure 1-1). A similar mechanism occurs at the epiphyseal growth plate towards the diaphysis; however, it is delayed, completing its ossification later in development.

When this critical process of bone homeostasis is disrupted various pathologies can arise. On the one hand, if the bone establishing osteoblast is affected and bone resorption outpaces bone formation this can lead to several complications such as osteopenia and osteoporosis, skeletal diseases where there are significant decreases in bone mineral density and a far greater risk of fracture. On the other hand, if the unique bone resorbing osteoclast is affected and bone formation outpaces bone removal, a net increase in bone mass and a resulting osteosclerosis and osteopetrosis can occur (Figure 1-2).

1.2. Osteopetrosis

Osteopetrosis is a heterogeneous family of inheritable bone remodeling disorders distinguished by failures of the aforementioned important osteoclast. Albers-Schönberg first characterized the condition over a hundred years ago via radiographic analysis of patients with an increased Bone Mineral Density (BMD).

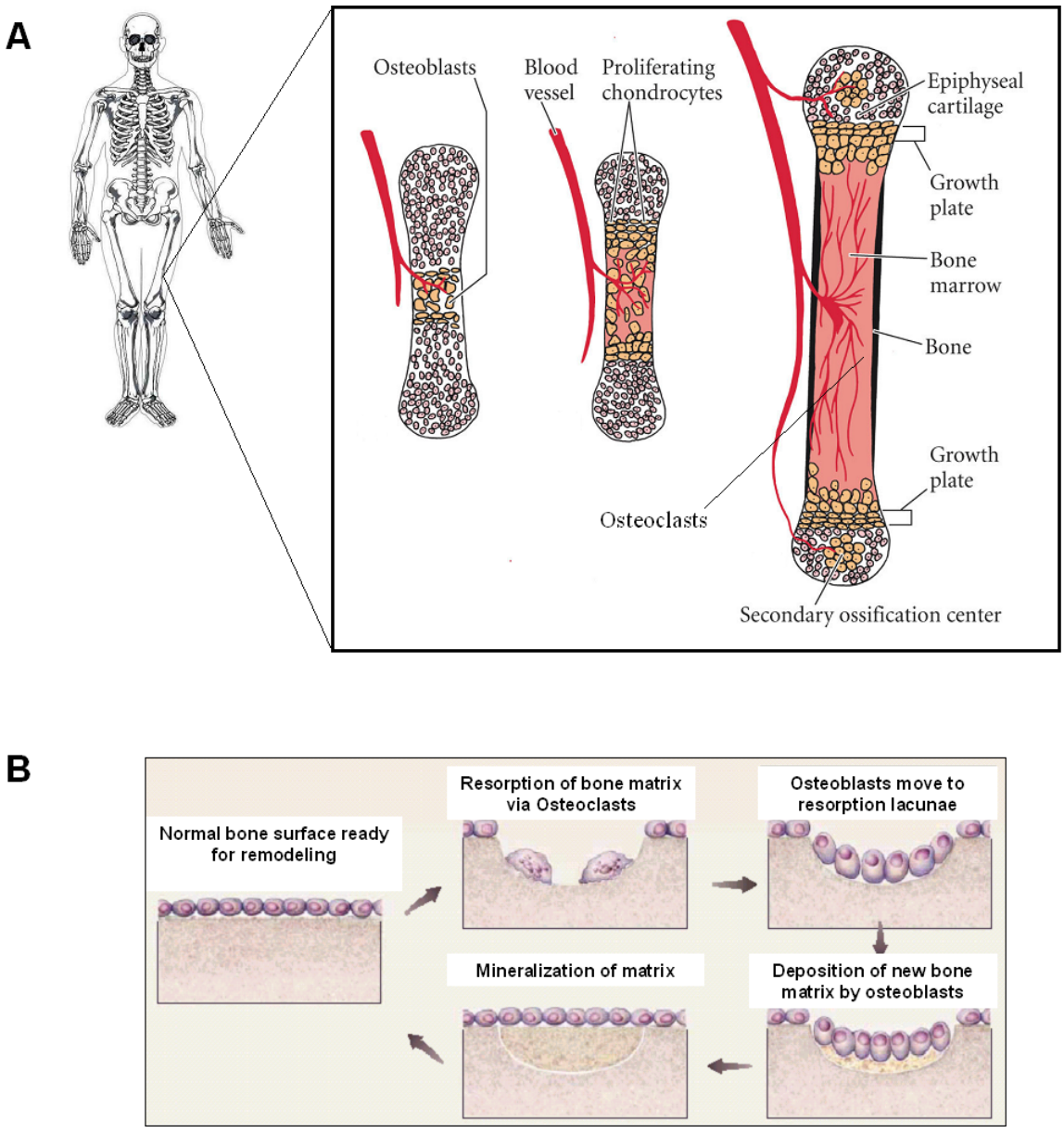

Figure 1-1: Bone formation and remodeling. (A) Diagram of endochondral ossification occurring in long bones and formation of medullary cavity. (B) Example of normal bone homeostasis involving bone formation and resorption. Disruption of this delicate balance due to malfunctioning osteoclasts can lead to osteopetrosis.

He identified it as “marble bone disease” after analysis revealed intense sclerosis of the skeleton. Widespread sclerosis is standard in the more severe cases with most bones including the skull, spine pelvis and appendicular bones being affected. A “bone in bone” pattern is generally visible with denser zones of calcification at the boundaries, less dense bones further in from this area, followed inside by even denser bone (Fattore et al., 2008) (Figure 1-2).

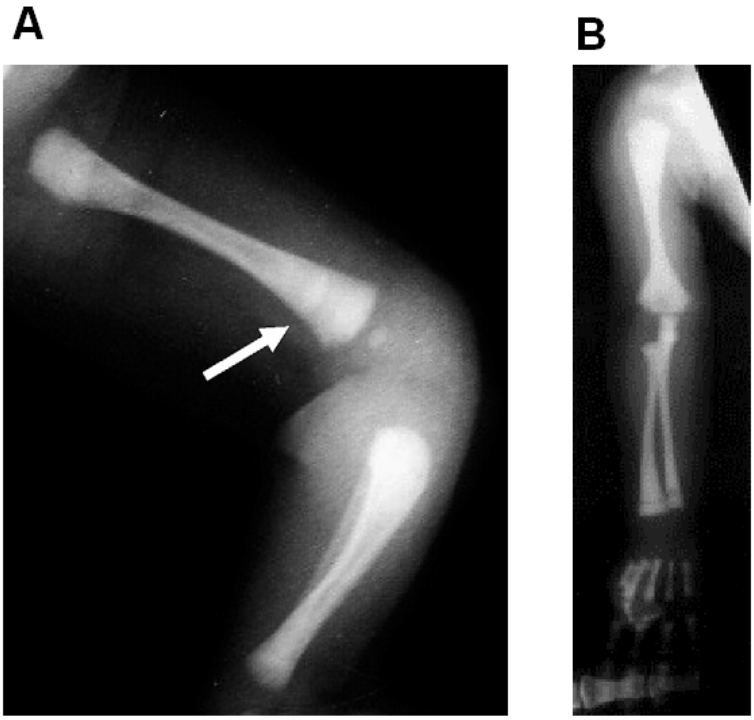

Figure 1-2: Radiographical examples of osteopetrosis. (A) Severe osteopetrotic femur and tibia. Increased bone density and notable decrease in bone marrow cavity. Arrow indicates funnel like appearance and alternating lucent bands. (B) Osteopetrotic arm with notable “bone in bone” appearance of the metacarpals (Adapted from Fattore et al., 2008, Wilson et al., 2000)

1.2.1. Role of the Osteoclast in Osteopetrosis

The failure of the osteoclast in osteopetrosis results from two main causes. On the one hand, there can be a block of differentiation of multipotent hematopoietic

stem cells into osteoclasts leading to a total lack of osteoclasts and an altered balance of bone remodeling. On the other hand, the bone resorbing function of the osteoclast can be directly affected.

There are several signals that are required for the proper development of an osteoclast. One of the first key steps in osteoclastogenesis involves the transcription factor PU.1. This important factor regulates the synthesis and expression of the Macrophage Colony Stimulating Factor (M-CSF) receptor (c-fms) on the osteoclast. This receptor is required for recognizing M-CSF that is produced by stromal cells and osteoblasts, which then continues the differentiation of osteoclast precursors (Roth et al., 1992, Hofbauer et al., 2001). At this stage, the Receptor Activator for Nuclear Factor κ B (RANK) receptor appears on the osteoclast and the binding of its ligand (RANKL), found on the outer membrane of the osteoblast, can then occur. This causes the precursors to become completely committed to the osteoclast lineage (Boyle et al., 2003, Tolar et al., 2004, Schoppet et al.,2002) (Figure 1-3). Disruption of any of these signals can severely disrupt the differentiation of the osteoclast and result in osteopetrosis. For example, knockout of PU.1 in a mouse model results in a total lack of osteoclasts and ensuing osteopetrosis (Tondravi et al., 1997). Similarly, the *op/op* mouse model has a mutation affecting the *m-csf* gene and has an absence of osteoclasts and osteopetrosis (Wiktor-Jedrzejczak et al., 1991, Yoshida et al., 1990). There are also rare cases seen in humans with mutations

affecting both RANK and RANKL. These patients are referred to as “osteoclast poor” and suffer the most severe form of osteopetrosis (Guerrini et al., 2008).

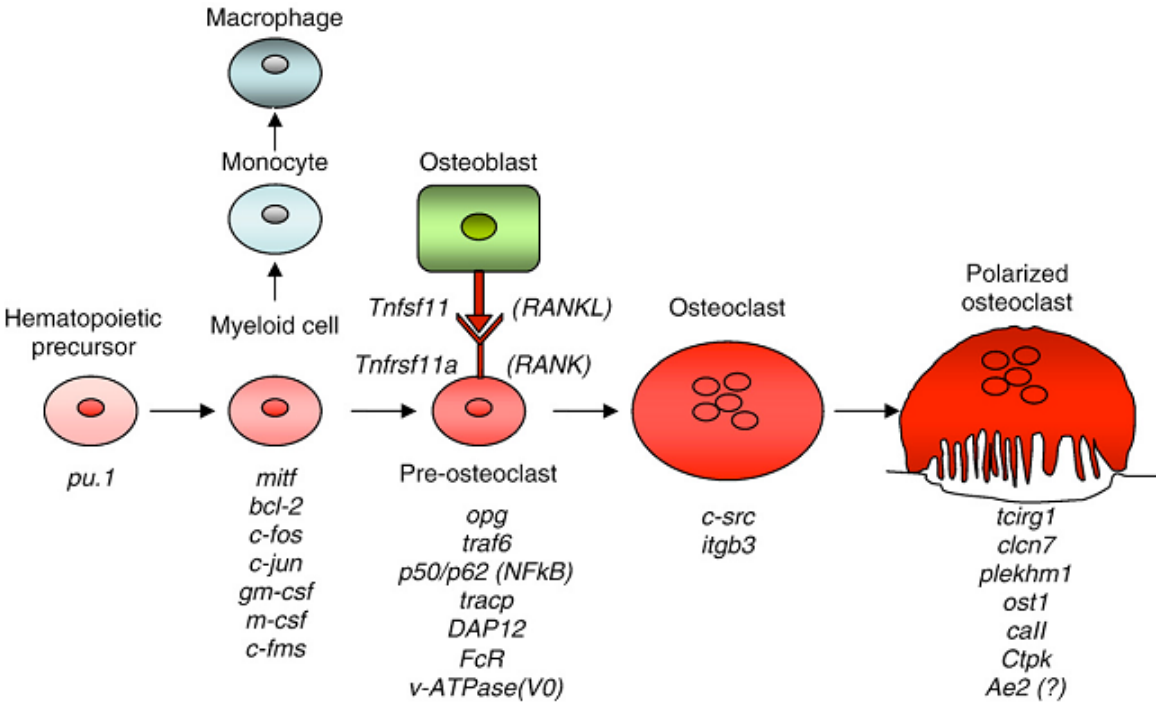

Figure 1-3:Osteoclast differentiation and function. Signals both internal and external to the hematopoietic precursor cell required for proper differentiation. (Adapted from Fattore et al., 2008)

If there is no mutation or alteration in the differentiation of the osteoclast, osteopetrosis can still develop due to a malfunction in the bone resorbing ability of the osteoclast. A normal osteoclast must be able to break down both the inorganic hydroxyapatite and organic collagen matrix of bone. In order to achieve this, a ruffled border is formed between the osteoclast and the bone surface. First, the cell attaches, polarizes, and becomes activated. A tight actin ring is formed along the bone surface in order to maintain a resorption lacuna where the

bone minerals can be dissolved and the matrix digested. Phosphatases, such as Tartrate Resistant Acid Phosphatase (TRAP) and proteases responsible for the digestion of collagens such as cathepsin K, are secreted into the resorption lacuna. Protons are also transported to the site to maintain a low enough pH for digestion (Baron, 1989, Zaidi, 2007, Balemans et al., 2005) (Figure1-4).

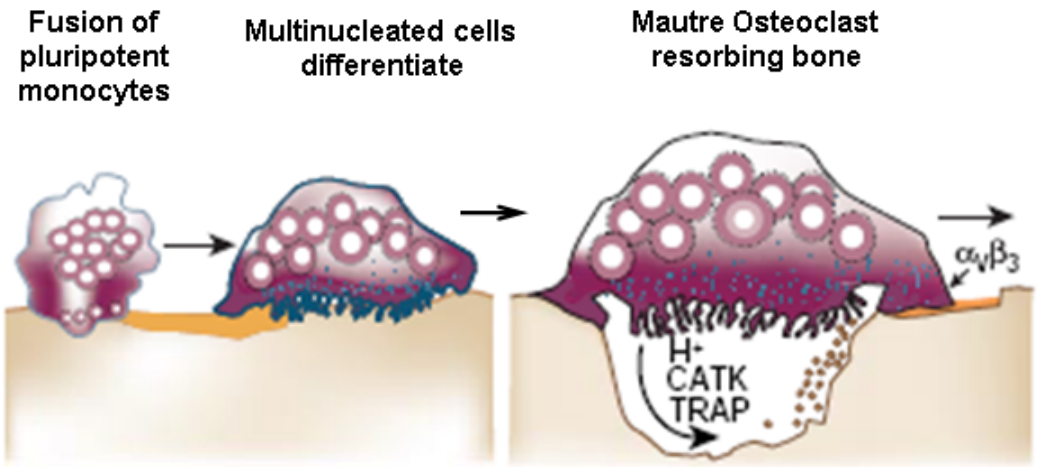

Figure 1-4: Example of a functioning osteoclast. First polarises, forms tight actin ring and ruffled border then releases enzymes such as cathepsin K to digest collagen and phosphatases as well as protons to facilitate bone resorption (Adapted from Boyle et al. 2003).

Mutations that result in osteopetrosis from either a defect in differentiation or an impairment in function of the mature osteoclast have proven to be very useful for the understanding of osteoclast development, action and the complicated balance of bone remodeling. To date, nearly all genes that are implicated in human osteopetrosis encode proteins that are involved in the function of mature osteoclasts (Balemans et al., 2005).

1.2.2. Forms of Osteopetrosis

Osteopetrosis is generally classified according to the manner of inheritance, age of onset and severity. Human cases are described as Autosomal Dominant Osteopetrosis (ADO), Intermediate Autosomal Recessive Osteopetrosis (IRO) or Malignant Infantile Autosomal Recessive Osteopetrosis (ARO). (Fattore et al., 2008)

ADO is the most frequent form of osteopetrosis, with an occurrence of approximately 5/100,000 observed mostly in adults. The disorder follows a much milder course with an increase in BMD, few fractures and normal life expectancy. (Fattore et al., 2008)

IRO, while only found to affect a minority of osteopetrotic patients, can also have significant effects. A mutation resulting in a lack of Carbonic anhydrase-2 (CA-II) activity can result in this form of osteopetrosis. CA-II is responsible for the conversion of H_2O and CO_2 into H_2CO_3, which is then used by the osteoclast to acidify the resorption lacuna (Figure 1-5). Without proper acidification, bone remodeling is impaired leading to an increase in incidence of fractures, developmental delay, and short stature. Interestingly, these patients also suffer from renal tubular acidosis in addition to the osteopetrotic symptoms (Tolar et al., 2004, Segovia-Silvestre et al., 2008).

ARO is the most severe form of osteopetrosis as well as the least common. Frequently found in children with consanguineous parents, approximately 1/250,000 people are affected (surprisingly more in Costa Rica, 3.4/100,000). The condition manifests early in life, generally around 3 months of age, with a mortality rate of over 75% by the age of four (Balemans et al., 2005). Almost all mutations resulting in malignant ARO involve defects in the function of the osteoclast. Most patients have normal if not slightly increased populations of osteoclasts; however, they are incapable of resorbing bone. The slight increase in osteoclast number is thought to be a compensatory mechanism implemented in an attempt to restore normal bone remodeling. Osteoclast failure produces bone with unresorbed calcified cartilage, remodeling sites that are compromised and micro fractures that go unchecked. This situation in turn results in an increase in BMD and low trauma fractures. In addition, the bone marrow compartment becomes occluded, affecting hematopoiesis and causes extra-medullary differentiation. This leads to a host of other symptoms including hepatosplenomegaly, anemia and pancytopenia (Balemans et al., 2005, Fattore et al., 2008). To date the only current treatment available is a bone marrow transplant; however, this course of action has only slightly better then a 50% success rate due to several complications including graft versus host disease (Wilson et al., 2000).

1.3. ARO

Currently there are three main genes whose loss of function have been observed in humans and in mice that are responsible for the majority of malignant ARO cases. Interestingly, thanks to the natural occurrence of several spontaneous mutant mouse models, these rare and severe forms of osteopetrosis can be studied in depth. In fact, much of what is known today about the osteoclast, both its differentiation and function, comes from the examination of these mice (Teitelbaum et al., 2003). Subsequent genetically modified mouse models have further helped clarify many aspects of ARO, including development of the first treatments for the disease using bone marrow transplants (Walker, 1975).

1.3.1. *TCIRG1*

The most commonly affected gene in ARO patients is the *TCIRG1* gene that encodes for the 116KDa a3 subunit of the Vacuolar proton ATPase (V-ATPase or H^+-ATPase) pump. This V-ATPase is generally found in the ruffled border of the fully differentiated osteoclast and accounts for approximately 60% of the mutations causing ARO in humans (Prinetti et al., 2008, Sobacchi et al., 2001). Normally the V-ATPase is responsible for acidifying and maintaining the pH of the resorption lacunae via extrusion of protons into the extracellular space (Figure 1-5). When the gene is mutated, the osteoclast can no longer resorb bone properly resulting in the host of difficulties already mentioned. This protein is also involved in processes in other tissues. In addition to bone, *TCIRG1* is expressed in the kidney where it helps control pH and the gastrointestinal tract

where the protein facilitates acidification and thereby absorption of calcium (Simeca et al. 2003, Sergovia-Silvestre et al. 2008). Similar to IRO, problems in other tissues outside the skeleton arise with mutations of *TCIRG1*. Without the necessary V-ATPase gastric acid levels become severely reduced which leads to considerable hypocalcemia and rachitic defects further compounding the malformed bone phenotype. (Schinke et al. 2008)

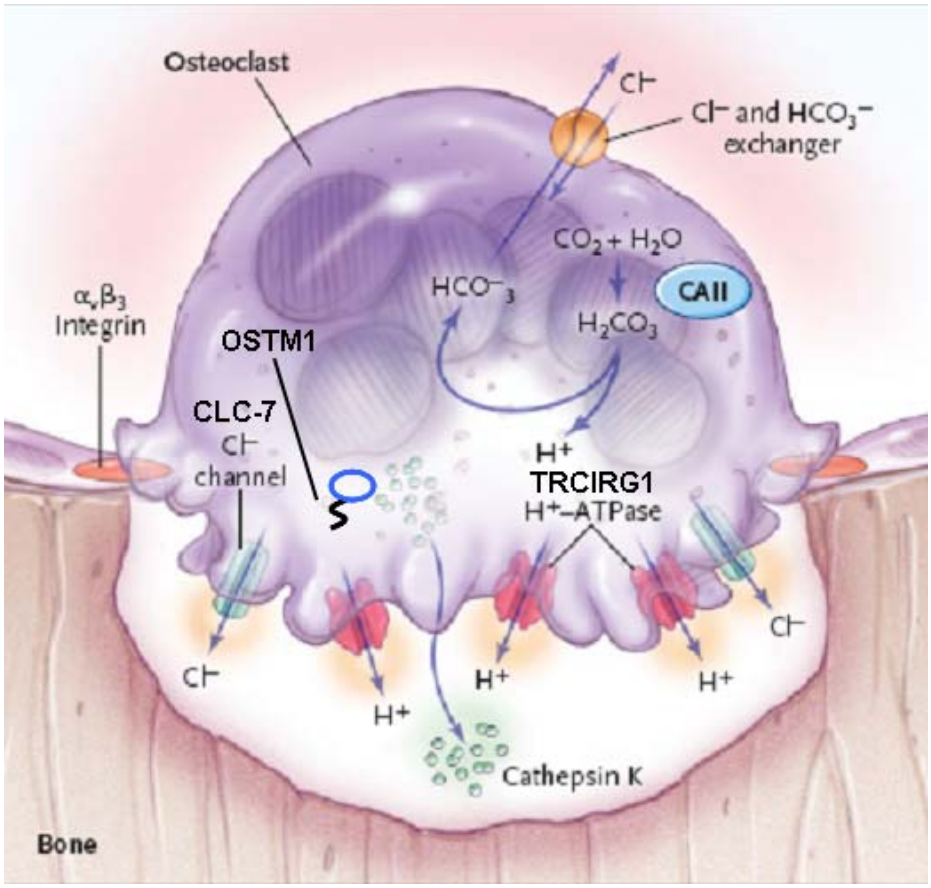

Figure 1-5: A resorbing osteoclast. CA-II is required for proper H_2CO_3 production. TCIRG1 is required for proper H^+-ATPase form and function of transporting protons to the resorption lacunae. CIC-7 is required for maintenance of the pH gradient in the resorption lacunae. OSTM1 with vital roles but function currently under investigation (Adapted from Fattore et al., 2008).

Using the *oc/oc* mouse model bearing a *Tcirg1* mutation has allowed for extensive study of this form of ARO. These mice mirror the majority of the features seen in the human patients and were in fact a key mouse model used to test hematopoietic stem cell treatments (Johansson et al., 2006).

1.3.2. *ClCN7*

The second largest cause of malignant ARO arises from mutations of the *CLCN7* gene. Mutations of this gene account for approximately 13% of cases of ARO in humans, and a heterozygous mutation of the gene can also result in ADO (Prinetti et al., 2008). *CLCN7* encodes for the CLC-7 chloride channel that is found on late endosomes and lysosomes. Primarily expressed in osteoclasts, it is translocated from the cytoplasm to the ruffled border when the osteoclast is polarizing and helps to control the pH of the resorption lacunae by maintaining the ion gradient via chloride anion flow (Kornak et al., 2001) (Figure 1-5). Like mutations of *TCIRG1*, loss of the chloride channel due to mutation results in a malfunctioning osteoclast and a disruption of bone homeostasis. Patients homozygous for the mutation suffer from the standard debilitating symptoms of malignant ARO.

Kornak et al. (2001) developed a knockout model of *Clcn7* in mice that proved valuable for better understanding of the channel and its function. It was in fact this mouse model that demonstrated the important role of CLC-7 in the

degradation of inorganic bone matrix (Sergovia-Silvestre et al. 2008, Henriksen et al. 2004).

These *Clcn7*$^{-/-}$ mice die on average at 6-7 weeks of age and have markedly impaired bone marrow cavities with large increases in total bone and trabecular bone volume (Kornak et al., 2001). These mice do not show an increase in osteoblast number but do suffer from anemia and splenomegaly, thus demonstrating another mouse model that closely resembles its human counterpart.

From the study of these mice it was found that *ClCN7* is expressed in several other tissues in addition to bone. Using a lacZ promoter, Kornak et al. (2001) showed that *Clcn7* is expressed (at lower levels compared to that of bone) in the cortex, hippocampus and cerebellum of the brain as well as the retinal pigment epithelium of the retina. Closer examination revealed these mice suffered considerable neurodegeneration on top of bone complications. The mice showed marked astrogliosis and microglia activation at the level of the cortex and hippocampus, with electron dense material found in neurons. The mice also showed degeneration of the retina (Kasper et al., 2005).

To better study the effects of *CLCN7* mutation on the brain Kasper et al. (2005) developed a transgenic line targeting *Clcn7* to terminally differentiated osteoclasts using a TRAP promoter. These mice were crossed with the *Clcn7*$^{-/-}$ to

obtain mice with rescue of the bone phenotype but mutation of *Clcn7* everywhere else. These mice had normal bone density; however, they still died at 12 weeks of age and showed severe neurodegeneration, loss of Purkinje cells in the cerebellum and degeneration of the retina. This neurodegenerative phenotype is thought to resemble a heterogeneous group of human progressive neuropathologies known as Neuronal Ceroid Lipofuscinoses (NCLs). NCLs are a group of disease that involve lysosomal storage complications mostly isolated to the central nervous system. They generally manifest as accumulations of autofluorescent lipofuscin like material in vesicles that lead to neurodegeneration and premature death (Mole, 2004, Tang et al. 2006). While similar to NCLs, the *Clcn7*$^{-/-}$ phenotype still has some key differences in that the lysosomes of these mice appear to function normally with a regular pH (Kasper et al., 2005).

Taken together, these results are an important piece of evidence showing that genes with important roles in osteoclast function and standard osteopetrotic symptoms can also have other important primary effects in other tissues, notably the brain.

1.3.3. *OSTM1*

Of particular interest to our lab and this thesis, mutations of the *OSTM1* gene account for another 4% of human ARO cases with the incidents being among the most severe (Prinetti et al., 2008). *OSTM1* encodes for Osteopetrosis associated transmembrane protein 1 that is a 38kDa putative type one transmembrane

protein (Chalhoub et al. 2003). OSTM1 is highly glycosylated (ten sites) and has been localized in the endoplasmic reticulum, Golgi apparatus and the intracellular compartment. With its C-terminal facing the cytosol, OSTM1 has been suggested as a possible β-subunit for ClC-7 that is required for maintenance and transport of the chloride channel (Lange et al., 2006). Its precise functions are still currently under investigation by our lab (Figure 1-5). With this in mind, it is still quite clear that a mutation of *Ostm1* results in the production of non-functional osteoclasts (Rajapurohitam et al., 2001) that in turn lead to a host of debilitating problems that are discussed further on.

1.3.4. RANK, RANKL and ARO

Spontaneous mutations of the aforementioned three genes do not account for all causes of malignant ARO. There still remains a gene, or possibly genes, that when mutated result in a serious disruption of bone remodeling and osteopetrosis. Two such genes encode for the all important RANK and RANKL signal. Previously thought to only occur in induced mouse models, recent studies have found individuals with mutations in the ligand RANKL and the receptor RANK that result in an osteoclast poor phenotype (Sobacchi et al. 2007, Guerrini et al., 2008). Thought to account for less then 3% of cases, these patients appear to have a slower disease progression then other malignant ARO occurrences but cannot in fact be treated in the standard fashion. Bone marrow transplants will not correct proper osteoclast differentiation; however, patients may in fact benefit from exogenous RANKL treatment (Prinetti et al. 2008,

Sobacchi et al. 2007). The cases, while rare, do highlight the very heterogeneous nature and need for further research of this novel genetic condition.

1.4. OSTM1 Human Patients

Humans with a mutation of *OSTM1* usually present within the first year of life with severe osteopetrosis, increased bone mineral density and pathological fractures. Endochondral ossification is completely abnormal with no discernable cartilage or bone resorption and intramembranous ossification is also affected, though the divergence is less striking (Maranda et al. 2008). In both areas of the skeleton, there is an aberrant amount of trabecular bone which in turn dramatically reduces the bone marrow spaces and results in anemia, thrombocytopenia, osteomyelitis and sepsis. Less than 30% of children live past the age of six with many succumbing to multi organ failure (Quarello et al. 2004, Ramirez et al., 2004).

1.4.1. Osteopetrosis and the Central Nervous System (CNS)

In addition to the hematopoietic defects that affect malignant ARO patients, the disruption of bone remodeling and subsequent malformations also affect the skull and by extension the CNS. Just as the bone marrow cavity becomes compromised, so too do the foramina of the skull. This leads to compression of cranial nerves, blood vessels and the spinal cord (Steward, 2003). Auditory, facial and trigeminal nerves, can be affected resulting in hearing loss, diminished eyesight and developmental delay. As well, with altered membranous ossification, the thickness of the skull is increased and the brain itself can be

overly compressed and cortical atrophy and hydrocephalous can ensue. Psychomotor retardation has also been observed and explained by stenosis of cranial arteries and venous drainage routes (Chlodo et al., 2007).

Neurological defects are observed in many malignant ARO patients; however, recently, only those with mutations in *CLCN7* or *OSTM1* have been shown to have primary neuropathologies. Patients with mutations in *TCIRG1* have neurological defects that are secondary, due solely to the effect of malformation of the skull and the resultant compression of the various nerves (Pangrazio et al., 2006). Conversely, as seen in the transgenic TRAP-*Clcn7* on a *Clcn7*$^{-/-}$ background, the mice that are rescued from the osteopetrotic bone phenotype, still develop neuropathologies and die (Kasper et al., 2005). The marked neurodegeneration in this mouse model is clearly not a result of occluded foramina or compression of the skull because bone remodeling is restored in these animals. Recently, it has been shown that mutations in *OSTM1* in humans also result in primary neuropathologies separate from problems in bone homeostasis (Chlodo et al., 2007, Maranda et al., 2008)

1.4.2. Case Study

Our laboratory (Maranda et al., 2008) examined and characterized a novel human *OSTM1* mutation that results in death at one year of age. The condition involved a point mutation in exon 1, resulting in a premature stop codon which may produce a shorter protein, that lacking the important transmembrane

domain, may be mislocalized and therefore either degraded or secreted (Figure 1-6A). This patient suffered standard osteopetrotic symptoms, including non traumatic fractures of the ribs and humerus and an above average BMD for her age. The patient also suffered numerous neurological defects including cerebral atrophy, general seizures and bilateral atrial subendymal heterotopias (Maranda et al. 2008). Heterotopia is a condition where a group of cells is found in the correct tissue of origin but in the wrong location (McInnes et al., 2007). In this case it resulted in a nodular mass of grey matter that was found protruding into the ventricle. (Figure 1-6B) Successive Magnetic Resonance Imaging (MRI) of the patient revealed progressive cerebral atrophy. There was also notable deafness and retinal degeneration with no evoked visual potentials. Electroretinograms revealed normal optic nerve conduction and a head Computed Tomography (CT) scan showed no signs of auditory or optic nerve compression.

Studies of other *OSTM1* patients have also shown notable cortical atrophy and even hypomyelination (Chlodo et al., 2007). Using ultrastructural analysis, others have found the presence of swollen unmyelinated axons that appear to have storage of excess carbohydrates and lipids (Alroy et al., 2007). Unlike the *Clcn7* knockout mouse model, where researchers suggest the phenotype resembles that of NCL, the *OSMT1* patients do not appear to have direct lysosomal problems.

Regardless, taken together these novel *OSTM1* human patients suggest a direct role of OSTM1 in the brain. A role so important that absence of *Ostm1* results in severe complications that are not secondary to the bone phenotype.

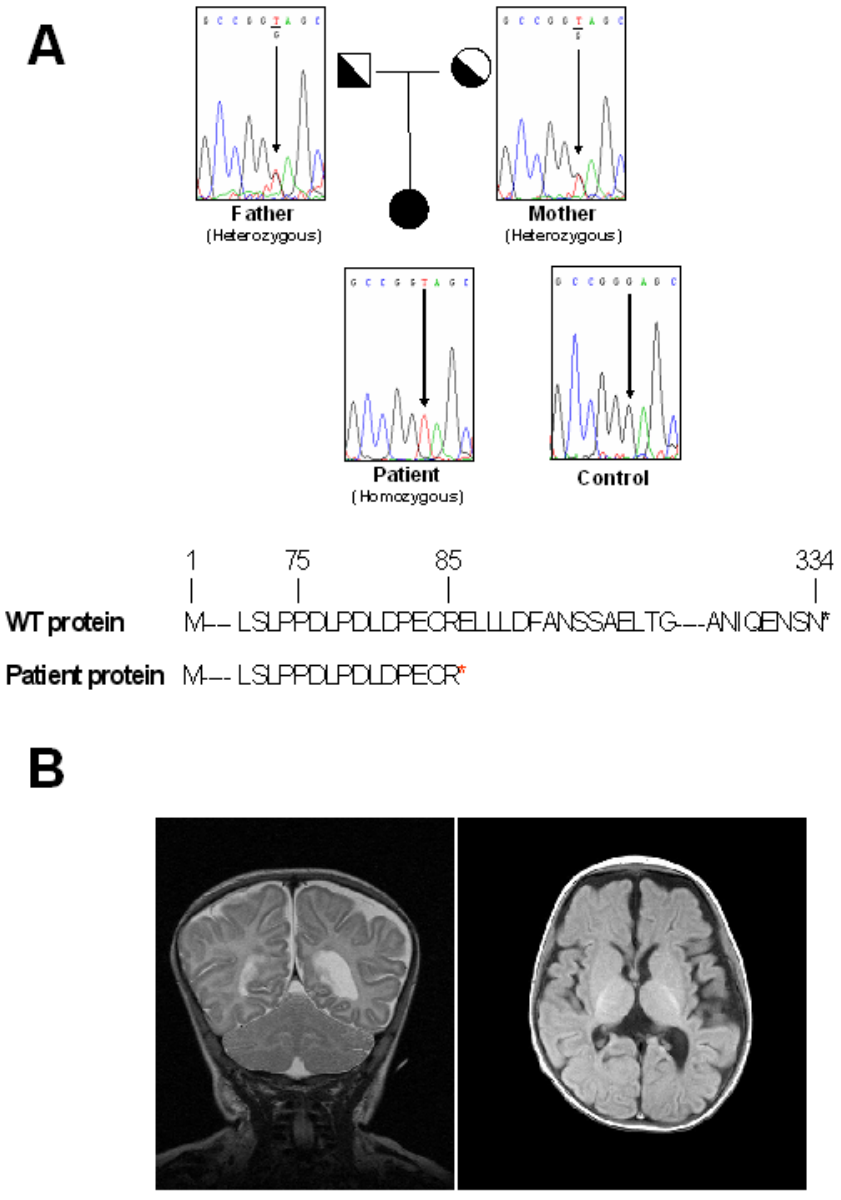

Figure 1-6: Study of an osteopetrotic human patient with a novel *OSTM1* mutation. (A) Point mutation that may result in the production of a truncated form of OSTM1. (B) Notable heterotopia seen in left ventricle in conjunction with cortical atrophy (Adapted from Journal of Bone Mineral Research 2008;23;296-300 with permission of the American Society for Bone and Mineral Research).

In both cases of *CLCN7* and *OSTM1* mutations, the novel roles for the genes outside of bone also reveal a major problem with classical treatment of this disease. Bone marrow transplants, while if successful are capable of correcting the bone phenotype, will not alleviate the severe problems at the level of the brain that until recently had gone unnoticed.

In order to better understand the roles of Ostm1, a suitable mouse model is required. A mouse model where the effects of this critical protein can be studied in a wide variety of tissues to better help characterize and treat human patients afflicted with the *OSTM1* mutation.

1.5. The Grey-Lethal Mouse

The *Ostm1* gene was discovered with the characterization of the spontaneous recessive osteopetrotic mouse mutant grey-lethal (*gl*) by our laboratory (Chalhoub et al., 2003, Grüneberg 1936). The *gl* mutation corresponds to a 7.5kb deletion of the *Ostm1* gene spanning 4.5 kb of the promoter region, all of exon 1 and 3kb of the first intron, resulting in a null phenotype. *gl/gl* mice habitually die at 3 weeks from the various bone and hematopoietic complications, further mimicking the severity of the human patients. This spontaneous mouse model is regarded as an excellent tool for the study of malignant ARO because the human *OSTM1* gene is 83% homologous to the mouse *Ostm1* gene. Most importantly the same gene is responsible for ARO as our laboratory discovered

the first *OSTM1* mutation in an osteopetrotic patient (Chalhoub et al., 2003, Quarello et al., 2004).

Of note, *Ostm1* is highly expressed in a variety of other tissues in addition to bone, including the spleen, thymus, kidney and brain. More specifically, in-situ hybridization showed *Ostm1* expression in the brain cortex, hippocampus and cerebellum. The gene is also found in melanocytes which explains the tell-tale grey coat color of the *gl/gl* mutant compared to that of the agouti color of the wild type or heterozygous *gl/+* (Figure 1-7) (Chalhoub et al., 2003).

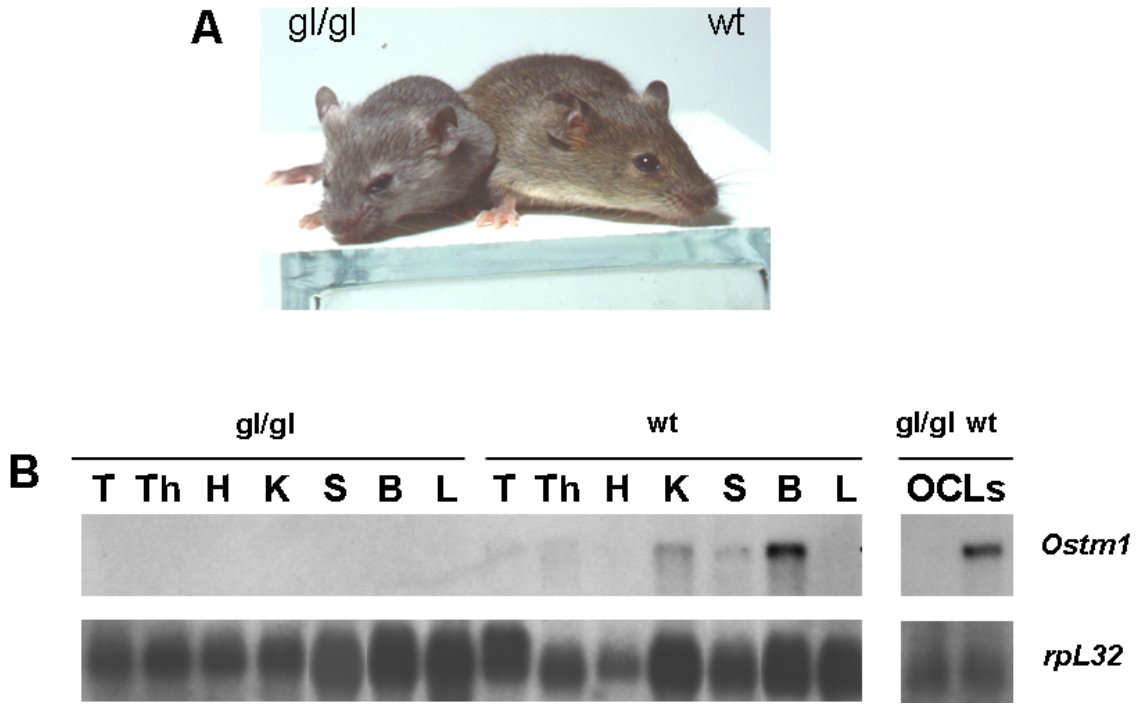

Figure 1-7: Expression of *Ostm1* in grey-lethal mouse. (A) Distinct grey coat color of *gl/gl* osteopetrotic mouse compared to that of agouti color of wild type. (B) Northern blot showing expression of *Ostm1* in various tissues. Note complete absence of mRNA in *gl/gl* mouse and normal high expression level in brain tissue compared to osteoclast cells (Adapted from Chalhoub et al., 2003).

Homozygous *gl/gl* mice exhibit typical osteopetrotic symptoms with an overabundance of trabecular bone and a thickening of the growth plate. These problems are caused directly from a functional defect in the osteoclast rather then a block in differentiation with up to a 10 fold decrease in resorptive activity. *gl/gl* mice have an increase in the osteoclast population as seen with TRAP staining, with individual osteoclasts displaying defective cytoskeletal reorganization as well as underdeveloped ruffled borders. Disruption of bone remodeling also results in a lack of tooth eruption and a reduced medullary space (Figure 1-8A) (Rajapurohitam et al., 2001).

A reduced bone marrow compartment in turn leads to defects in hematopoiesis. *gl/gl* mice show mild anemia, a marked decrease in the B cell population and an altered T cell population (Figure 1-8B). There is a significant decrease in double positive CD4+CD8+ T cells in the thymus and an increase in single positive CD4+ and CD8+ cells suggesting a possible shift in differentiation (Pata et al., 2008). A bone marrow transplant can in fact correct the bone and hematopoietic phenotype of the *gl/gl* mutant further demonstrating the importance of *Ostm1* in proper bone remodeling (Walker, 1975).

1.5.1. PU.1 transgenic mice

In an effort to rescue the bone and hematopoietic phenotypes seen in the grey-lethal mouse, Pata et al. (2008) targeted *Ostm1* to the hematopoietic multipotent myeloid and lymphoid progenitors using a PU.1 promoter in a BAC transgene.

A

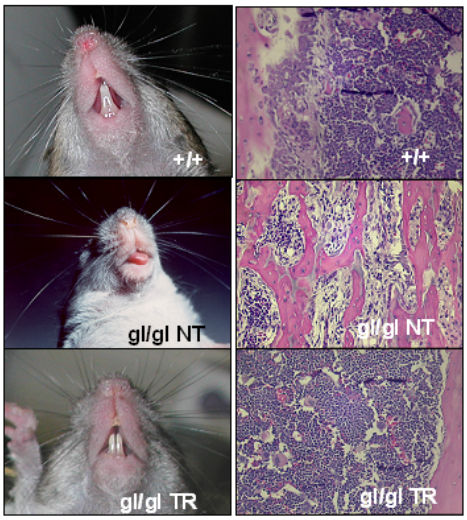

B

		Spleen			Thymus		
		Myeloid (%)		Lymphoid (%)	Lymphoid (%)		
Mice	n	CD11b+	CD11b+/ Ly6-G+	B220+	CD4+CD8+	CD4+	CD8+
+/+ NT	6	11.5 ± 0.6	5.2 ± 0.8	61.9 ± 7.0	88.6 ± 3.8	7.0 ± 0.8	2.7 ± 1.4
+/+ TR	4	9.4 ± 2.3	4.3 ± 0.8	55.1 ± 7.2	89.0 ± 3.5	6.5 ± 1.6	2.8 ± 1.4
gl/gl NT	5	15.6 ± 2.0**	10.2 ± 4.7 **	39.9 ± 8.9 *	36.2 ± 13.1 **	45.3 ± 20.4 *	16.0 ± 7.2*
gl/gl TR1	5	8.7 ± 1.2	4.0 ± 0.5	59.2 ± 2.8	87.6 ± 1.1	7.5 ± 1.3	3.4 ± 0.3
gl/gl TR2	3	11.3 ± 0.9	4.2 ± 0.8	55.6 ± 4.5	89.4 ± 0.5	7.0 ± 0.2	2.3 ± 0.7

Data are expressed as the means % ± SD compared to wild type non-transgenic (+/+ NT)

*p<0.05 **p<0.005 ***p<0.001

Figure 1-8: Bone and Hematopoietic phenotypes of *gl/g*l and PU.1-*Ostm1-gl/gl* mice. (A) Lack of tooth eruption and reduced bone marrow compartment seen in *gl/g*l mice and corrected in transgenic PU.1-*Ostm1-gl/gl* mice. (B) Notable decrease in B lymphoid cell population and altered T cell population in *gl/gl* mice. Return to normal levels of both myeloid and lymphoid cell populations in transgenic PU.1-*Ostm1-gl/gl* mice. (Adapted from Pata et al., 2008)

Recall that PU.1 is an early transcription factor found throughout hematopoietic differentiation (Figure 1-3). A BAC transgene was used in order to include regulatory elements found 14kb upstream from the transcription start site (Huang

et al., 2008) and the coding sequence was replaced with *Ostm1* cDNA (Figure 1-9).

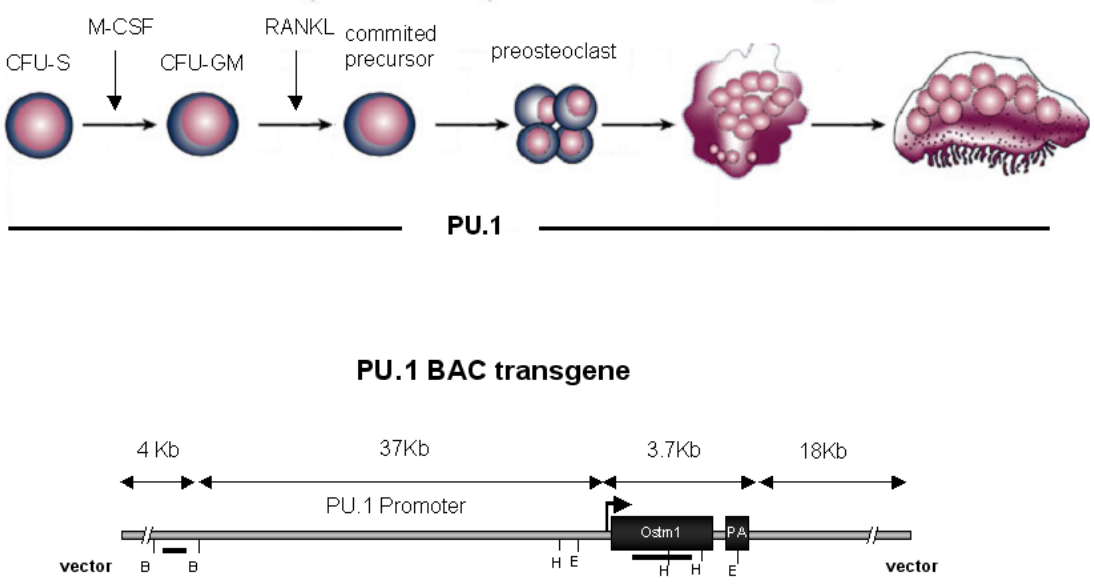

Figure 1-9: Expression of PU.1 and the PU.1 BAC transgene construct. PU.1 is expressed very early in hematopoietic differentiation and maintained through to development of the osteoclast. A BAC was used to include the regulatory elements of the PU.1 promoter found 14kb upstream. (Adapted from Boyle et al., 2003 and Pata et al., 2008)

PU.1 was used to target *Ostm1* to the osteoclast lineage because a previous attempt using a TRAP promoter failed to rescue the bone and hematopoietic phenotype of the *gl/gl* mouse. As mentioned earlier, TRAP is only expressed in fully committed osteoclast precursors. Targeting *Ostm1* only to these mature cells was insufficient to prolong the short three week life span of the *gl/gl* osteopetrotic mouse (Pata et al., 2008).

Once the PU.1-*Ostm1* transgene was established, transgenic mice were crossed with heterozygous *gl/+* mice in order to obtain transgenic PU.1-*Ostm1-gl/gl* mice. These mice were then analysed and a complete rescue of the bone phenotype was observed. PU.1-*Ostm1-gl/gl* mice showed normal tooth eruption and normal development of the bone marrow cavity (Figure 1-8A). As well, using FACS analysis, a complete rescue of the hematopoietic phenotype with a return to normal myeloid and lymphoid cell populations was obtained (Figure 1-8B). PU.1-*Ostm1-gl/gl* mice also lived past three weeks of age. Interestingly, this complete phenotypic rescue was achieved with very low transgene expression. The PU.1-*Ostm1* transgene was expressed at several fold lower than that of the endogenous *Ostm1*.

Functional rescue of the hematopoietic and osteoclast defects, obtained via early multilineage expression of *Ostm1,* demonstrates it is not only required in late osteoclastogenesis. *Ostm1* has roles in other hematopoietic lineages, such as myelopoiesis and lymphopoiesis where it seems a cross talk mechanism between different hematopoietic cells is required for proper osteoclast activation and function (Pata et al., 2008). This is in stark contrast to ClC-7 where targeting *Clcn7* to late precursors and mature osteoclasts using a TRAP promoter was adequate enough to rescue the bone phenotype (Kasper et al. 2005).

Hypothesis and Approach

Based on the information presented here, we used the PU.1-*Ostm1-gl/gl* mouse to study the role of *Ostm1* in other tissues, specifically the brain. Mutations in *Tcirg1* and *Clcn7* genes can lead not only to severe osteopetrosis but complications in other tissues as well. Mutations of *Clcn7* specifically can result in a severe neurological phenotype (Kasper et al., 2005). This coupled with the prominent neurological phenotype seen in human *OSTM1* patients and the high expression of *Ostm1* in mouse brain tissue suggests a possible critical role for *OSTM1* outside of bone. We then hypothesized, that by following the development of PU.1-*Ostm1-gl/gl* mice, we should be able to determine the role of *Ostm1* in the brain. Furthermore, we developed additional transgenic mice with targeted *Ostm1* expression to specific cell types in the brain, to determine if the function of *Ostm1* is cell autonomous and which cells require *Ostm1* for proper homeostasis and survival.

Chapter 2
Methods and Materials

2.1 Mice

All mice were backcrossed on a C57BL/6^{J} background for at least ten generations and maintained in a 12-hour light/dark cycle at 22-26^{o}C with laboratory chow and tap water ad libitum. All procedures and protocols were approved by the local Institutional Animal Care and Use Committee and comply with guidelines of the Canadian Committee for Animal Protection (Appendix 1)

2.1.1.Grey-Lethal mice

The mouse strain GL/Le *dl*^{J}+/+*gl* was obtained from The Jackson Laboratory (Bar Harbour Maine).

2.1.2. PU.1-*Ostm1-gl/+* Mice

PU.1-*Ostm1-gl/+* mice produced in our lab have been previously described (Pata et al. 2008). The expression of the *Ostm1* cDNA was placed under control of the PU.1 promoter in a BAC transgene. These mice have been shown to express *Ostm1* in the multipotent myeloid progenitors including the osteoclast lineage. Four lines were described and two were analysed in more detail (line 737 having 2 copies and line 761 having 8 copies).

2.1.3. SYN-*Ostm1* Mice Expression

The coding sequence of the *Ostm1* gene was obtained via digestion of a previously described pBS-gl plasmid with XmaI and SpeI (Pata el al 2008). A previously described plasmid was used as a cloning vector (Luca et al. 2005)

(A generous gift from Dr. Manfred W. Killimann, Department of Cell and Molecular Biology, Uppsala University, Uppsala Sweden.). The leptin receptor cDNA from the original plasmid was removed via BspeI and SpeI digestions. *Ostm1* cDNA was then inserted (BspeI is compatible with XmaI) downstream of the 4.3kb Synapsin I specific promoter and rat growth hormone intron and upstream of the simian virus 40 late polyadenylation signal (Figure 2-1A). A linearized PmeI/Sma I 6.6kb transgene fragment was then injected (1 ng/μl) into fertilized mouse oocytes isolated from F1 (C3H x C57BL/6^J) x C57BL/6^J crosses and transferred to pseudo pregnant females. Founders were subsequently identified and crossed as described below. Two transgenic founders, with different numbers of transgene copies (hereafter designated lines 214 and 215), were used to establish transgenic lines for the following experiments.

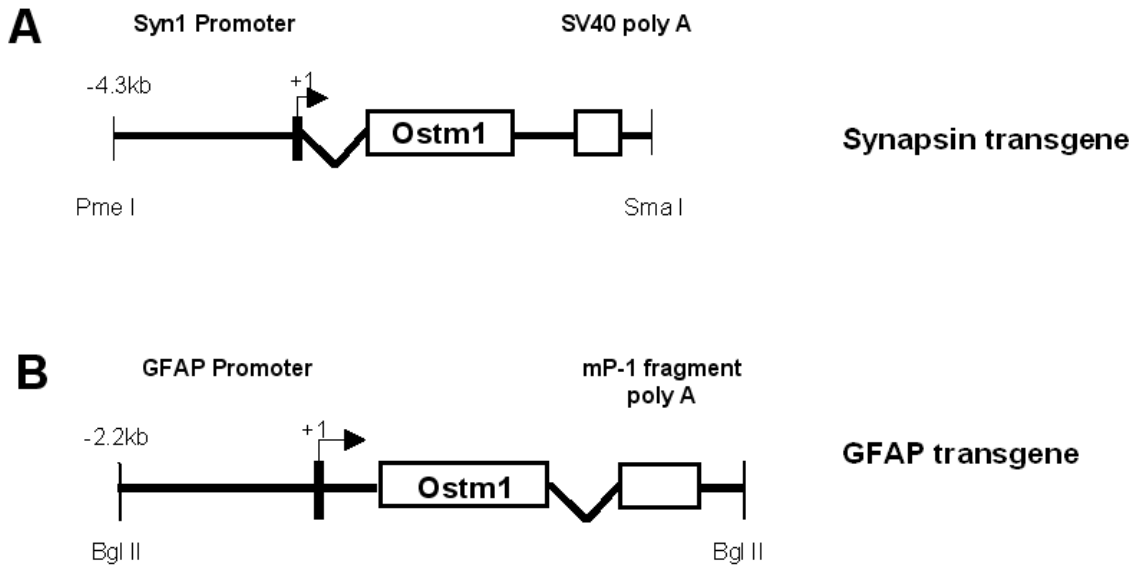

Figure 2-1: Structure of the transgenes used in this study. (A) The SYN-*Ostm1* transgene specific for neurons. (B) The GFAP-*Ostm1* transgene specific for astrocytes.

2.1.4. GFAP-*Ostm1* Mice Expression

The coding sequence of the *Ostm1* gene was obtained via digestion of a previously described pTRAP-*gl* plasmid with BamHI (Pata el al 2008). A previously described plasmid was used as a cloning vector (Brenner et al. 1996) (a generous gift from Dr. Michael Brenner, Department of Neurobiology and Civitan International Research Center, University of Alabama-Birmingham, Birmingham, AL, USA). The *lacZ* cDNA from the original plasmid was removed via BamHI digestion. *Ostm1* cDNA was then inserted downstream of the 2.2kb GFAP specific promoter, upstream of a mouse protamine-1 gene fragment containing a stabilizing intron and polyadenylation signal (Figure 2-1B). A linearized Bgl II 3.8kb transgene fragment was then injected (1 ng/μl) into fertilized mouse oocytes isolated from F1 (C3H x C57BL/6^{J}) x C57BL/6^{J} crosses and transferred to pseudo pregnant females. Founders were subsequently identified and crossed as described. The founders were obtained and one line (hereafter designated 244) was established and used in the subsequent experiments.

2.1.5. Genotyping of Mice

Genotyping was performed by PCR on DNA isolated by salt preparation from mouse tail biopsies. Tails were first digested overnight at 55^{o}C in digestion buffer (50mM Tris-HCl pH8, 100mM EDTA pH8, 100mM NaCl, 1% SDS and 150μg proteinase K). DNA was then precipitated with 5M NaOH and 100% EtOH and resuspended in TE buffer (10mM Tris-HCL pH8, 1mM EDTA pH8). *Ostm1*

genotyping used the gl For 1, gl For 2, gl Rev 1 and gl Rev 2 primers (see Table 1). The PCR reaction was carried out in buffer containing 10mM Tris-HCl pH 8.3, 50mM KCl and 1.5mM MgCl2. Cycling conditions were 30 cycles as follows: 94^{o}C, 30 seconds, 65^{o}C, 30 seconds, 72^{o}C 30 seconds with a 10 minute final elongation at 72^{o}C. This assay distinguished individual alleles wild-type (+/+), heterozygous (*gl*/+) and homozygous (*gl/gl*) mice by producing a 236bp amplicon for the wild-type allele and a 330 amplicon for the mutated allele respectively. The PU.1-*Ostm1*, SYN-*Ostm1* and GFAP-*Ostm1* transgenic lines were genotyped using PU.1 For, HSPC Rev 1, SYN For 1, RGH Rev 1, GFAP-gl For 1 and mp-1 Rev 1 primers respectively (see Table 1). PCR conditions for both PU.1 and SYN transgenic lines were the same as *Ostm1* genotyping. For the GFAP-*Ostm1* transgene the cycling conditions were 35 cycles at 94^{o}C, 30 seconds, 60^{o}C, 30 seconds, 72^{o}C, 30 seconds with a 10 min final elongation at 72^{o}C. The genotyping of the transgenic lines were carried out in buffer containing 10 mM Tris-HCl pH 8.3, 50mM KCl, 1.5 mM MgCl2 and 10% DMSO. The resulting specific amplicons of 500bp for PU.1, 450bp for SYN-Ostm1, 500bp for GFAP-*Ostm1* were visualized in 1X TBE 1.5% agarose gels stained with Ethidium Bromide (EtBr).

2.1.6.Crosses

SYN-*Ostm1* positive mice were crossed with PU.1-*Ostm1-gl/*+ mice to generate F1 double transgenic SYN-*Ostm1*-PU.1-*Ostm1-gl/*+ mice. F1 animals were then intercrossed to obtain all three genotypes for experimental sets and analysis.

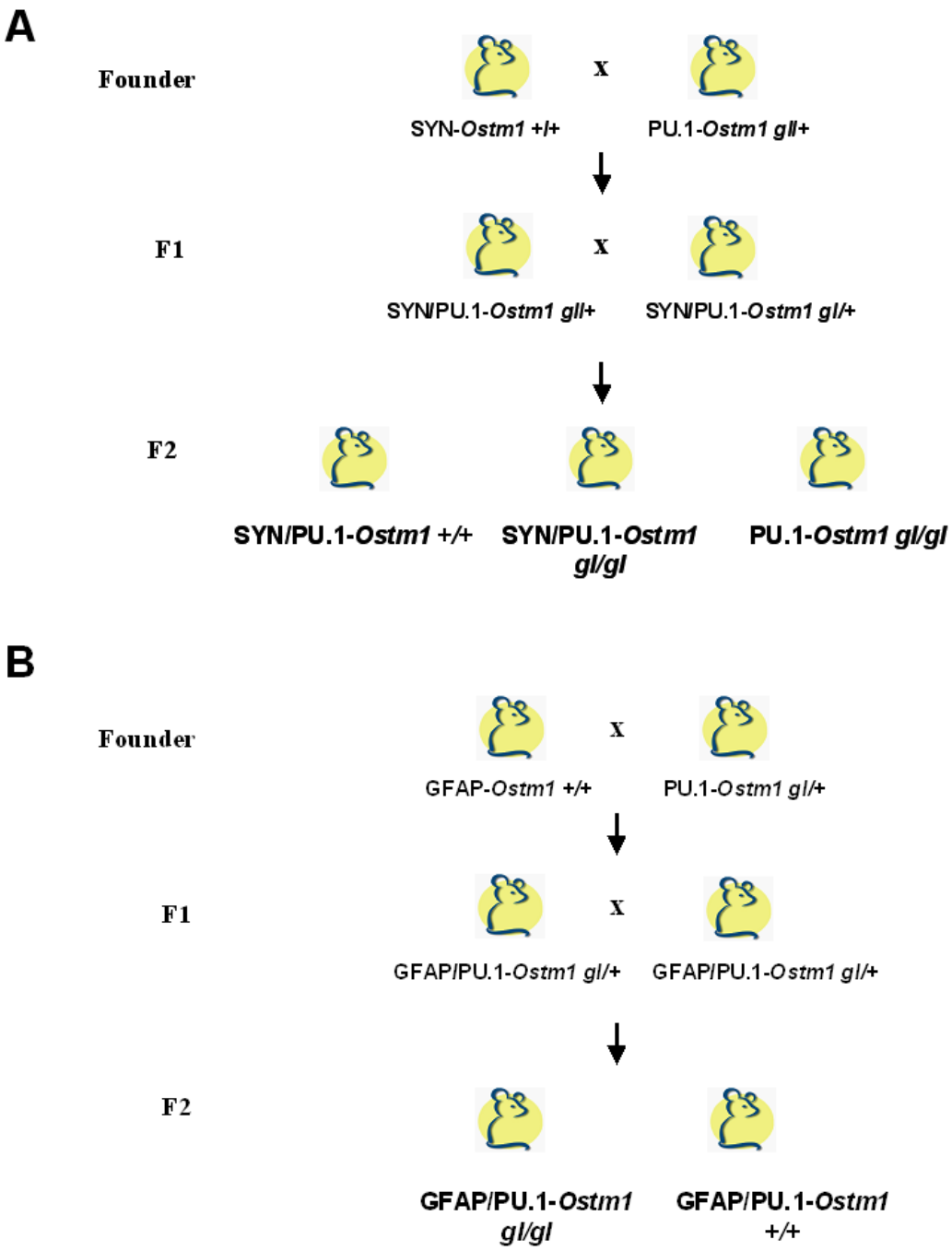

Figure 2-2: Mating scheme used to generate mice analyzed in this study. (A) Mice positive for the SYN transgene were crossed with heterozygous PU.1-*Ostm1-gl/+* mice to generate F1 animals that are positive for both transgenes and heterozygous for *Ostm1* (*gl/+*). The F1 animals were then intercrossed to obtain transgenic wild type for *Ostm1*, single transgenic PU.1-*Ostm1-gl/gl* and double transgenic SYN-*Ostm1*-PU.1-*Ostm1-gl/gl* mice. (B) A similar set of crosses was carried out to obtain mice transgenic for both GFAP-*Ostm1* and PU.1-*Ostm1* and homozygous for the *Ostm1* mutation (*gl/gl*).

Similarly, GFAP-*Ostm1* positive mice were crossed with PU.1-*Ostm1-gl/+* mice to generate F1 double transgenic GFAP-*Ostm1*-PU.1-*Ostm1-gl/+* mice. F1 animals were then intercrossed to obtain double transgenic GFAP-*Ostm1*-PU.1-*Ostm1-gl/gl* mice for analysis (Figure 2-2).

2.2. Primary Cell Culture

2.2.1 Astrocytes

Primary cultures of cerebral cortical astrocytes were obtained from neonatal wild type and grey-lethal mice. Cerebral hemispheres were dissected into small blocks after removal of meninges and then incubated in PBS containing 0.25% trypsin. After a short incubation, dissociated cells were suspended in Dulbecco's modified Eagle medium (Invitrogen), supplemented with 5% fetal bovine serum, 5mg/ml glucose, and 100U/ml of penicillin, and 1 μg/ml of streptomycin. After confluent astrocyte cell layer was obtained, free floating microglia were removed with the supernatant and oligodendrocytes and neurons were detached by agitation on a shaking platform (Hertz et al., 1998, Saura, 2007)

2.3 Molecular Analysis

2.3.1.Southern blot for copy number of SYN and GFAP transgenic lines

2.3.1.1. DNA Digestion and analysis

10 μl of genomic DNA was digested overnight at 37^{o}C with Hpa I for the Syn transgene and XhoI for the GFAP transgene and run in a 0.7% TAE 1X (40mM Tris Acetate, 1mM EDTA) agarose gel. The gel was then treated for 30 minutes in denaturing solution (1M NaCl, 0.5M NaOH) followed by 20 minutes in

neutralizing solution (3M NaCl, 0.5M Tris HCl pH 7.4). DNA was then transferred to a nylon membrane overnight by capillarity using 20X SSC (3M NaCl, 0.3M sodium citrate pH 7.0) Cross linking of the DNA to the membrane was then achieved by exposure to UV light for 10 minutes.

2.3.1.2. Radioactive Probe Labeling and Membrane Hybridization

The DNA template for the probe was prepared by PCR amplification on mouse genomic DNA of a 300bp sequence corresponding to exon 1 of *Ostm1* using HSPC Exon 1 For and P10 5' Rev (see Table 1). Cycling conditions were the same as *Ostm1* genotyping. The digestion product was then run in agarose gel, isolated by electroelution and precipitated at –20^{o}C with 100% EtOH and 0.2M NaCl. 100ng of DNA template was then used to prepare the ^{32}P dCTP labelled probe by nick translation using DNA pol I.

Nylon membranes were then pre-hybridized for at least 3 hours at 65^{o}C with 2mM denatured salmon sperm DNA in 5X SSC (1.5M NaCl, 75mM sodium citrate), 10X Denhart (2% ficoll, 2% polyvinylpyrrolidone, 2% BSA) and 0.1% SDS. Radiolabeled probe was then added and allowed to hybridize overnight at 65^{o}C. Membranes were then washed under increasingly stringent conditions: SSC 1X (0.3M NaCl, 15mM sodium citrate) SDS 1%; then SSC 0.1X (0.03M NaCl, 1.5mM sodium citrate) SDS 0.1% to remove non-specific hybridization of the probe and then exposed film at –80^{o}C for 3 to 5 days.

The expected specific bands resulting from Hpa I digestion of the SYN-*Ostm1* transgene are 6.6kb transgene and 5.0kb endogenous *Ostm1*. The expected specific bands resulting from XhoI digestion of the GFAP-*Ostm1* transgene are 3.8kb transgene and 14.8kb endogenous *Ostm1.*

2.3.1.3. Determination of transgene integrity and copy number

Using Image Quant Version Build software (Molecular Dynamics), resulting films were analysed and the expected bands for both the SYN-*Ostm1* transgene and GFAP-*Ostm1* transgene were quantified for total pixels along with the expected endogenous *Ostm1* bands. A ratio of the transgene to the endogenous was then taken to evaluate the number of copies in each transgenic line.

2.3.2. mRNA Expression

2.3.2.1. RNA isolation

Total RNA was isolated from cells and tissues using TRIzol (Gibco) and a polytron homogenizer according to the manufacturer's instructions. RNA was then resuspended in diethyl pyrocarbonate (DEPC) treated water and the concentration was quantified by UV spectroscopy absorbance reading at 260 nm.

2.3.2.2. Northern Blot

10μg of RNA were subjected to electrophoresis on denaturing formaldehyde (11.5%) 1.5% agarose gel and run in 10X MOPS buffer (0.2M 3-N-morpholino-2-hydroxypropanesulfonic acid, 50mM Sodium acetate-$3H_20$, 10mM EDTA pH 7).

RNA was then transferred to a nylon membrane overnight by capillarity using 20X SSC (3M NaCl, 0.3M sodium citrate pH 7.0). Cross linking of the RNA to the membrane was then achieved by exposure to UV light for 10 minutes.

The DNA template for the probe was prepared by PCR amplification on mouse *Ostm1* cDNA of a 1kb sequence using the following primers: HSPC Exon 1 For, HSPC Exon 6 Rev for detecting endogenous and transgenic *Ostm1*, GFAP for (Ex1) and GFAP rev (Ex5) for detecting GFAP expression from mRNA. Previously described rpL32 (Vacher et al. 1990) specific for the transcript of the ribosomal protein L32 was used as an internal control. The subsequent radioactive labelling and membrane hybridization were carried out as previously described above.

2.3.2.3. RT-PCR

Reverse transcription reactions were performed on DNAase treated total RNA. 2μg of total RNA were incubated for 15 minutes at room temperature with 0.5μl of DNAse. The enzyme was then denatured by incubation for 10 minutes at 75°C with 2.5mM EDTA. Following an additional 15 minutes incubation at 70°C in the presence of oligodT primers, cDNA was then transcribed from the RNA using SuperScript II Reverse Transcriptase (Invitrogen) by incubation for 50 minutes at 42°C with RT buffer mix (0.5mM dNTPs, 10mM DTT,50mM Tris-HCl pH 8.3, 75mM KCl, 3mM MgCl2). The enzyme was then inactivated by incubation for 15 minutes at 70°C and 1/10 dilution (0.2μg of cDNA) was used to perform PCR for the genes of interest listed in Table II for 30-35 cycles. PCR conditions of 94°C

for 30 seconds, 65^{o}C for 30 seconds, 72^{o}C for 30 seconds in buffer containing 10mM Tris-HCl pH 8.3, 50mM KCl, 1.5mM MgCl2 were used to generate amplicons with two exceptions. RT-PCR of the SYN-*Ostm1* and GFAP-*Ostm1* transgenes have annealing temperatures of 60^{o}C and include 10% DMSO in the PCR buffer.

2.3.2.4. qPCR analysis

cDNA was prepared as above and quantitative qPCR was performed on a Mx3005 Stratagene using SYBR Green Mastermix (Qiagen, Mississauga, Ontario, CA) according to the manufacturer's instructions. PCR amplification was performed in a 25μl reaction mix containing 0.5μl cDNA sample. Thermal cycling was initiated with one cycle at 95^{o}C for 15min to denature cDNA and to activate the HotStarTaq DNA polymerase. PCR conditions were then carried out for 40 cycles of 95^{o}C, 30 seconds, 60^{o}C, 30 seconds and 72^{o}C seconds. Ribosomal protein S16 was used as an internal control. The primers used were SYN Endo for 1, SYN Endo Rev 1, qOstm1 for 1, qOstm 1 Rev 1, as well as qS16 FOR and qS16 REV (see Table II). qPCR products were visualized on agarose gel with EtBr to ensure the presence of a single amplicon. The *Ostm1* transgene expression is represented by a ratio of wild-type non-transgenic mouse (endogenous *Ostm1* expression alone) to that of transgenic mouse (transgenic *Ostm1* + endogenous *Ostm1* expression). The data were presented as a fold increase. Results were then analyzed and differences in cycle threshold normalized to S16 were obtained.

2.4. Biochemical analysis

2.4.1. Antibodies and reagents

The following antibodies and reagents were used in this analysis: rabbit anti-Beclin-1 (SantaCruz), rabbit anti-Akt, rabbit anti-phospho-Akt (ser473), rabbit anti-mTOR, rabbit anti-phospho-mTOR (Ser 2481), rabbit anti-p70 S6 Kinase, rabbit anti-phospho p70 S6 Kinase (Thr 389) (Cell Signaling), mouse anti-golgin-97 (Molecular Probes), mouse anti-β-actin, rabbit anti-LC3 (Sigma). Horseradish Peroxidase (HRP) labeled goat anti-mouse and goat anti-rabbit IgG (BioRad)

2.4.2. Protein Extracts

Tissues were processed by the manual Potter-homogenizer method in phosphor-protein lysis buffer (50mM Na Pyrophosphate, 50mM NaF, 50mM NaCl, 5mM EDTA, 5mM EGTA, 40mM B-glycerophosphate, 10mM HEPES pH 7.4, 0.1% Triton X-100, 0.1% NP-40, 2mM Na Orthovanadate, 1mM PMSF and 1/1000 protease inhibitor cocktail (PIC) (Sigma)). Following a 30 minute incubation on ice, samples were centrifuged for 15 minutes at 4^{o}C at 12,000 rpm. Supernatant was collected as total protein extract.

2.4.3. Western Blot

The concentrations of protein extracts were evaluated using the Bradford assay (BioRad). Equal amounts of protein were boiled for 10 minutes in sample buffer (190mM Tris-HCl pH 6.8, 6% SDS, 30% glycerol, 0.006% bromophenol blue and 5% β-mercaptoethanol) and separated by denaturing SDS-PAGE (4% stacking,

6.5 and 15% resolving). Proteins were then electro-transferred to Polyvinylidene Fluoride (PVDF) membranes at 300mA for 1 hour. The membrane was then incubated for 1 hour in blocking solution containing 5% skim milk in TBS-T 1X (25mM Tris-HCl pH 7.5, 0.9% NaCl and 0.1% Tween). The membrane was then washed with TBS-T 1X and incubated overnight at 4^{o}C with primary antibody diluted (1:200 for phospho-mTOR, 1:5000 for β-actin, 1:1000 for others) in TBS-T 1X with 5% BSA. Following washes in TBS-T 1X, the membrane was then incubated for 1 hour at room temperature with the appropriate HRP coupled secondary antibody diluted (1:10,000) in 5% skim milk in TBS-T 1X. Signal was then detected using ECL Western Blotting Detection kit (Amersham GE Heathcare) and autoradiography. Membranes were incubated 30 minutes at 55^{o}C with stripping solution (2% SDS, 62.5mM Tris-HCl pH 6.7,0.6% B-mercaptoethanol) to remove antibodies and reprobed.

2.5. Immunohistological analysis

2.5.1. Antibodies and reagents

The following antibodies and reagents were used in this analysis: mouse anti-NeuN (Chemicon), mouse anti-calbindin-D-28K, mouse anti-GFAP (Sigma) and rabbit anti-IbaI (Wako).

2.5.2. Tissue and Section preparation

Anesthetized mice were perfused with 20ml of PBS 1X followed by ice-cold 4% paraformaldehyde in PBS 1X, pH 7.4 over 10 minutes. Brains and eyes were

removed, post fixed overnight then embedded in paraffin. For cytoarchitectural studies, sections (4μm) were stained by hematoxylin and eosin. For immunohistochemistry, sections were subjected to protease antigen retrieval (0.1% trypsin in 0.1% CaCl2, 20mM Tris-HCl, pH 8.0), peroxydase quenching and incubated overnight at 4°C with primary antibodies. The sections were then immunolabeled with the R.T.U. VECTASTAIN Universal ABC kit using DAB substrate kit (Vector Laboratories) and counterstained with hematoxylin. Images were captured with a Zeiss Axiovert microscope.

2.6. Ultrastructural analyses

Anesthetised mice were perfused with PBS 1X followed by ice-cold fixative (1% paraformaldehyde and 2.5% glutaraldehyde in PBS 1X, pH 7.4) over 10 minutes. Brains were then removed and post-fixed 2 hours in the same fixative. Floating sections (50μm) were then post-fixed in 1% OsO_4 in cacodylate buffer and dehydrated in ethanol series before embedding and polymerization in LR White Resin (Electron microscopy Science). Hippocampal ultra-thin sections were placed on nickel grids and stained with 1% uranyl acetate in 70% ethanol. Grids were viewed on a Jeol 1200-Ex transmission electron microscope (Jeol, Inc. Peabody, MA).

2.7. MRI Scans

All MRI studies were performed at the Small Animal Imaging Lab (SAIL) at McGill University. During imaging, the mice were anesthetised with isoflurane and

placed in the Bruker 7T Pharmascan MRI Scanner with constant monitoring of respiratory rate and maintenance of body temperature. Following a 3-plane localizing scan, coronal 3D Fast Imaging with Steady State Precession (FISP) images were acquired with 4 phase acquisitions at 0, 90, 180 and 270 degrees. Images were reconstructed offline and combined using complex sum averaging. To eliminate banding artifacts from 3D volumes, images were acquired with the following parameters: TR=6 ms, TE=3 ms, flip angle = 30°, matrix=128X128X64, FOV=18x18x9 mm^3, NEX=4, and 33 minute scan duration (Bangerter et al., 2004). Following imaging, mice were removed from the MRI and placed under a heat lamp until they regained consciousness and were then returned to their cage. Images were analyzed using Medical Image Processing, Analysis and Visualization (MIPAV) software. (Center for Information Technology, National Institutes of Health)

Table 1: Genotyping Primers

Primer Name	Sequence
gl For 1	5’-CCT CTG GGAA GAC TAA TAC TTG CTG-3’
gl Rev 1	5’-GCC TGG AAC AGA GCA AAG C-3’
gl For 2	5’-GCT ACA TCT GGG TCC TTT CG-3’
gl Rev 2	5’-CGC TTG CTT TTG TCT GTT ACC TTT GTG TTC-3’
PU.1 For	5’-GCC TTT CTC CCT CCC AGC C-3’
HSPC Rev 1	5’-CAA GTC CTG CAC CTC CAA CAG C-3’
SYN For 1	5’-ATT TAG TAC CGC CGA CAG AGC CTT-3’
RGH Rev 1	5’-AGT TGG GAT GCC CTC ACA CTA GAA-3’
GFAP-gl For 1	5’-CCG TGG TTG CTG TGT CTG TGT T-3’
mp-1 Rev 1	5’-TCT CAC GTC AGG AGT TTG ATG G-3’
HSPC Exon 1 For	5’-GTC GGC ACC CAG GCT TTC-3’
P 10 5’ Rev	5’-AGC GTT AGT TCT ACC TGT TGT-3’
HSPC Exon 6 Rev	5’-CTG CAG TCC CAA CAT TTC GTG AG-3’
GFAP Exon 1 For	5’-GCT TCC TGG AAC AGC AAA AC-3’
GFAP Exon 5 Rev	5’-CGG CGA TAG TCG TTA GCT TC-3’

Table 2: RT-PCR Primers

Primer Name	Sequence
β-Actin For	5’-TGA CGA TAT CGC TGC GCT G-3’
β-Actin Rev	5’-ACA TGG CTG GGG TGT TGA AG-3’
RT SYN For A	5’-AGC GAG GAA GCG GAA GAG GAA-3’
RT SYN Rev A	5’-AGC GAG GAA GCG GAA GAG GAA-3’
RT Ostm1 Ex 3 For	5’-CCT GCT TTG AGC ATA ACC TGC-3’
RT Ostm1 Ex 6 Rev	5’-CTG CAG TCC CAA CTT TCG TGA G-3’
GFAP-gl For 1	5’-CCG TGG TTG CTG TGT CTG TGT T-3’
mp-1 Rev 1	5’-TCT CAC GTC AGG AGT TTG ATG G-3’
qPCR SYN Endo For 1	5’-AGA AAC CCA GCC AGG ATG T-3’
qPCR SYN Endo Rev 1	5’-GTC TTT CGC CAG CCT CTT CT-3’
qOstm1 For 1	5’-GTG GTT GCT GTG TCT GTG TTC-3’
qOstm1 Rev 1	5’-CAG GAG ACT TCC GCC ACA G-3’
qS16 For	5’-GCT ACC AGG GCC TTT GAG ATG-3’
qS16 Rev	5’-AGG AGC GAT TTG CTG GTG TGC-3’

Chapter 3

Results

3.1. Neurodegeneration in PU.1-*Ostm1-gl/gl* mice

Grey-lethal mice die regularly at three weeks of age due to a host of complications caused by severe malignant ARO. Targeting *Ostm1* to the multipotent myeloid progenitors using a PU.1 promoter is sufficient to rescue the bone and hematopoietic defects and transgenic PU.1-*Ostm1-gl/gl* mice in fact have an extended life span longer then three weeks. It is also known that *Ostm1* is highly expressed in the brain, among other tissues. (Chalhoub et al., 2003, Pata et al., 2008) These mice provide an excellent model for studying the exact roles of *Ostm1* in other tissues and cell types.

Surprisingly, PU.1-*Ostm1-gl/gl* mice live past three weeks; however, their overall health deteriorates progressively and rapidly. All the transgenic *gl/gl* mice were dead after 6-7 weeks as shown by Kaplan-Meier survival analysis (Figure 3-1),

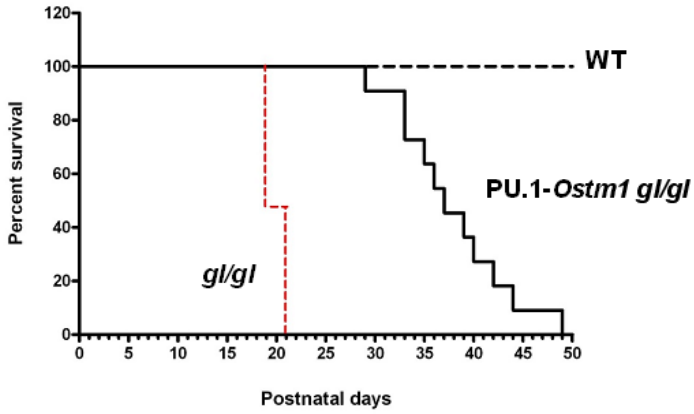

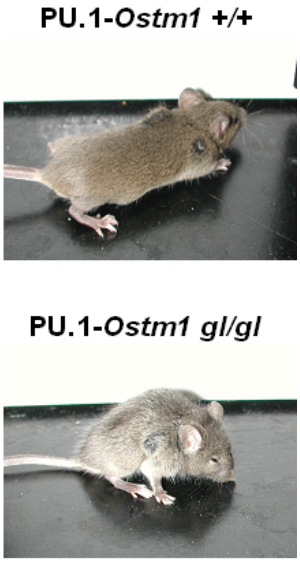

Figure 3-1: Survival of PU.1-*Ostm1-gl/gl* mice. Kaplan-Meier survival analysis showing average 6-7 week lifespan of PU.1-*Ostm1-gl/gl*. Note grey coat color persists in transgenic *gl* mice as transgene only target the hematopoietic lineage with mutation still present elsewhere including melanocytes.

while all wild type transgenic mice did not show any phenotype. Since *Ostm1* is highly expressed in the CNS, including the cortex, hippocampus and cerebellum, we hypothesized that perhaps these mice were suffering from neuronal abnormalities leading to their decrease in survival.

3.1.1. Immunohistological analysis of PU.1-*Ostm1-gl/gl* mice

3.1.1.1. CNS

Using histological staining and immunohistochemistry on sections of brain from 5 and 6 week old mice we did in fact see notable differences. Hematoxylin and Eosin (H&E) staining of sections demonstrated almost total loss of the CA3 region of the hippocampus compared to that of wild type mice positive for the PU.1-*Ostm1* transgene. (Figure3-2A). Similar sections stained with the antibody NeuN specific for a neuron nuclear protein revealed significant losses of cortical neurons at all layers of the cortex in PU.1-*Ostm1-gl/gl* mice (Figure 3-2B). As well, at the level of the cerebellum, there was a loss of Purkinje cells as seen by calbindin immunostaining (Figure3-2C). The loss of Purkinje cells was only visible after 6 weeks, compared to losses in the cortex and hippocampus which were visible after 5 weeks. This suggests a possible progressive nature of the neurodegeneration.

In addition to neurons, astrocytes have several critical roles in the brain, from maintaining the blood brain barrier and modulating the amount of neurotransmitter molecules in the extracellular space to tempering synaptic

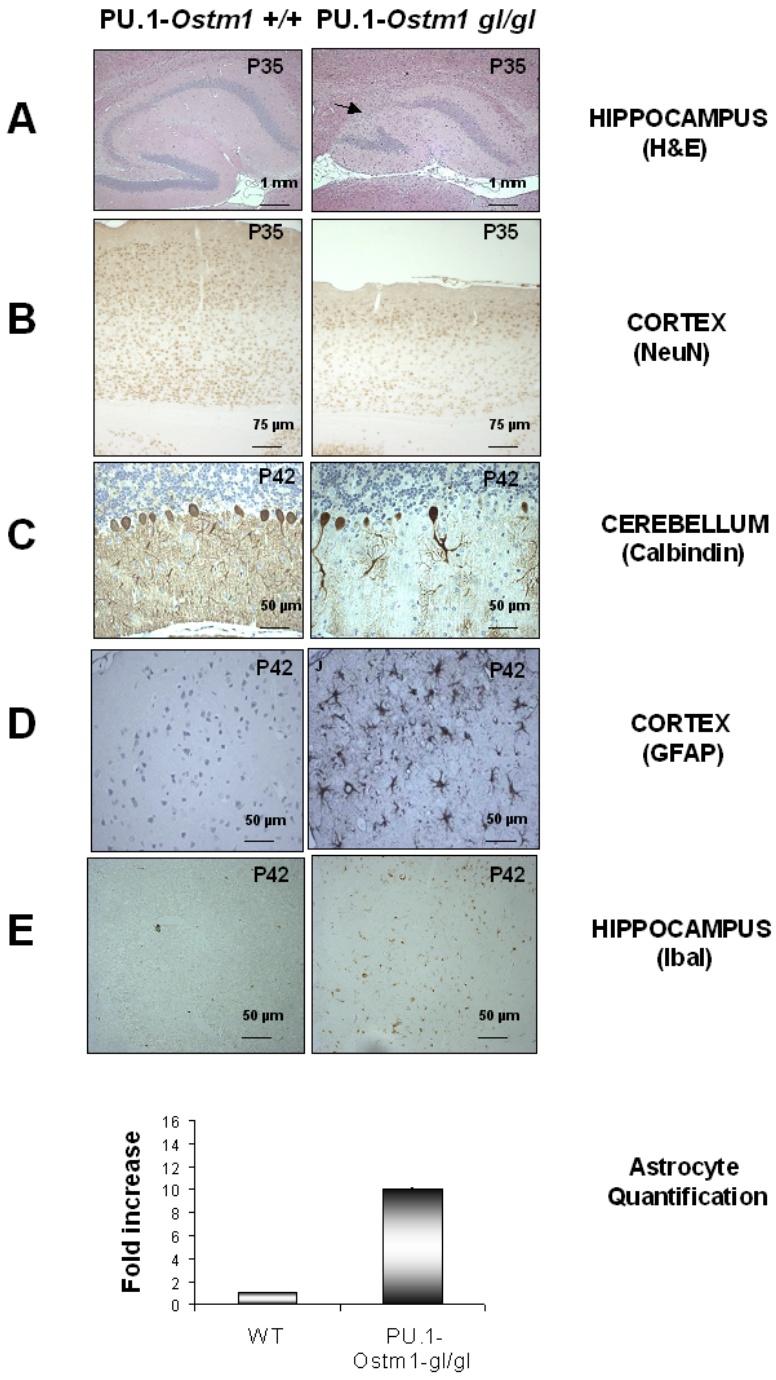

Figure 3-2: Immunohistological analysis of brain sections of PU.1-*Ostm1-gl/gl* transgenic mice. (A) H&E stain of Hippocampus. Arrow indicates loss of CA3 region. (B) NeuN staining specific for neurons. Significant loss of cortex in PU.1-*Ostm1-gl/gl* mice. (C) Calbindin staining specific for Purkinje cells demonstrated marked loss after 6 weeks in PU.1-*Ostm1 gl/gl* mice. (D) GFAP marker for mature astrocytes showed notable astrogliosis and inflammation in cortex of PU.1-*Ostm1-gl/gl* brain. (Quantification of astrogliosis at bottom) (E) Iba1 stain for reactive microglia showed presence of numerous active cells in cortex.

function itself via direct communication with neurons (Rouach et al., 2008). They also play an important role during neuronal cell death. Both acute and chronic brain traumas can result in astrogliosis. During astrogliosis, astrocytes become highly activated and undergo proliferation in an attempt to isolate the affected areas from the rest of the brain. This may involve the remodeling of the blood brain barrier and or reconstruction of the brain circuits surrounding the damaged region. This reaction inevitably results in the formation of a permanent glial scar (Rodriguez et al., 2009, Pekny et al. 2007). Glial Fibrillary Acidic Protein (GFAP) is a major intermediate filament generally regarded as an excellent marker for mature astrocytes (Messing et al., 2003). Following immunostaining for GFAP expression, we saw considerable astrogliosis at the level of the cortex in PU.1-*Ostm1-gl/gl* mice with a ten fold increase in GFAP-positive stained cell number compared to the wild type at 6 weeks (Figure3-2D).

Microglia, while not actually a brain cell type, are another group of myeloid cells that are in fact found in the CNS. Microglia are the resident immune cells of the brain that are considered the “macrophages” of the brain and maintain constant vigilance by removing dead cells and debris during times of stress, damage or infection (Allen et al., 2009). We used a specific marker for microglia, Iba1 for staining. As seen in Figure 3-2E, a significant level of active microglia was present in the cortex in PU.1-*Ostm1-gl/gl* mice compared to that of wild type at six weeks (Figure3-2E).

Further evidence for a progressive development of the neurodegenerative phenotype came from the examination of the non-transgenic *gl/gl* mouse. At three weeks of age, just before death, the *gl* mutant showed no discernable loss of cortex compared to that of wild type. All regions of the hippocampus appeared intact (data not shown); however, sections immunostained for GFAP did reveal mild astrogliosis with a 2 fold higher number of GFAP-positive cells signifying the presence of cell death and inflammation, as yet undetectable at three weeks (Figure3-3).

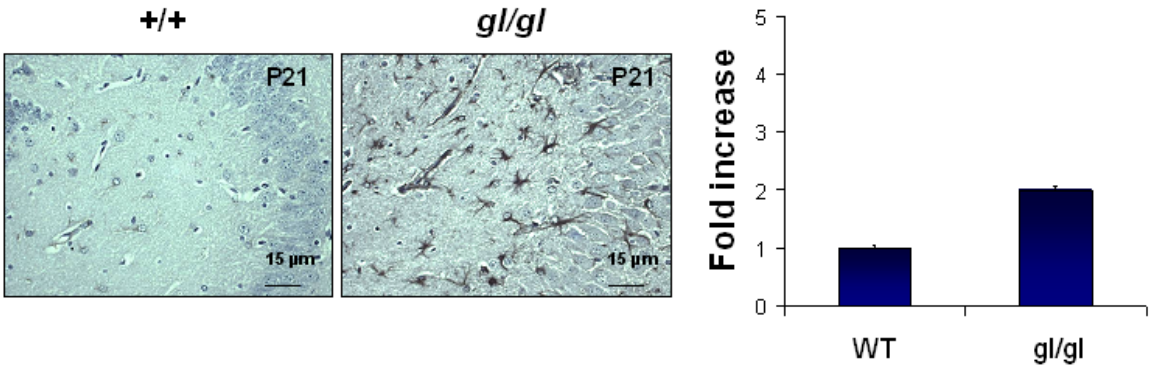

Figure 3-3: Immunohistological analysis of *gl/gl* brain. GFAP staining of *gl/gl* brain reveals mild astrogliosis at the level of the cortex.

3.1.1.2. Retina

Recall that osteopetrotic mice with loss of *Clcn7* also have significant retinal degeneration in addition to the neuronal phenotype. This, coupled with the retinal dystrophy seen in the human *OSTM1* patient that was separate from the prominent bone phenotype, led to the examination of the retina of the PU.1-*Ostm1-gl/gl* mouse.

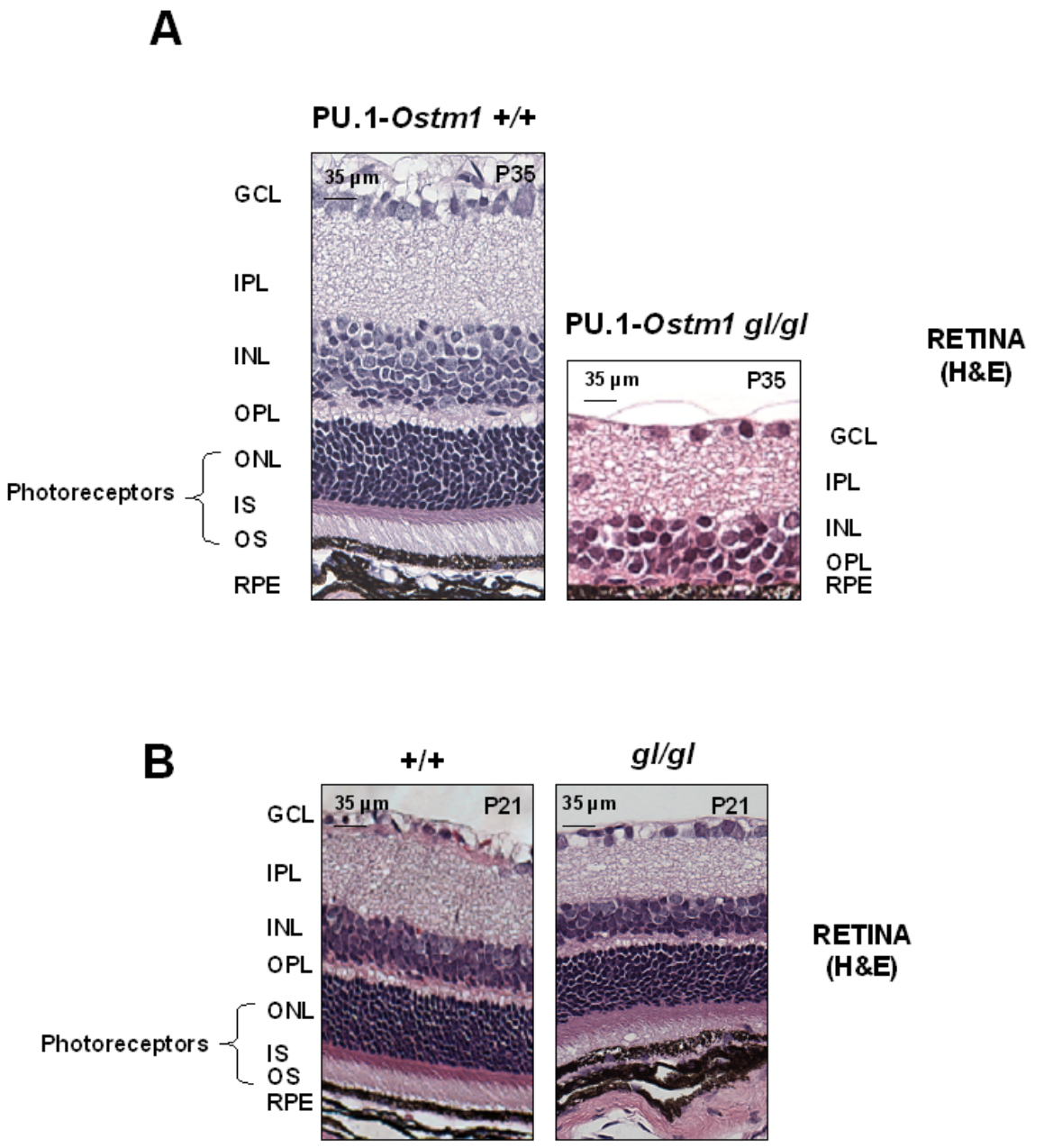

Figure 3-4: Histological analysis of retinal sections from 3 and 5 week old mice. (A) Note complete loss of photoreceptors in PU.1-*Ostm1-gl/gl* retinal sections. (B) H&E stain of the retina shows no degeneration with all layers present and no detectable loss of photoreceptors in *gl/gl* retinal sections. (GCL) = Ganglion Cell Layer, (IPL) = Inner Parietal Layer, (INL) = Inner Nuclear Layer, (OPL) = Outer Parietal Layer, (ONL) = Outer Nuclear Layer, (IS) = Inner Segments, (OS) = Outer segments, (RPE) = Retinal Pigment Epithelium.

Hematoxylin and eosin stains of retinal sections of 5 week old mice exposed major retinal degeneration in PU.1-*Ostm1-gl/gl* mice. There was a complete loss of both the inner and outer segments of the photoreceptors, as well as an absence of the Outer Nuclear Layer (ONL), normally found to contain the cell bodies of rods and cones (Figure 3-4A). Like the neurodegeneration seen only after 5 weeks, the loss of whole layers of the retina was progressive in nature. Retinal sections of 3 week old *gl/gl* mice were analyzed using hematoxylin and eosin and all regions appeared intact (Figure 3-4B). Once the bone and hematopoietic phenotypes were corrected using the PU.1 transgene, only then was severe retinal atrophy detected, just as was observed with degeneration of the CNS.

3.1.2. Autophagy in PU.1-*Ostm1-gl/gl* mice

3.1.2.1. Ultrastructural analysis

We next characterized more closely the neurodegenerative phenotype using ultrastructural analysis. Electron microscopy of hippocampal sections from 5 week old PU.1-*Ostm1-gl/gl* mice showed numerous osmium dense vesicles in the neuronal cytoplasm. This abnormal accumulation of vesicles may account for the prominent axonal swelling also observed in these neurons (Figure 3-5A). At higher magnification these vesicles appeared to be double membrane bound and contained dense inclusions possibly identifying them as autophagosomes (Figure 3-5B).

3.1.2.2. Biochemical Analysis

Autophagosomes are double membrane bound vesicles that are formed when the bulk degradation process of autophagy is stimulated. Autophagy is a physiological response used by the cell during times of cell growth, starvation, and stress (Levine et al., 2008, Marino et al., 2004, Mizushima, 2007). Unlike the ubiquitin proteasome system that targets small short lived cytoplasmic proteins,

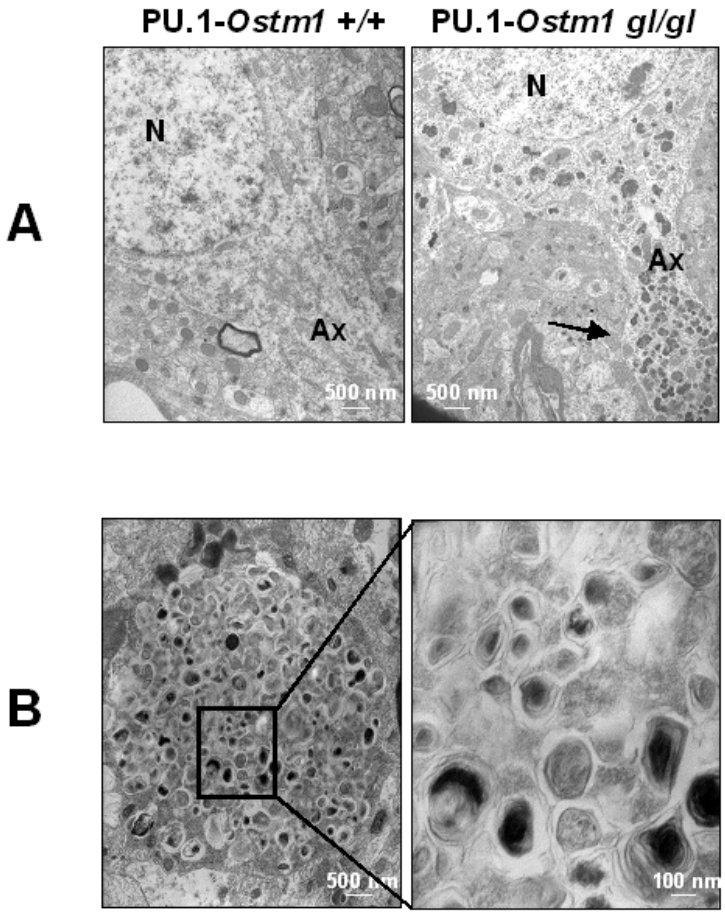

Figure 3-5: Ultrastructural analysis of hippocampal sections of 5 week old PU.1-*Osmt1-gl/gl* mice. (A) Accumulation of numerous vesicles in the neuronal cytoplasm and axons that may account for the significant axonal swelling indicated by the arrow (N= nucleus, Ax = Axon). (B) Higher magnification of a cross section of PU.1-*Ostm1-gl/gl* hippocampal axon reveals presence of double membrane bound vesicles with dense inclusions resembling autophagosomes.

autophagy is used to remove large misfolded proteins or damaged organelles for macromolecule recycling and improved survival (Klionsky et al., 2000, Mizushima et al., 2002). Autophagy begins with the sequestration of the cytoplasmic material by a unique membrane known as a phagophore stemming from the endoplasmic reticulum. (Simonsen et al., 2008, Axe et al., 2008). The vesicle is then expanded and completed to form the spherical autophagosomes. The autophagosomes then mature, join with endosomes and are transported via microtubules to the lysosomes where they fuse and their contents are degraded (Figure 3-6). Microtubule associated protein I Light Chain 3 (LC3) represents a specific marker of autophagy. LC3 is a cytoplasmic protein that is modified following cleavage of its C terminal region, allowing attachment of a phosphatidylethanolamine group. This modification changes LC3 from its cytoplasmic form (LC3-I) to LC3-II that inserts into the membrane of an autophagosome. LC3-II is the marker for autophagosome accumulation (Kabeya et al., 2000, Shacka et al., 2008).

Since we hypothesized that the vesicles detected by electron microscopy represent true autophagosomes, we next quantified expression of LC3-I and LC3-II protein in brain extracts from PU.1-*Ostm1-gl/gl* mice by Western blot. In contrast to the presence of only LC3-I in brain extracts of 6 week old wild type mice, we detected in brain extracts from 6 week old PU.1-*Ostm1-gl/gl* mice an increase in LC3-I expression and even more importantly an increase in LC3-II expression. Quantification of these proteins showed, when compared to the wild type mice, a ratio of LC3-I to LC3-II had an increase of approximately 70% in

PU.1-*Ostm1-gl/gl* mice, suggesting a significant accumulation of autophagosomes (Figure 3-7A).

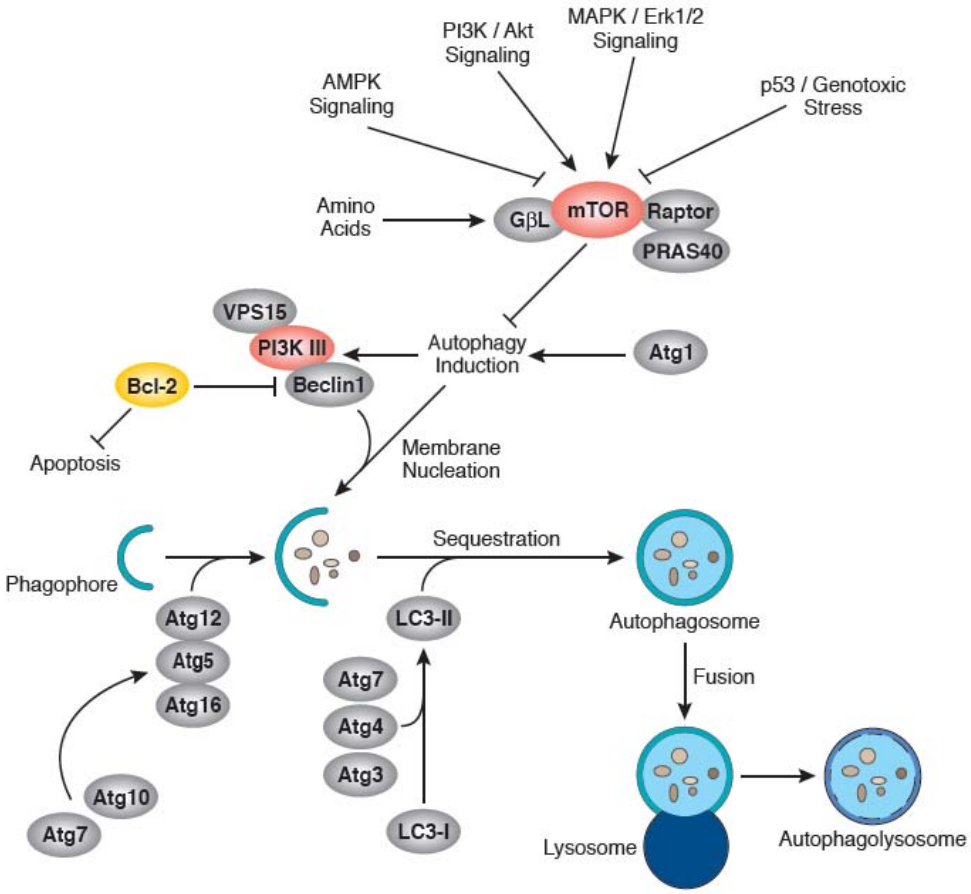

Figure 3-6: Regulation of Autophagy and Autophagosome formation. Autophagosomes start as Phagophores, envelop macromolecules and organelles, mature and are transported to the lysosome for degradation (LC3-II found on outer membrane of autophagosome). Two main pathways regulate autophagy. Beclin-1 via the PI3K III and mTOR that when phosphorylated inhibits autophagy via S6K (Adapted from Cell Signalling).

In order to further verify the involvement of autophagy in the neurodegenerative phenotype of the PU.1-*Ostm1-gl/gl* mice, we examined the signalling pathways known to be involved in the stimulation of autophagy. Two main pathways regulate autophagy. One pathway involves the Beclin-1 protein and the other

pathway implicates the Mammalian Target of Rapamycin (mTOR) kinase protein. Beclin-1 regulates autophagosome formation in mammals via increased expression of the protein and its interaction with class III phosphatidylinositol 3-kinase (PI3K) (Figure 3-6) (Cecconi et al., 2008, Liang et al., 2006, Simonsen et al. 2009). mTOR is a serine/threonine kinase, that when phosphorylated, acts by inhibiting autophagosome formation. Normally mTOR is regulated by the class I PI3K/Akt pathway. Akt, when phosphorylated, keeps mTOR phosphorylated thereby inhibiting autophagy (Degtyarev et al., 2008). mTOR acts via phosphorylation of further downstream effectors, such as the 70kDa ribosomal protein S6 Kinase (S6K) that prevent autophagosome formation. A decrease in Akt signalling can result in a decrease in phosphorylated mTOR and a stimulation of autophagy (Nicklin et al., 2009, Tang et al., 2008) (Figure 3-6).

The analysis of brain extracts of 6 week PU.1-*Ostm1-gl/gl* mice with Western blot revealed a ≅ 50% decrease in phosphorylated mTOR compared to wild type. We next examined the upstream and downstream regulators of the mTOR pathway and found a similar ≅ 34% decrease of phosphorylated Akt and a ≅ 38% decrease of phosphorylated S6K, further suggesting the particular involvement of the mTOR pathway in PU.1-*Ostm1-gl/gl* mice that results in a major stimulation of autophagy in neuronal cells (Figure 3-7B). In contrast, analysis of the Beclin-1 pathway showed no relative increase in Beclin-1 expression in PU.1-*Ostm1-gl/gl* brain extracts compared to wild type, suggesting most likely no involvement of this pathway (Figure 3-7C).

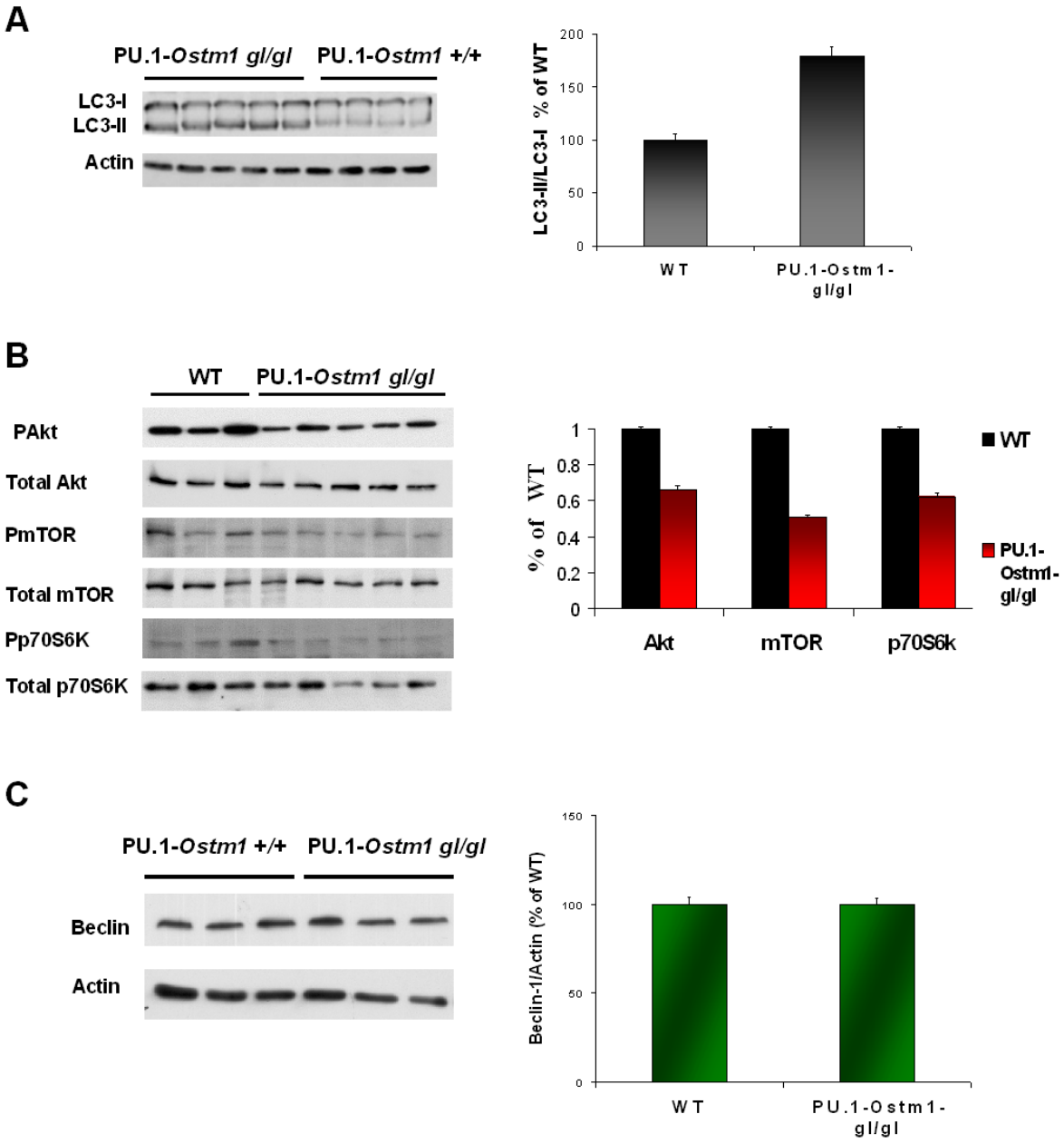

Figure 3-7: Analysis of autophagy signalling pathways in PU.1-*Ostm1-gl/gl* mice. (A) Marked increase in LC3-II protein expression in PU.1-*Ostm1-gl/gl* brain extract compared to PU.1-*Ostm1* wild type demonstrated stimulation of autophagy. Normalized quantification on the right. (B) Notable decrease in phosphorylated mTOR in PU.1-*Ostm1-gl/gl* mice compared to that of wild type. Examination of upstream regulator (pAkt) and downstream effectors (Pp70S6K) confirmed mTOR result and demonstrates involvement of the mTOR pathway in stimulation of autophagy in the CNS of PU.1-*Ostm1-gl/gl* mice. Normalized quantification on the right. (C) Analysis of Beclin-1 protein showed no significant difference between wild type and PU.1-*Ostm1-gl/gl* mice.

3.2. Targeted expression of *Ostm1* to neurons

In an effort to better understand the role of *Ostm1* in normal brain cell homeostasis, we developed another transgenic line by targeting *Ostm1* specifically to neurons using the rat Synapsin-1 promoter (SYN-*Ostm1*). Synapsins are abundant small synaptic vesicle proteins that coat the cytoplasmic surface of the vesicle and are found in the neuronal pre-synaptic terminal (Bennett et al., 1991, Fdez et al., 2006, Hosaka et al., 1999, Street et al., 2005). Other neuronal gene regulatory sequences that are used to direct expression in the brain are restricted to only certain cellular subtypes or the promoters overlap in specificity with other non-neural cell types such as glial cells. Conversely, synapsin is found exclusively in neurons of all types. (Gaffield et al, 2007, Hoesche et al, 1993, Schoch et al., 1996, Thiel et al, 1991).

3.2.1. SYN-*Ostm1* transgenic mice

3.2.1.1. Transgenic lines

With this in mind the SYN-*Ostm1* transgene was established (Figure 3-8A). We next analyzed the integrity of the transgene and the number of copies in each line by Southern blot. Two lines were developed, line 214 with 2 copies and line 215 with 10 copies (Figure3-8B).

3.2.1.2. Expression

Specific expression of the SYN-*Ostm1* transgene in the brain was then verified by Northern blot. The 1kb mRNA transcript of the transgene was detected only in

the brain in comparison to the 3kb mRNA transcript of the endogenous *Ostm1* mRNA transcript that was present in all tissues analysed (Figure 3-8C).

Further confirmation of brain specific expression was obtained by RT-PCR (Figure 3-8D). Two amplicons were observed in the brain due to the nature of the primers used. The forward primer was located at the end of the promoter region of the transgene with the reverse primer at the start of the *Ostm1* coding sequence thereby spanning the rat growth hormone (RGH) intron (Figure 3-8A). The difference of 198bp in the two amplicons corresponds to the RGH intron, which demonstrated that only partial excision of the intron in the transgene occurred. This result was observed in both transgenic lines (Figure 3-8D).

The differences in expression between lines 214 and 215 were quantified by qPCR analysis. Again due to the nature of the primers, the SYN-*Ostm1* transgene could not be quantified exclusively. Instead, primers were selected that spanned the *Ostm1* coding sequence; thus, both the endogenous and transgenic *Ostm1* expression were detected. The result was represented by a ratio of wild-type non-transgenic mouse expression (endogenous *Ostm1* alone) to that of transgenic mouse expression (transgenic *Ostm1* + endogenous *Ostm1*) (Figure 3-8D). Line 214 was found to have a $\cong$ 5 fold increase in *Ostm1* expression while line 215 had over a $\cong$ 35 fold increase in *Ostm1* expression that corroborated with the number of copies in each transgenic line.

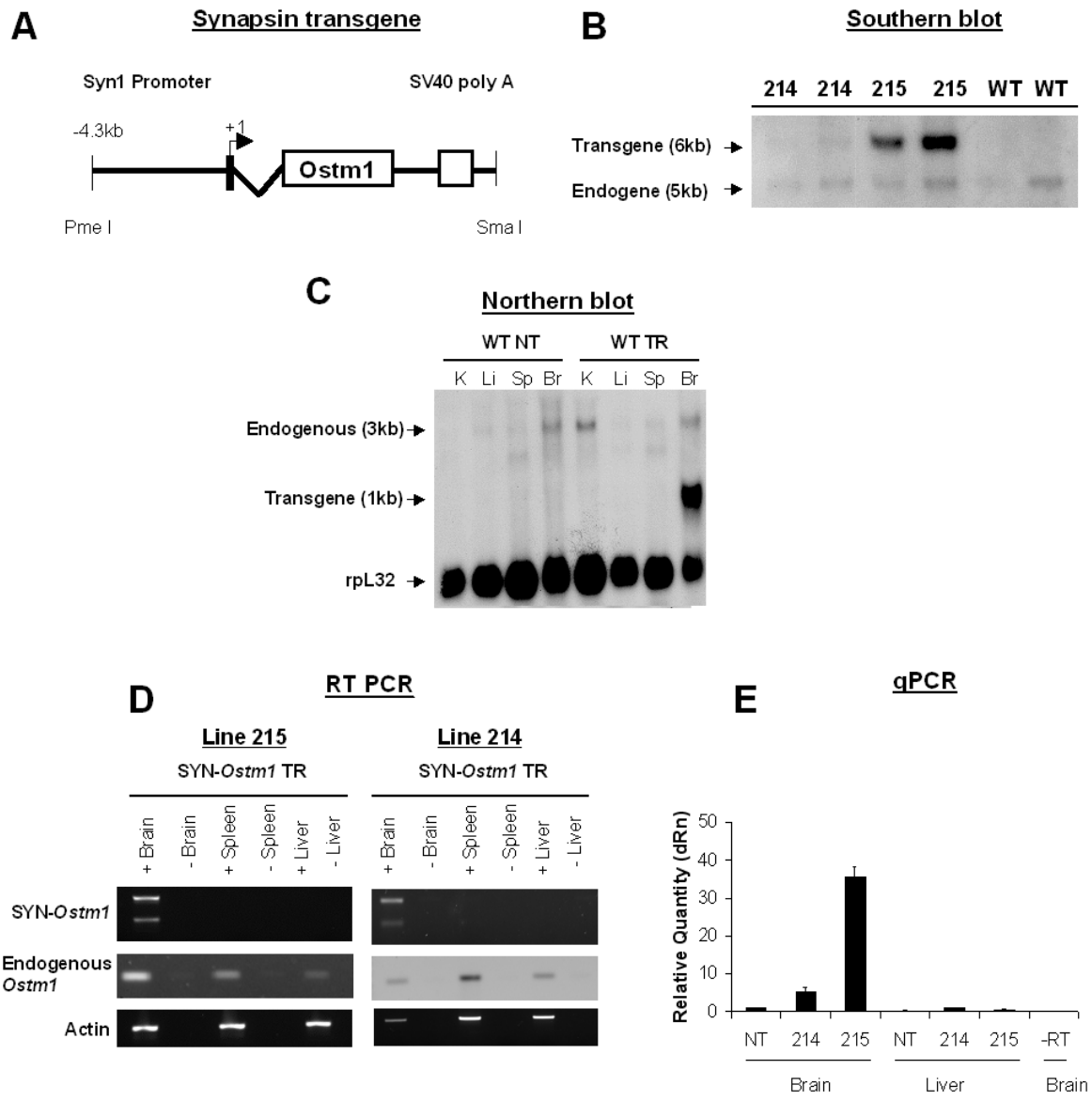

Figure 3-8:Characterization of SYN-*Ostm1* transgenic mice. (A) Construct of Synapsin transgene used to target *Ostm1* specifically to neurons (B) Southern blot of transgenic founder mice 214 and 215 genomic DNA. (C) Northern blot of SYN-*Ostm1* mRNA showed specific transgene expression in the brain. (D) Brain specific expression detected by RT-PCR. (E) Quantitative expression of SYN-*Ostm1* (Endogenous + transgenic) in brain by qPCR (n=2). Expression represented as fold increase relative to non transgenic endogenous expression of *Ostm1.*

3.3. Rescue of the Neurodegenerative Phenotype

3.3.1. SYN-*Ostm1*-PU.1-*Ostm1-gl/gl* mice

Mice positive for the SYN-*Ostm1* transgene were then crossed with heterozygous *gl/+* mice positive for the PU.1-*Ostm1* transgene to obtain double transgenic SYN-*Ostm1*-PU.1-*Ostm1-gl/gl* mice (Figure 2-2A). Specifically, the low SYN-*Ostm1* expresser 214 line was crossed with the low expressing PU.1-*Ostm1* 737 line and the high SYN-*Ostm1* expressing line 215 was crossed with the higher PU.1-*Ostm1* expressing line 761. These mice have complete rescue of the bone and hematopoietic phenotypes as well as targeted expression of *Ostm1* in neurons. The *gl* mutation still resides in the rest of the tissues as evidenced by the grey coat color of the animals. Both the 214-737-*gl/gl* and 215-761-*gl/gl* mice were then analyzed and compared to wild type controls.

Recall that single transgenic PU.1-*Ostm1-gl/gl* mice die regularly on average at 6-7 weeks (Figure 3-1). Until now, all double transgenic SYN-*Ostm1*-PU.1-*Ostm1-gl/gl* mice from both sets of crosses lived past 6-7 weeks and showed a normal life span, with the oldest living to almost two years old (data not shown). Single transgenic Syn-*Ostm1-gl/gl* littermates still die at three weeks due to the standard bone and hematopoietic defects.

3.3.2. Immunohistological analysis of SYN-*Ostm1*-PU.1-*Ostm1-gl/gl* brain

Using histological staining and immunohistochemistry on sections of brain from 6 week old SYN-*Ostm1*-PU.1-*Ostm1-gl/gl* mice, we found a complete rescue of the neurodegenerative phenotype. Histologically, staining with H&E showed normal

hippocampal structures with no loss of the CA3 region (Figure 3-9A). As well, sections stained with NeuN antibody showed no loss of cortex in either the 215-761-*gl/gl* or the 214-737-*gl/gl* lines compared to that of wild type (Figure 3-9B). Consistently, at the level of the cerebellum, there was no loss of Purkinje cells as detected by calbindin immunostaining (Figure3-9C). As well, at the level of the cortex, there was no notable astrogliosis or inflammation. This was established via GFAP staining where there was no significant increase in activated astrocyte numbers (Figure 3-8D). Furthermore, 214-737-*gl/gl* and 215-761-*gl/gl* sections analysed and immunostained for IbaI showed no reactive microglia at the level of the cortex compared to wild type sections (Figure 3-9E).

3.3.3. MRI analysis of SYN-*Ostm1*-PU.1-*Ostm1-gl/gl* mice

Complete rescue of the neurodegenerative phenotype was further confirmed using non-invasive MRI of both 214-737-*gl/gl* and 215-761-*gl/gl* mice. Using this approach, we were able to detect and follow the course of the neurodegeneration in a time scale manner. In addition, the neurodegenerative phenotype in the PU.1-*Ostm1-gl/gl* mice and rescue of the phenotype of the SYN-*Ostm1*-PU.1-*Ostm1-gl/gl* mice were also observed *in vivo*. Scans were performed at 4, 5 and 6 weeks of age further highlighting the progressive nature of the neurodegeneration. Consistent with our immunohistochemical analysis, there was a noticeable loss of brain cortex in the PU.1-*Ostm1-gl/gl* starting at 5 weeks and an even more apparent reduction at 6 weeks (Figure 3-10).

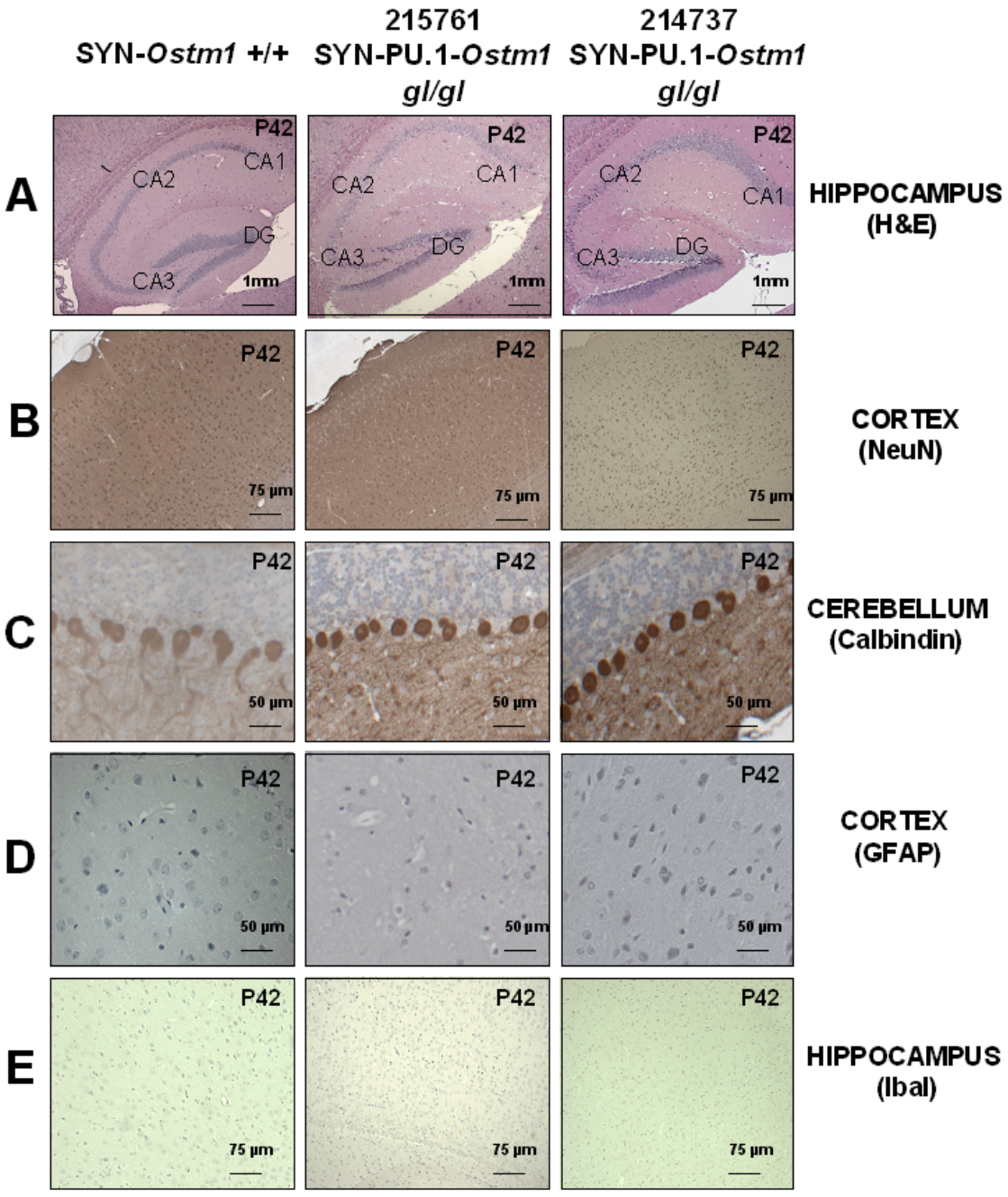

Figure 3-9: Immunohistological analysis of SYN-*Osmt1*-PU.1-*Ostm1-gl/gl* brain sections. (A) All regions of Hippocampus are identical to wild type controls following H&E staining. (B) No significant loss of cortex in both 215761-*gl/gl* and 214737-*gl/gl* following neuronal specific NeuN antibody staining. (C) Specific Calbindin staining of Purkinje cells demonstrated no cell loss at 6 weeks (D) GFAP marker staining for mature astrocytes showed no astrogliosis or inflammation in cortex of SYN-*Ostm1*-PU.1-*Ostm1-gl/gl* brain. (E) Iba1 antibody staining for microglia showed no reactive cells in either line and are indistinguishable from wild type controls.

There were also some features of the neurodegenerative phenotype that previously and histologically had gone unnoticed. In conjunction with the strong reduction of cortex layers, there was a significant thinning of the corpus callosum and prominent enlargement of the lateral and 3rd ventricles in the PU.1-*Ostm1-gl/gl* mice at 6 weeks (Figure 3-10). *In vivo* CNS analysis of both 6 week old double transgenic 215-761-*gl/gl* and 214-737-*gl/gl* lines, showed normal development of the cortex and corpus callosum and ventricle size was comparable to wild type controls (Figure 3-10).

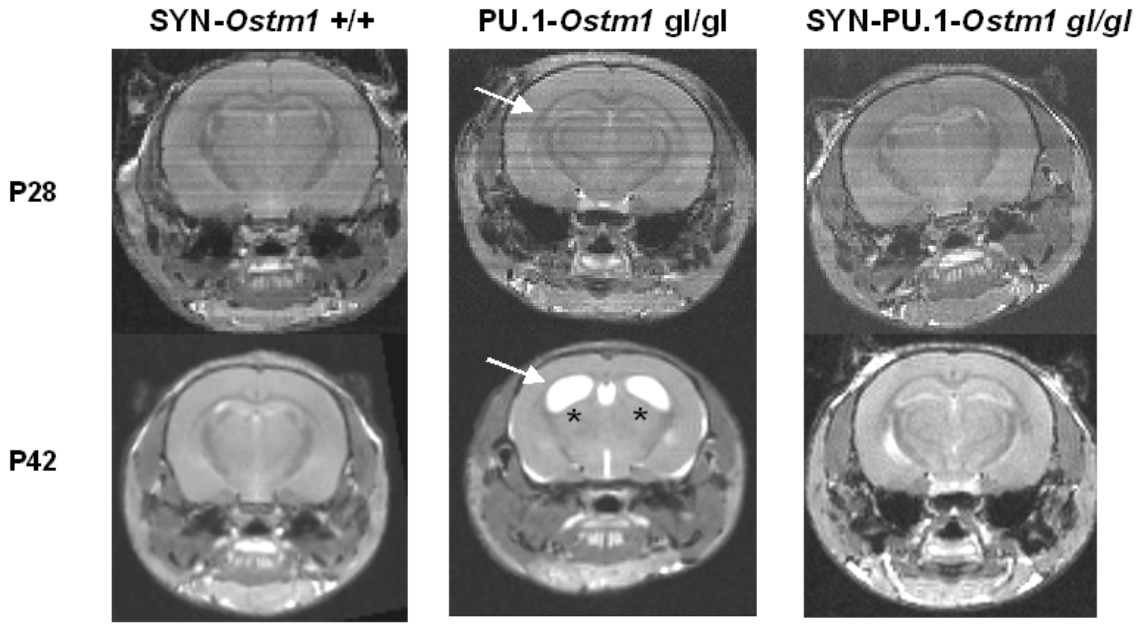

Figure 3-10: MRI analysis of single and double transgenic mice. Progressive nature of neurodegeneration clearly is present. Arrows indicate corpus callosum that is significantly thinner in PU.1-*Ostm1-gl/gl* mouse after 6 weeks compared to 4 weeks. Stars indicate sizeable increase of lateral and 3rd ventricles and loss hippocampus. Neurodegeneration in SYN-*Ostm1*-PU.1-*Ostm1-gl/gl* mice was undetectable with no change in cortex, corpus callosum or ventricle structures.

3.3.4. Histological analysis of SYN-*Ostm1*-PU.1-*Ostm1-gl/gl* retina

Next, we analyzed retinal sections of 6 week old double transgenic SYN-*Ostm1*-PU.1-*Ostm1-gl/gl* mice. H&E staining showed unaffected photoreceptors with both the inner and outer photoreceptor segments present. Additionally, no deficit in the ONL cell layer was detected (Figure 3-11). In contrast, retinal sections of older (9 week) SYN-*Ostm1*-PU.1-*Ostm1-gl/gl* mice revealed severe retinal degeneration. Absence of photoreceptors and a loss of the ONL cell layer similar to the PU.1-*Ostm1-gl/gl* phenotype were detected in 9 week old retinal sections (Figure 3-11). This result suggested that the SYN-*Ostm1* transgene while capable of preventing the neurodegenerative phenotype in the brain was only able to delay the retinal degenerative phenotype.

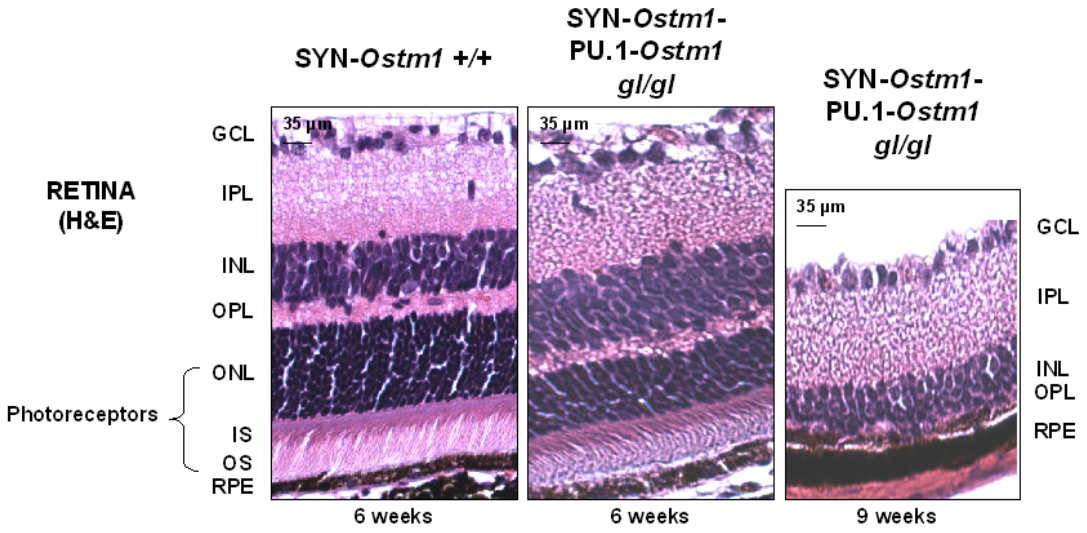

Figure 3-11: Histological analysis of retinal sections from SYN-*Ostm1*-PU.1-*Ostm1-gl/gl* mice. Retinal organization at 6 weeks in double transgenic SYN-*Ostm1*-PU.1-*Ostm1-gl/gl* mice is similar to wild type control. Retinal degeneration appears delayed and detectable at 9 weeks. (GCL) = Ganglion Cell Layer, (IPL) = Inner Parietal Layer, (INL) = Inner Nuclear Layer, (OPL) = Outer Parietal Layer, (ONL) = Outer Nuclear Layer, (IS) = Inner Segments, (OS) = Outer segments, (RPE) = Retinal Pigment Epithelium.

3.3.5. Autophagy in SYN-*Ostm1*-PU.1-*Ostm1-gl/gl* mice

Further evidence of cellular rescue of the neurodegenerative phenotype came from molecular analysis of protein expression related to autophagy in 6 week old brain extracts from SYN-*Ostm1*-PU.1-*Ostm1-gl/gl* by Western blot. We evaluated protein expression of LC3-I and LC3-II in 6 week old mice. There was no significant increase in LC3-II expression, with mostly LC3-I present in the double transgenic mice (Figure 3-12). Compared to the wild type mice, the ratio of LC3-I to LC3-II in SYN-*Ostm1*-PU.1-*Ostm1-gl/gl* mice was similar. This suggested, most likely that autophagy was not stimulated in these animals and correlated with the rescue of the neurodegenerative phenotype.

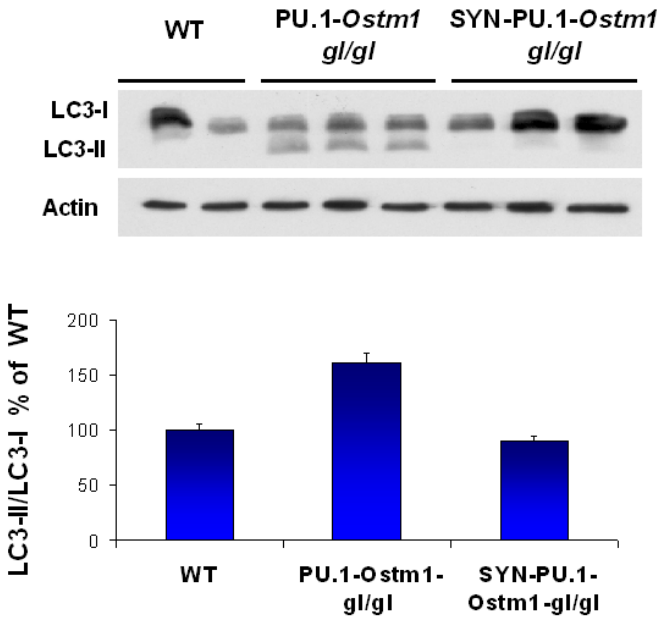

Figure 3-12: Molecular characterization of autophagy in SYN-*Ostm1*-PU.1-*Ostm1-gl/gl*. No significant increase in LC3-II to LC3-I ratio in 6 week old brain extracts from SYN-*Ostm1*-PU.1-*Ostm1-gl/gl* suggests no stimulation of autophagy (Seen in both 214-737-*gl/gl* and 215-761-*gl/gl* lines). Normalized quantification show similar value for double transgenic and wild type extracts compared to single transgenic PU.1-*Ostm1-gl/gl*.

3.4. Neurodegeneration in PU.1-*Ostm1-gl/gl* mice is cell autonomous

Study of the SYN-*Ostm1*-PU.1-*Ostm1-gl/gl* transgenic lines demonstrated an important role for *Ostm1* in neurons but we do not know if this function is cell autonomous. We do know however, that *Ostm1* is also expressed in other brain cell types such as astrocytes. Cultured astrocytes from wild type neonatal pups showed high levels of *Ostm1* expression as detected by Northern blot analysis. As control, astrocytes from *gl/gl* littermates showed a complete absence of *Ostm1* expression (Figure 3-13A). Does the lack of *Ostm1* expression in astrocytes have an effect on the astrogliosis and inflammation observed in the PU.1-*Ostm1-gl/gl* mice? In an effort to better understand the role of *Ostm1* in the brain as a whole, we developed additional transgenic lines by targeting *Ostm1* expression to astrocytes with the specific Glial Fibrillary Acidic Protein (GFAP) promoter (GFAP-*Ostm1*).

GFAP, as previously mentioned, is an intermediate filament expressed primarily by astrocytes, a cell type that has many important roles in the CNS (Su et al., 2004). Researchers have shown that restoring certain gene activity to astrocytes can in fact affect brain disease progression. Amyotrophic Lateral Sclerosis (ALS) for example, is a fatal human neurological disorder that involves the progressive loss of motor neurons. Transgenic ALS mouse models that specifically target astrocytes, either through removal of causal mutant genes such as Superoxide Dismutase (SOD1) or over express rescue genes such as transcription factor Nuclear Factor Erythroid 2-Related Factor 2 (Nrf2), while not capable of total

rescue can in fact delay the onset of the disease and extend survival (Vargas et al., 2008, Yamanaka et al., 2008). Based on these results, we decided to target specific *Ostm1* expression to astrocytes in transgenic mice and follow the evolution of neurodegeneration in double transgenic GFAP-*Ostm1*-PU.1-*Ostm1-gl/gl* mice.

3.4.1. GFAP-*Ostm1* transgenic mice

3.4.1.1. Transgenic lines

Given aforementioned possibility of neurodegenerative rescue via targeting astrocytes, the GFAP-*Ostm1* transgene was established and transgenic founders were produced (Figure 3-13B). We next analyzed the integrity of the transgene and the number of copies in each founder by Southern blot. Three lines were developed, line 244 with 2 copies, line 299 with 4 copies and line 308 with 16 copies (Figure3-13C). Line 308 did not breed satisfactorily and unfortunately line 299 did not express the transgene.

3.4.1.2. Expression

Specific expression of the GFAP-*Ostm1* transgene in the brain was then verified by RT-PCR (Figure 3-13D). The transgene was detectable only in brain extracts of transgenic mice while the endogenous *Ostm1* mRNA was observed in all tissues.

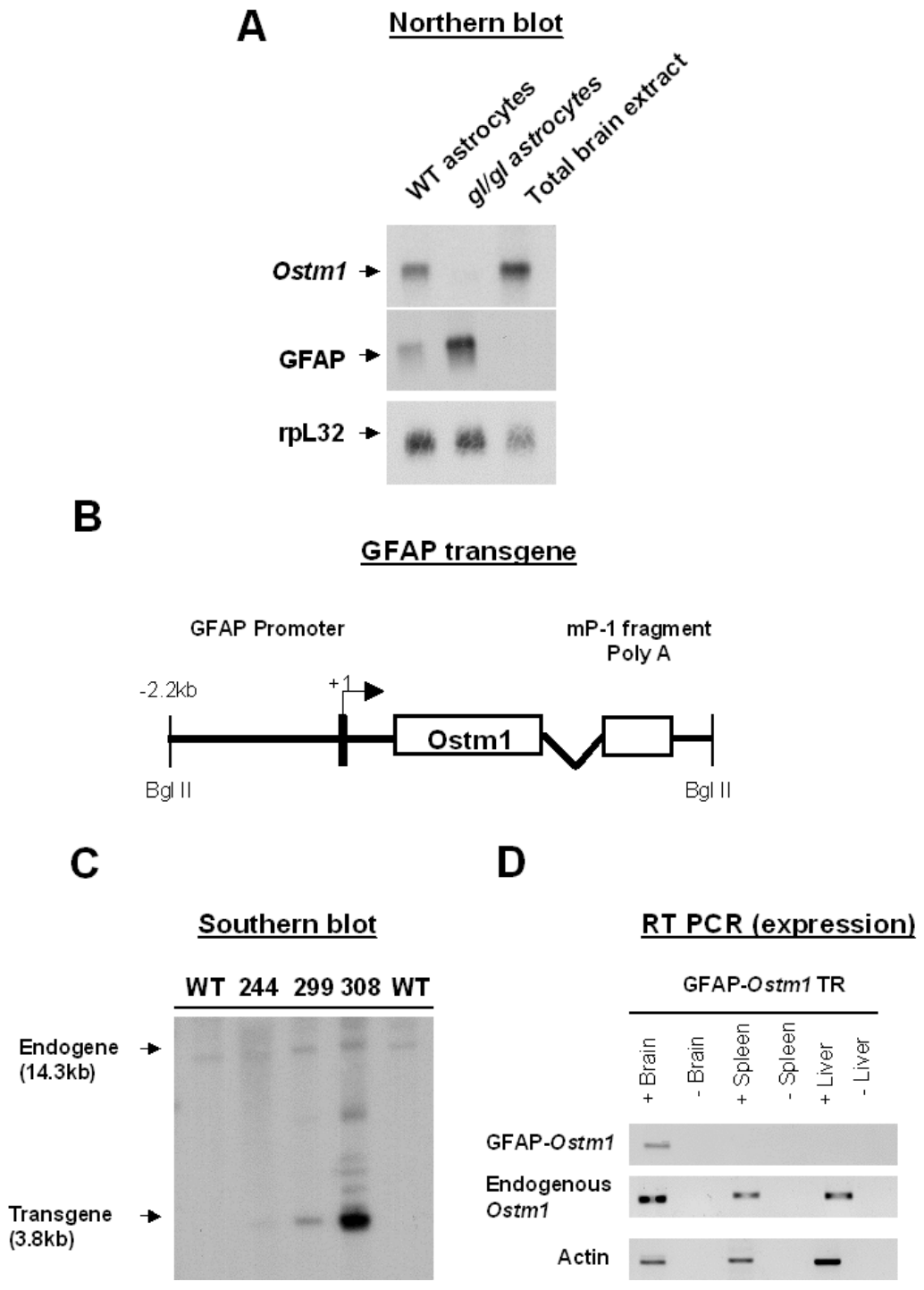

Figure 3-13: Characterization of GFAP-*Ostm1* transgenic mice. (A) Northern blot of cultured astrocytes from wild type and *gl/gl* pups showed expression of *Ostm1* in astrocytes (GFAP positive). (B) Structure of the GFAP transgene used to target *Ostm1* specifically to astrocytes. (C) Southern blot of lines 244, 299 and 308. (D) Specific transgene expression in the brain was verified by RT-PCR.

3.4.2. GFAP-*Ostm1*-PU.1-*Ostm1-gl/gl* mice

Mice positive for the GFAP-*Ostm1* transgene were then crossed with heterozygous *gl/+* mice positive for the PU.1-*Ostm1* transgene to obtain double transgenic GFAP-*Ostm1*-PU.1-*Ostm1-gl/gl* mice, as previously done with the Synapsin transgene (Figure 2-2BA). Specifically, line 244 positive for the GFAP-*Ostm1* transgene was crossed with the PU.1-*Ostm1* expressing line 761. These mice display complete rescue of the bone and hematopoietic phenotypes as well as specific transgene expression of *Ostm1* in astrocytes. The *gl* mutation still resides in the other tissues as evidenced by the grey coat color of these mice. The resultant 244-761-*gl/gl* mice were then phenotypically analyzed.

Recall that PU.1-*Ostm1-gl/gl* mice died regularly at 6-7 weeks and double transgenic SYN-*Ostm1*-PU.1-*Ostm1-gl/gl* mice showed no overt degenerative phenotype and had normal life spans. Interestingly, all double transgenic GFAP-*Ostm1*-PU.1-*Ostm1-gl/gl* exhibited a progressive deterioration of their health similar to that observed in the single transgenic PU.1-*Ostm1-gl/gl* mice. At present, all the GFAP-*Ostm1*-PU.1-*Ostm1-gl/gl* produced mice died between 7-8 weeks (data not shown), while wild type transgenic GFAP-*Ostm1* mice did not show any adverse phenotype.

3.4.2.1 Immunohistological analysis of GFAP-*Ostm1*-PU.1-*Ostm1-gl/gl* brain

Using histological staining and immunohistochemistry on 7 week old brain sections of GFAP-*Ostm1*-PU.1-*Ostm1-gl/gl* mice we detected the benchmark

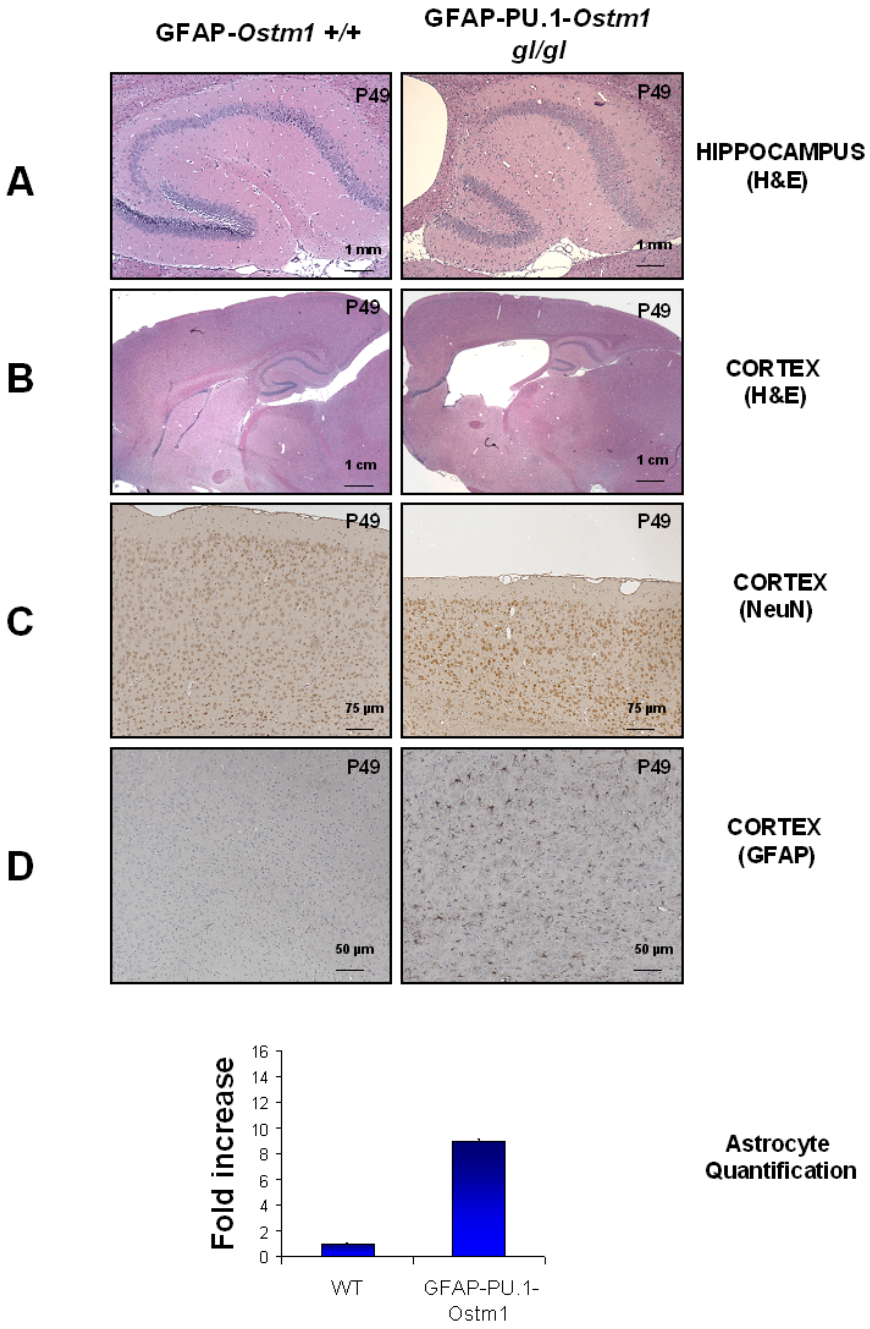

Figure 3-14: Immunohistological analysis of GFAP-*Osmt1*-PU.1-*Ostm1-gl/gl* brain sections. (A) H&E staining of Hippocampus. Notable loss of CA3 region and prominent protrusion of lateral ventricle. (B) H&E staining of cortex shows major enlargement of lateral ventricle and compression of hippocampus in GFAP-*Osmt1*-PU.1-*Ostm1-gl/gl* brain (C) Neuronal NeuN immunostaining shows significant reduction of cortex cell layers in GFAP-*Ostm1*-PU.1-*Ostm1-gl/gl* mice. (D) GFAP marker for mature astrocytes detects notable astrogliosis and inflammation in cortex of GFAP-*Ostm1*-PU.1-*Ostm1-gl/gl* brain. (Quantification of astrogliosis at bottom)

neurodegeneration. Histologically, staining with H&E showed nearly total loss of the CA3 region of the hippocampus (Figure 3-14A). Interestingly, a major morphological change in the CNS was detected by histology (Figure 3-14B). First, similar to the swelling observed with MRI analysis of PU.1-*Ostm1-gl/gl,* the lateral ventricles in the GFAP-*Osmt1-gl/gl* brain sections were abnormally large with complete lack of the hippocampal CA3 region (Figure 3-14A-B). Second, immunostaining with NeuN antibodies showed marked loss of cortical neurons of all layers in the cortex compared to that of wild type (Figure 3-14C). At the level of the cortex, there was also marked astrogliosis and presence of inflammation in GFAP-*Ostm1*-PU.1-*Ostm1-gl/gl* sections stained with GFAP antibody (Figure 3-14D). An ≅ 9 fold increase in GFAP-positive cell number was quantified in the transgenic GFAP-*Ostm1-gl/gl* cortex compared to that of wild type.

3.4.2.2. Histological analysis of GFAP-*Ostm1*-PU.1-*Ostm1-gl/gl* retina

Hematoxylin and eosin staining of retinal sections of 7 week old mice exposed the initiation of major retinal degeneration in GFAP-*Ostm1*-PU.1-*Ostm1-gl/gl* mice. There was close to a complete loss of the outer segments of the photoreceptors as well as a thinning of the Outer Nuclear Layer (ONL) (Figure 3-15), a slightly delayed but similar phenotype to the one detected in PU.1-*Ostm1-gl/gl* transgenic mice (Figure 3-4).

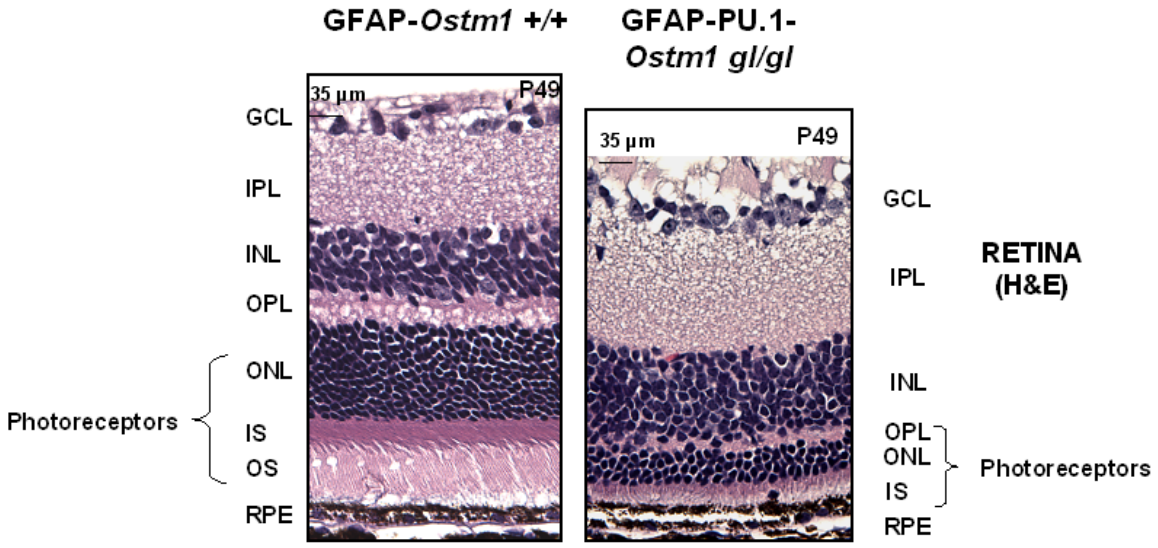

Figure 3-15: Histological analysis of retinal sections from 7 week old mice. Note the progression of photoreceptor loss with no outer segments detected in GFAP-*Ostm1*-PU.1-*Ostm1-gl/gl* retinal sections. Thinning of the Outer Nuclear layer also observed. (GCL) = Ganglion Cell Layer, (IPL) = Inner Parietal Layer, (INL) = Inner Nuclear Layer, (OPL) = Outer Parietal Layer, (ONL) = Outer Nuclear Layer, (IS) = Inner Segments, (OS) = Outer segments, (RPE) = Retinal Pigment Epithelium.

3.4.2.3. Autophagy in GFAP-*Ostm1*-PU.1-*Ostm1-gl/gl* mice

With the manifestation of the severe neurodegenerative phenotype in the GFAP-*Ostm1*-PU.1-*Ostm1-gl/gl* mice, we next studied the protein expression levels of LC3-II in brain extracts of these mice for the possible involvement of autophagy. Using Western blot, an increase in LC3-I and LC3-II expression was observed. Quantification of these proteins showed a ratio of LC3-I to LC3-II increase of ≅ 78% in GFAP-*Ostm1*-PU.1-*Ostm1-gl/gl* mice, akin more to PU.1-*Ostm1-gl/gl* levels than that of wild type. This suggested a significant stimulation of autophagy in the CNS of these mice and similar to the one detected in single transgenic PU.1-*Ostm1-gl/gl* mice. (Figure 3-16).

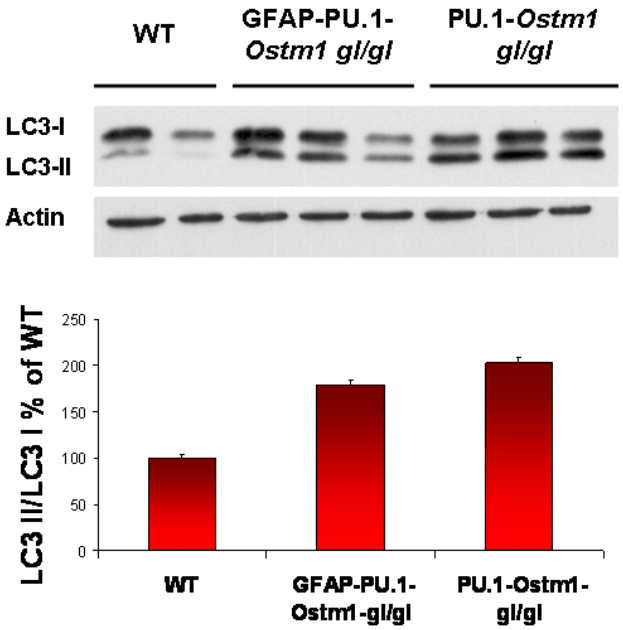

Figure 3-16: Molecular characterization of autophagy in GFAP-*Ostm1*-PU.1-*Ostm1-gl/gl*. Marked increase in LC3-II protein expression in GFAP-*Ostm1*-PU.1-*Ostm1-gl/gl* brain extract compared to wild type demonstrated stimulation of autophagy. Normalized quantification below.

Chapter 4
Discussion

Bone homeostasis is an intricate and dynamic process that is carried out by two main cell types. On the one hand there are the osteoblasts responsible for the formation of bone and on the other hand there are the osteoclasts whose main function is the resorption of bone. This delicate balance is maintained throughout life from early development to maintenance of the skeleton.

When bone remodeling is disrupted, several complications can arise, specifically, a problem involving the osteoclast can result in osteopetrosis. Either through complications that impair osteoclast differentiation resulting in a lack of bone resorbing cells or a malfunction that directly affects the ability of the osteoclast to resorb bone, “marble bone disease” can occur.

Of particular interest to our lab, a mutation of the *OSTM1* gene results in the most severe form of osteopetrosis. These patients have an increased non-functional osteoclast population that results in an increased BMD and a malformed bone marrow compartment. They also suffer a host of other difficulties including hematopoietic defects and 75% of patients die by the age of four years. To date, the only current treatment available for these patients is a bone marrow transplant.

From the study of various mouse models and human patients, it has been shown that genes responsible for ARO can have primary effects in other tissues, separate from disruptions in bone remodeling.

The objective of this study was to elucidate the role of *Ostm1* in the CNS. The grey-lethal mouse mutant, that most closely mirrors the *OSTM1* human patients, is consistently lethal at three weeks; therefore, a transgenic line targeting *Ostm1* to the multipotent myeloid progenitors via a PU.1 promoter was used. In addition, we developed additional transgenic mice, targeting *Ostm1* expression to specific cell types in the CNS, to better understand the function of *Ostm1*.

Loss of *Ostm1* leads to neurodegeneration

PU.1-*Osmt1-gl/gl* mice have complete rescue of the bone and hematopoietic phenotype and live past three weeks; however, they still die at 6-7 weeks. Knowing that *Ostm1* is highly expressed in the brain and given the cases of primary neuropathologies in human *OSTM1* patients, we suspected the mice were suffering from neurodegeneration that was leading to their decrease in survival (Chalhoub et al., 2003, Maranda et al., 2008).

Using histological and immunohistochemistry, we did in fact see a severe neurodegenerative phenotype in the CNS of PU.1-*Ostm1-gl/gl* mice, highlighted by substantial losses of cortical layers, a complete loss of the CA3 region of the hippocampus and notable inflammation and astrogliosis.

Evidence that the neurodegenerative phenotype was progressive in nature came from the examination of *gl/gl* non transgenic brain sections. These mice showed no morphological changes to either the hippocampus or the cortex; however,

there was a detectable presence of astrogliosis at the level of the cortex. While no overt loss of neurons could be observed at three weeks via histological and immunohistochemical techniques, mature astrocytes were activated in the *gl/gl* cortex, presumably to help deal with damage to the CNS, that was, as of yet, undetectable.

The progressive neurodegenerative phenotype of the PU.1-*Ostm1-gl/gl* presented several similarities to another ARO mouse model. The TRAP-*Clcn7*-*Clcn7*$^{-/-}$ mouse is a transgenic line targeting *Clcn7* to terminally differentiated osteoclasts using a TRAP promoter. These mice were crossed with the *Clcn7*$^{-/-}$ to obtain a rescue of the bone phenotype and presented a severe neurodegenerative phenotype. The mice showed losses of CNS regions, similar to that of the PU.1-*Ostm1-gl/gl* mice, with a loss of the CA3 region as well as marked astrogliosis (Kasper et al., 2005). It has been suggested that the primary role of *Ostm1* is to serve as a β-subunit for the CLC-7 chloride channel that protects and ensures its proper localization (Lange et al., 2006). The neurodegenerative phenotype observed in the PU.1-*Ostm1-gl/gl* mouse could then simply be explained as a malfunction of CLC-7 that resulted from the absence of *Ostm1*. This hypothesis seems unlikely because TRAP-*Clcn7*-*Clcn7*$^{-/-}$ die regularly at 8-9 weeks, while PU.1-*Ostm1-gl/gl* mice die 3 weeks earlier, suggesting *Ostm1* has a more essential role in the CNS.

Interestingly, the severe neurodegenerative phenotype of PU.1-*Ostm1-gl/gl* mice shares some characteristics of another well characterized neurological disorder found in humans. Alzheimer's is an aging neurodegenerative disease that results in widespread neuronal loss and decreased synaptic density. There are two notable pathologic signs of Alzheimer's disease: one involves neurofibrillarly tangles inside the neurons made up primarily of a microtubule stabilizer Tau; the other involves senile plaques that are deposited in the extracellular matrix, made up principally of fibrillar aggregates of amyloid-β peptide (Aβ) (Duyckaerts et al, 2009, Yilmazer-Hanke 1998). Like osteopetrosis there are several mouse models that aid in the study of this debilitating disease. Mice with mutations in the amyloid precursor protein (*App*) and presenilin-1 (*ps-1*) genes develop Aβ peptide fragments as a result of faulty App processing that form detectable plaques at an early age. (Duff et al., 1996, Hsiao et al., 1996). While both the PU.1-*Ostm1-gl/gl* CNS phenotype and Alzheimers are progressive in nature, the mutation of *Ostm1* causes a more rapid effect that takes considerably less time to develop. The *App/Ps-1* mouse model does have some aspects in common with the PU.1-*Ostm1-gl/gl mice* such as considerable activation of astrocytes at the level of the cortex in regions where plaques are detected at an early age before significant neuronal cell loss. As well, comparable regions of the hippocampus become affected in the Alzheimer's mouse model with losses of the CA3 region and layers of the cortex (Matsuoka et al., 2001, Yu et al, 2005). Currently, the specific loss of the CA3 region in the hippocampus over other areas such as the CA1, CA2 and the dentate gyrus regions in both Alzheimer

mouse models and transgenic *gl/gl* mice cannot be explained. Perhaps these neurons are more susceptible or less robust than other neuronal cell types in the CNS or perhaps these cells rely more heavily on autophagy.

Autophagy in the CNS of PU.1-*Ostm1-gl/gl* mice was first brought to our attention after ultrastructural analysis was carried out on hippocampal neurons. An accumulation of vesicles was noted in the neuronal cytoplasm of PU.1-*Ostm1-gl/gl* sections. Closer investigation of the vesicles showed they appeared to be double membrane bound autophagosomes and may have been the cause of the significant axonal swelling that was also observed. Examination at the molecular level confirmed the presence of autophagosomes in the CNS of PU.1-*Ostm1-gl/gl* mice and implicated autophagy in the neurodegenerative phenotype.

These findings again parallel those of the Alzheimer's mouse mutant. *App/ps-1* mice, like PU.1-*Ostm1-gl/gl* mice, accumulate autophagosomes in their cortical neurons and exhibit considerable axonal swelling (Boland et al., 2008, Nixon 2007).

It has been shown that autophagy is used by all tissues at varying degrees for the recycling of large macromolecules. Studies have shown that basal autophagy in the CNS and more specifically in neurons is quite high. Autophagosomes are generally not detected in neurons and their projections because turnover of the autophagosome via fusion and degradation by the lysosome is so rapid

(Mizushima et al., 2006, Settembre et al. 2008, Yue et al., 2008) This would suggest that the increase in autophagosomes observed in the CNS of PU.1-*Ostm1-gl/gl* mice is due either to an over stimulation of this physiological response or to an impaired clearance of the double membrane bound autophagosomes.

Two main pathways, the Beclin-1 pathway and the mTOR pathway, regulate autophagy. Alterations or perturbations of these proteins and their effectors can have dramatic effects on the cells ability to clear unwanted proteins and organelles. It has been shown that even a heterozygous deletion of *Beclin-1* in *App/ps-1* mice can dramatically increase Aβ accumulation, deposition and neurodegeneration (Pickford et al., 2008).

With this in mind, we next inspected the regulation of autophagy. mTOR normally inhibits autophagy when phosphorylated and a decrease in the phosphorylated protein results in an increase of autophagy. Analysis of brain extracts of PU.1-*Ostm1-gl/gl* mice suggested a major augmentation of autophagy via notable decreases in phosphorylated mTOR and its downstream effectors. The other main pathway of Beclin-1 did not appear to be involved with no difference detected in Beclin-1 expression.

It does not appear that the accumulation of autophagosomes in PU.1-*Ostm1-gl/gl* mice is the result of over stimulation of autophagy. As the name states, mTOR

can be inhibited and by extension autophagy can be stimulated via the administration of Rapamycin. PU.1-*Osmt1-gl/gl* mice were subjected to Rapamycin treatment and no change in LC3-II expression and autophagosome accumulation was observed (data not shown). This suggested that the stimulation of autophagy in PU.1-*Ostm1-gl/gl* mice is already at a maximum.

Therefore, the problem may lie in the ability of the cell to remove the autophagosomes. Normally an autophagosome, forming from a nascent phagophore and originating from the endoplasmic reticulum, is then transported via microtubules, fusing with endosomes along the way, until it reaches the lysosome, where it fuses and is finally degraded (Shakcka et al., 2008, Simonsen et al., 2008). An alteration at any of these steps could result in an accumulation of autophagosomes. It has previously been shown that lysosomes of *gl/gl* mice have a normal pH and therefore likely function properly (Lange et al., 2006). While the exact function of *Osmt1* is still currently under investigation by our lab, preliminary results suggest it may have an important role in microtubule transport. As mentioned, autophagosomes formed in the distal region of a neuron must travel by retrograde transport up the axon toward the neuronal cell body where the majority of the lysosomes are concentrated (Nixon 2007). If *Ostm1* is involved in transport, then its absence could severely impede the movement and eventual degradation of the autophagosomes.

Taken all together, these results, along with the progressive nature of the neurodegeneration, suggest that perhaps basal autophagy is being disrupted. If the trafficking of autophagosomes is impaired due to an absence of Ostm1, then normal autophagy used by the cell for remodeling and cell survival would be affected and start an accumulation of aggregates and autophagosomes. This would in turn result in a stimulation of autophagy via the mTOR pathway in an effort to remove the vesicles, thereby exacerbating the situation. Neurons would continue to accumulate autophagosomes which in turn would result in axonal swelling and cell death.

Separate from the CNS phenotype, PU.1-*Ostm1-gl/gl* mice also suffered a distinct retinal atrophy. Retinal sections from 5 week old mice showed a complete loss of the photoreceptor layer as well as the ONL. This retinal degeneration is definitely due to a primary defect as a result of *Ostm1* mutation and not a secondary effect caused by optic nerve compression for two reasons. First, there is no occlusion of foramina of the skull in *gl/gl* or PU.1-*Ostm1-gl/gl*. Second, when optic nerve damage occurs as a result of compression for example, the first cells to be affected are the ganglion cells and not the photoreceptors as observed in the PU.1-*Ostm1-gl/gl* mice (Berkelaar et al., 1994).

Rescue of the *Ostm1* neurodegenerative phenotype

In order to better understand the role of *Ostm1* in the CNS, we next developed a transgenic line targeting *Ostm1* to neuronal cells using a specific synapsin promoter. Synapsins are abundant synaptic vesicle proteins found in the pre-synaptic nerve terminal (Bennett et al., 1991, Fdez et al., 2006, Hosaka et al., 1999, Street et al., 2005). Once the transgene and the resulting founders were established and specific expression was verified, we then crossed two lines (214 and 215) with differing copy number and expression to transgenic PU.1-*Ostm1-gl/*+ mice to obtain double transgenic SYN-*Ostm1*-PU.1-*Ostm1-gl/gl* mice. These mice, with complete rescue of the bone and hematopoietic phenotype and *Ostm1* targeted to the neurons, were then analyzed.

We observed a complete rescue of the neurodegenerative phenotype in SYN-*Ostm1*-PU.1-*Ostm1-gl/gl* mice with no loss of hippocampus or cortical layers and no detectable inflammation. There also appeared to be no simulation of autophagy and double transgenic SYN-*Ostm1*-PU.1-*Ostm1-gl/gl* mice consistently live past 7 weeks and demonstrated normal life spans. Taken together this suggested that *Ostm1* has a cellular autonomous role in neuronal cells.

Interestingly, both SYN-*Ostm1* transgenic lines 214 and 215 showed complete phenotypic rescue with no major CNS morphological changes, no stimulation of autophagy and normal life spans. The significant differences in transgene

expression levels did not appear to affect neuronal function. It appears *Ostm1* does not have a dose dependence effect. Both lines expressed *Ostm1* at higher levels then the endogenous, with line 215 expressing *Ostm1* at much higher levels. This lack of dose dependence is supported by the studies of the PU.1-*Ostm1* transgenic lines, where the transgene was expressed at levels well below the endogenous, yet there was still complete bone and hematopoietic rescue (Pata et al. 2008).

Additional evidence of complete rescue of the neurodegenerative phenotype came from *in vivo* analysis of the CNS using MRI. Using this non invasive technique, we observed normal CNS structures with no significant differences between SYN-*Ostm1*-PU.1-*Ostm1-gl/gl* and wild type mice. It also highlighted the progressive nature of the neurodegenerative phenotype as scans were performed at 4, 5 and 6 weeks and showed the extensive deterioration of the CNS in PU.1-*Ostm1-gl/gl* mice. After 6 weeks, the hallmark loss of the cortex was observed as well as notable loss of the hippocampus.

Surprisingly, additional features of the PU.1-*Ostm1-gl/gl* brain phenotype that had previously gone undetected were revealed. There was substantial thinning of the corpus callosum after 6 weeks that suggested a possible problem involving hypomyelination and a severe enlargement of the ventricles. The change in ventricle size displayed significant heterogeneity, with some mice displaying severe enlargement of the lateral and 3rd ventricles, while others showed no

major change in ventricle size but significant Cerebrospinal Fluid (CSF) in the subarachnoid space. Normal flow of the CSF moves through foramina from the lateral ventricles to the 3rd and 4th ventricles and finally into the subarachnoid space (Johnston M, 2003). The significant change in ventricle size could be due to the loss of cortex, whereby the standard pressure of the CSF expands the ventricles, taking the space left vacant by the neuronal loss. The specific ventricles that become enlarged could also be affected by the variance in foramina size. Another possibility could involve hydrocephalus in osteopetrosis. Previous studies have documented swelling of the brain and hindbrain compression that was associated with ARO in human patients (Al-Tamimi et al., 2008). Ependymal cells found in the choroid plexus and lining the ventricles normally produce CSF. These cells, in conjunction with the cilia also found on the surface of the ventricles, are responsible for the production and distribution of cerebrospinal fluid (Rekate 2009). Changes affecting these cells can have dramatic results that can lead to swelling of the brain and hydrocephalus. Mutations in the cilia, for example, have previously been shown to result in considerable hydrocephalus of the brain in a mouse mutant model (Banizs et al., 2005). As *Ostm1* may play a role in microtubule transport, there may be a cilia defect that has thus far gone undetected and could account for swelling observed in mice and in humans.

Interestingly, studies in human patients have revealed cases where hydrocephalic conditions have been accompanied by subependymal

heterotopias (Palm et al., 1986). Heterotopias are of particular interest, as a human *OSTM1* patient demonstrated significant subependymal heterotopia with a nodular mass of grey matter that failed to migrate properly and was found protruding into the ventricle (Figure 1-6B) (Maranda et al., 2008). MRI analysis theoretically allows for the investigation of heterotopias in osteopetrotic grey-lethal mice. Duration of our previous scans was insufficient for the level of sensitivity necessary to detect any protrusions into the ventricles. To date, no record of heterotopias have been reported in other mouse models of osteopetrosis. Longer scan times of PU.1-*Ostm1-gl/gl* mice could produce images of high enough resolution to identify heterotopias and develop a better understanding of the role of *Ostm1* in osteopetrosis and the CNS.

We next analyzed retinal sections of double transgenic SYN-*Ostm1*-PU.1-*Ostm1-gl/gl* mice. At 6 weeks there was neither loss of photoreceptors nor any deficit of the ONL cell layer. In contrast, retinal sections of older (9 week) SYN-*Ostm1*-PU.1-*Ostm1-gl/gl* mice revealed severe retinal degeneration with complete absence of photoreceptors ONL similar to the PU.1-*Ostm1-gl/gl*.

Work by our lab using *in situ* hybridization has shown that *Ostm1* is highly expressed in the higher layers of the retina such as the ganglion cell layer (GCL) and the lowest layer in the retinal pigment epithelium (RPE). Conversely, there is very little *Ostm1* expression in the photoreceptors themselves. Studies have shown that synapsin is expressed in the GCL as well as the Inner Nuclear Layer

(INL) and the Inner Plexiform Layer (IPL) but is not expressed in the photoreceptors (Haas et al., 1990). This would suggest that the delay of the retinal degenerative phenotype in SYN-*Ostm1*-PU.1-*Ostm1-gl/gl* mice is the result of *Ostm1* complementation in the higher layers of the retina. It also suggests that the loss of photoreceptors in PU.1-*Ostm1-gl/gl* mice is not cell autonomous for the photoreceptors but rather is a non cell autonomous secondary consequence of absence of *Ostm1* elsewhere in the retina. The fact that there is still severe degeneration in the retina of the double transgenic mice points to a second role of *Ostm1* in the retina separate from functions in the GLC, INL and IPL. The RPE is a critical layer of the retina whose main function is the removal of disks from the outer segments of the photoreceptors. Mutations affecting RPE function habitually lead to photoreceptor cell death and retinal degeneration (Krock et al., 2007, Tolmachova et al., 2006). As mentioned, *Ostm1* is highly expressed in the RPE; therefore, its absence in mice may severely impair removal of outer segment disks and lead to the notable progressive photoreceptor cells loss.

If there are two important roles of *Ostm1* in the retina, then there is no expression of *Ostm1* in the higher layers such as the GCL and no expression in the RPE in PU.1-*Ostm1-gl/gl* mice, resulting in a severe more immediate phenotype with a complete loss of photoreceptors at 5 weeks. In the double transgenic SYN-*Ostm1*-PU.1-*Ostm1-gl/gl* retina there is complementation at the level of the GCL but still an absence of *Ostm1* at the level of the RPE that results in a delayed

retinal degeneration seen at 9 weeks. These results revealed that while the SYN-*Ostm1* transgene is capable of preventing the neurodegenerative phenotype, there are additional important roles of *Ostm1* separate in the peripheral nervous system.

Ostm1 **neurodegeneration is cell autonomous**

In an effort to better understand if the role of *Osmt1* in the CNS is cell autonomous, we next developed a transgenic line targeting *Ostm1* to another important brain cell type, the astrocyte. Astrocytes were targeted for two primary reasons. First, astrocytes are non neuronal brain cells that have many important roles in the CNS and showed expression of *Ostm1*. A lack of *Ostm1* in astrocytes could therefore have affected the level of astrogliosis and inflammation observed in the PU.1-*Ostm1-gl/gl* mice. Secondly, astrocytes were selected over another important brain cell type such as microglia because of their origin. Microglia differentiate from hematopoietic stem cells and become the resident macrophages in the brain (Ritter et al., 2006). The PU.1-*Ostm1* transgene therefore is expressed in microglia and their function should not be affected by an absence of *Ostm1* in PU.1-*Ostm1-gl/gl* mice.

Astrocytes were also targeted because previous studies have shown that astrocytes in certain degenerative disease models can in fact delay onset and progression of neuronal cells loss (Vargas et al., 2008, Yamanaka et al., 2008).

With this in mind, *Ostm1* was targeted to astrocytes using a GFAP promoter. GFAP is an intermediate filament found primarily in these cells (Brenner et al., 1996, Su et al., 2004). Once the transgene and the resulting founders were established with no adverse phenotype and specific expression was verified, we then crossed line 244 with transgenic PU.1-*Ostm1-gl/+* mice to obtain double transgenic GFAP-*Ostm1*-PU.1-*Ostm1-gl/gl* mice. These mice with complete rescue of the bone and hematopoietic phenotype and *Ostm1* targeted to the astrocytes were then analyzed.

Examination of GFAP-*Ostm1*-PU.1-*Ostm1-gl/gl* mice compared to single transgenic PU.1-*Ostm1-gl/gl* mice showed no delay in neurodegeneration of the CNS. There was considerable damage to the CA3 region of the hippocampus and loss of cortex after 7 weeks. There was also notable enlargement of the 3rd ventricles observed in H&E stained sections of the cortex that were found protruding against the hippocampus itself. This morphological change only previously observed in MRI analysis probably went undetected by histological examination due to processing of the sections. There was also marked astrogliosis that appeared similar to that of single transgenic PU.1-*Ostm1-gl/gl* brain sections.

Investigation at the molecular level also demonstrated a significant stimulation of autophagy in the CNS of these mice similar to the one detected in single transgenic PU.1-*Ostm1-gl/gl* mice. This further demonstrated a similar onset and

progression of the neurodegenerative phenotype and furthermore suggests that the role of *Ostm1* in the CNS is most likely cell autonomous.

In retinal sections of 7 week old GFAP-*Ostm1*-PU.1-*Ostm1-gl/gl* mice, H&E staining revealed the start of significant retinal degeneration with nearly a complete loss of the outer segments of the photoreceptors and a thinning of the ONL. Compared to retinal sections of PU.1-*Ostm1-gl/gl* mice that show complete photoreceptor loss after 5 weeks, there did appear to be a delay in the retinal degenerative phenotype in GFAP-*Ostm1*-PU.1-*Ostm1-gl/gl* mice. This may be explained by expression of GFAP in the retina. GFAP itself is not expressed in any layer of the retina; however, it is expressed in Müller cells. Müller cells are a type of glial cell found in the retina. Specifically, they are form radial glial cells derived from neuroepithelial cells. Normally they do not express GFAP; however, in situations of stress or damage and degeneration they do accumulate the GFAP intermediate filament protein (Eisenfeld et al., 1984, Noctor et al., 2001). Interestingly, recent studies have shown that following injury to retinal layers, Müller cells can proliferate and dedifferentiate to become retinal progenitors that can replace photoreceptors and even earlier neuronal lineages such as retinal neurons (Bernardos et al., 2007). The GFAP-*Ostm1* transgene could therefore be expressed in the Müller cells in the retina once loss of photoreceptors is initiated. New photoreceptors may even be generated from transgenic Müller cells thereby delaying the standard retinal degenerative phenotype.

Conclusions and perspectives

Osteopetrosis is a heterogeneous family of genetic bone diseases that results from a malfunction in the bone resorbing osteoclast. Both the *gl/gl* and transgenic *gl/gl* mouse models provide excellent opportunities to study the most severe form of malignant infantile osteopetrosis caused by a mutation of the *Ostm1* gene.

Specific expression of *Ostm1* in multipotent myeloid progenitors rescues the bone and hematopoietic phenotypes in homozygous PU.1-*Ostm1 gl/gl* BAC transgenic mice. This rescue however, is not sufficient for a normal lifespan which presented a novel function of *Ostm1* in neuronal cell development.

PU.1-*Ostm1-gl/gl* mice exhibit severe progressive neurodegeneration in conjunction with an accumulation of autophagosomes and a stimulation of autophagy via inhibition of the mTOR pathway. These mice also display severe retinal degeneration with a loss of photoreceptors and the ONL after only 5 weeks.

The importance of *Ostm1* in the CNS and the retina as seen in PU.1-*Ostm1-gl/gl* mice corroborates with the primary neuropathology previously documented in an *OSTM1* patient.

Targeting *Ostm1* to neuronal cells and astrocytes, using specific Synapsin and GFAP promoters respectively, helped further elucidate the role of *Ostm1* in the

CNS. Complete phenotypic rescue in double transgenic SYN-PU.1-*Ostm1-gl/gl* mice in conjunction with the unchanged neurodegenerative phenotype in double transgenic GFAP-PU.1-*Ostm1-gl/gl* mice suggests a cellular autonomous gene activity of Ostm1 in neuronal cells.

Future experiments should characterize the PU.1-*Ostm1-gl/gl* neurodegenerative phenotype in even greater detail. Longer MRI scans could produce images at higher resolution that would allow for the possible detection of heterotopias previously undetected in any osteopetrotic mouse model.

As well, the notable thinning of the corpus callosum observed in MRI scans of PU.1-*Ostm1-gl/gl* mice suggest a possible hypomyelination that could be further investigated using histological and immunohistochemical techniques.

The role of Cilia and CSF in the osteopetrotic mouse could also be studied. Examination of cilia size and shape in the ventricles of PU.1-Ostm1-gl/gl mice could reveal yet another important role of Ostm1 in the CNS.

It would also be interesting to examine the cause of autophagy in PU.1-*Ostm1-gl/gl* mice. Is the observed stimulation of autophagy and accumulation of autophagosomes a result of blocked autophagosome clearance or are there other complications in the cell affecting autophagy? In other neurodegenerative diseases, such as Huntington's, there is a block of the ubiquitin-proteasome

protein degradation system by the malformed Huntington protein. Without the standard system, the cell then uses autophagy to recycle and remove all unwanted macromolecules which in turn leads to a stimulation in autophagy and an accumulation of autophagosomes. (Rubinsztein 2006, Wang et al., 2008) Experiments could be carried out on PU.1-*Ostm1-gl/gl* neuronal cells to determine if the proteasome is in fact functional and if this is the primary cause of autophagy stimulation.

Furthermore, experiments should be carried out to continue studying of the role of *Ostm1* in the retina. Our lab has previously developed a transgenic line targeting *Ostm1* to melanocytes using a tyrosinase promoter (Tyr-*Ostm1*). Transgenic mice crossed with heterozygous *gl*/+ mice to obtain transgenic Tyr-*Ostm1-gl/gl* mice showed rescue of the grey coat color defect but still die at 3 weeks due to the standard osteopetrotic defects. The Tyr-*Ostm1* transgene is expressed at the level of the RPE and could help determine the exact role and required location of *Ostm1* for proper retinal development. Development and analysis of triple transgenic Tyr-*Ostm1*-SYN-*Ostm1*-PU.1-*Ostm1-gl/gl* mice could provide complete complementation at the level of the retina. If after 9 weeks all layers of the retina were intact this would suggest there are in fact two roles for Ostm1, one in the higher layers and one in the RPE.

Sadly our results also indicate that treatment for this debilitating disease is even more difficult. Standard treatments of *OSTM1* osteopetrotic patients involve bone

marrow transplants. While this course of action can alleviate the bone pathology, the patient will still suffer from the absence of *OSTM1* in the brain. One possible solution could involve the use of stem cells. It has recently been shown that the transplantation of modified human CNS stem cells into brains of a mutant mouse model for NCL can improve the outcome of the disease. The modified stem cells that were grown as neurospheres were able to engraft, migrate and even impart neuroprotection of the host's CNS (Tamaki et al., 2009). This course of treatment in conjunction with bone marrow transplants could represent novel therapeutic avenues for *OSTM1* human patients.

Bibliography

Allen N. J, Barres B. A (2009). Glia-more then just brain glue. Nature 475, 675-677

Alroy J, Pfanni R, Ucci A, Lefranc G, Frattini A, Megarbane A (2007). Electron Microscope Findings in Skin Biopsies from Patients with Infantile Osteopetrosis and Neuronal Storage Disease. Ultrastructural Pathology *31*, 333-338

Al-Tamimi Y. Z, Chumas P. D (2008). Patients with autosomal-recessive osteopetrosis presenting with hydrocephalus and hindbrain posterior fossa crowding. J. Neurosurg. Pediatrics *1*,103–106,

Axe E. L, Walker S. A, Manifava M, Chandra P, Rioderick H. L, Habermann A, Griffiths G, Ktistakis N. T (2008). Autophagosome formation from membrane compartments enriched in phosphatidylinositol 3-pjhosphate and dynamically connected to the endoplasmic reticulum. J. Cell Biol. *182*, 685-701

Balemans W, van Wesenbeeck L, Van Hul W (2005). A Clinical and Molecular Overview of the Human Osteopetroses. Calcif. Tissue Int. *77*, 263-274

Bangerter N, Hargreaves B, Vasanawala S, Pauly J, Gold G, Nishimura D (2004). Analysis of Multiple Acquisition SSFP. Magn. Reson. Med. *51,* 1038-1047

Banizs B, Pike M. M, Millican C. L, Ferguson W. B, Komlosi P, Sheetz J, Bell P. D, Schwiebert E. M, Yoder B. K (2005). Dysfunctional cilia lead to altered ependyma and choroid plexus function, and result in the formation of hydrocephalus. Development *132*, 5329-5339

Baron R (1989). Molecular mechanisms of bone resorption by the osteoclast. Anat. Rec. *224*, 317-324

Bennett A. F, Hayes N. V. L, Baines A. J (1991). Site specificity in the interactions of synapsin I with tubulin. Biochem. J*. 276*, 793-799

Berkelaar M, Clarke D. B, Wang Y. C, Bray G. M, Aguayo A. J (1994). Axotomy results in delayed death and apoptosis of retinal ganglion cells in adult rats. J. Neuroscience *14*, 4368-4374

Bernardos R. L, Barthel L. K, Meyers J. R, Raymond P. A. (2007). Late-stage neuronal progenitors in the retina are radial Müller glia that function as retinal stem cells. J. Neurosci. *27*, 7028-7040.

Blair H. C, Zaidi M,. Schlesinger P. H (2002) Mechanisms Balancing Skeletal Matrix Synthesis and Degradation. Journal of Biochem*. 364*, 329-341

Boland B, Kumar A, Lee S, Platt F. M, Wegiel J, Yu W. H, Nixon R. Autophagy Induction and Autophagosome Clearance in Neurons: Relationship to Autophagic Pathology in Alzheimer's Disease (2008). The Journal of Neuroscience *28*, 6926-6937

Boyle W.J, Simonet W. S, Lacey D. L (2003). Osteoclast differentiation and activation. Nature *423*, 337-341

Brenner M., Messing A. (1996). GFAP Transgenic Mice. Methods *10*, 351-364

Castellano Chlodo D, DIRocco M, Gandolfo C, Morana G, Buzzi D, Rossi A (2007). Neuroimaging Findings in Malignant Infantile Osteopetrosis due to OSTM1 Mutations. Neuropediatrics *38*, 154-156

Cecconi F, Levine B (2008). The Role of Autophagy in Mammalian Development: Cell Makeover Rather than Cell Death. Developmental Cell *15*, 344-356

Chalhoub N, Benachenhou N, Rajapurohitam V, Pata M, Ferron M, Frattini A, Villa A, Vacher J (2003) Grey-lethal mutation induces severe malignant autosomal recessive osteopetrosis in mouse and human. Nature *9*, 399-406

Degtyarev M, De Maziere A, Orr C, Jie L, Lee B. B, Tien J. Y, Prior W. W, van Dijk S, Wu H, Gray D. C, Davis D. P, Stern H. M, Murray L. J, Hoeflich K. P, Klumperman J, Friedman L. S, Lin K (2008). Akt inhibition promotes autophagy and sensitizes PTEN-null tumors to lysosomotropic agents. J. Cell Biol. *183*, 101-116

Del Fattore A, Cappariello A, Teti A (2008). Genetics, pathogenesis and complications of osteopetrosis. Bone *42*, 19-29

Duff K, Eckman C, Zehr C, Yu X, Prada C. M, Perez-Tur J, Hutton M, Buee L, Harigaya Y, Yager D, Morgan D, Gordon M. N, Holcomb L, Refolo L, Zenk B, Hardy J, Younkin S (1996). Increased amyloid-□42(43) in brains of mice expressing mutant presenilin 1. Nature *383*, 710-713

Duyckaerts C, Delatour B, Poitier M. C (2009). Classification and basic pathology of Alzheimer disease. Acta Neuropathol. *118*, 5-36

Eisenfeld A. J, Bunr-Milam A. H, Sarrhy P. V (1984). Muller Cell Expression of Gliol Fibrillory Acidic Protein offer Genetic and Experimental Photoreceptor Degeneration in the Rat Retina. Invest. Ophthalmol. Vis. Sci. *25,* 1321-1328

Fdez E, Hilfiker S (2006). Vesicle pools and synapsins: New insights into old enigmas. Brain Cell Biology *35*, 107-115

Gaffield M. A, Betz W. J (2007). Synaptic Vesicle Mobility in Mouse Motor Nerve Terminals with and without Synapsin. The Journal of Neuroscience *27*, 13691-13700

Grüneberg, H. (1936). Grey-lethal, a new mutation in the house mouse. J. Hered. *27*, 105–109

Guerrini M. M, Sobacchi C, Cassani B, Abinun M, Kilic S. S, Pangrazio A, Moratto D, Mazzolari E, Clayton-Smith J, Orchard P, Coxon F. P, Helfrich M. H, Crockett J. C, Mellis D, Vellodi A, Tezcan I, Notarangelo L. D, Rogers M. J, Vezzoni P, Villa A, Frattini A (2008). Human Osteoclast-Poor Osteopetrosis with Hypogammaglobulinemia due to TNFRSF11A (RANK) Mutations. The American Journal of Human Genetics *83*, 64-76

Haas C. A, DeGennaro L. J, Müller M, Holländer H (2004). Synapsin I expression in the rat retina during postnatal development. Experimental Brain Research *82*, 25-32

Henriksen K, Gram J, Schaller S, Dahl BH, Dziegiel MH, Bollerslev J, Karsdal MA (2004). Characterization of osteoclasts from paitents harboring a G215R mutation in CLC-7 causing autosomal dominant negative osteopetrosis type II. Am. J. Pathol. *164*, 1537-1545

Hertz L, Peng L, Lai, J. C, (1998). Functional Studies in Cultured Astrocytes. Methods: A Companion to Methods in Enzymology *16*, 293-310

Hoesche C, Sauerwald A, Veb R. W, Krippl B, Kilimann M. W (1993). The 5'-Flanking Region of the Rat Synapsin I Gene Directs Neuron-specific and Developmentally Regulated Reporter Gene Expression in Transgenic Mice. The Journal of Biological Chemistry *268*, 26494-26502

Hofbauer LC, Neubauer A, Heufelder AE, (2001). Receptor activator of nuclear factor kappaB ligand and osteoprotegerin: potential implications for the pathogenesis and treatment of malignant bone disease. Cancer *92*, 460-470

Hosaka M, Sudhof T. C (1999). Homo- and Heterodimerization of Synapsins. The Journal of Biological Chemistry *274*, 16747-16753

Hsiao K, Chapman P, Nilsen S, Eckman C, Harigaya Y, Younkin S, Yang F, Cole G (1996). Correlative memory deficits, Aβ elevation and amyloid plaques in transgenic mice. Science *274*, 99-102

Huang G, Zhang, P, Hirai H, Elf S, Yan X, Chen Z, koschmieder S, Okuno Y, Dayaram T, Growney J. D, Shivdasani R. A, Gilliland D. G, speck N. A, Nimer S. D, Tenen D. G (2008). PU.1 is a major downstream target of AML1 (RUNX1) in adult mouse hematopoiesis. Nature Genetics *40*, 51-60

Johansson M, Jansson L, Ehinger M, Fasth A, Karlsson S, Richter J (2006). Neonatal hematopoietic stem cell transplantation cures oc/oc mice from osteopetrosis. Exp. Hematol. *34*, 242-249

Johnston M (2003). The importance of lymphatics in cerebrospinal fluid transport.. Lymphat. Res. Biol. *1*, 41-44

Kabeya Y, Mizushima N, Ueno T, Yamamto, Kirisako T, Noda T, Kominami E, Ohsumi Y, Yoshimori T (2000). LC3, a mammalian homologue of yeast Apg8p, is localized in autophagosome membranes after processing. J. EMBO *19*, 5720-5728

Kasper D, Planells-Cases R, Fuhrmann J. C, Scheel O, Zeitz O, Ruether K, Schmitt A, Poet M, Steinfeld R, Schweizer M, Kornak U, Jentsch T. J (2005). Loss of the chloride ClC-7 leads to lysosomal storage disease and neurodegeneration. EMBO Journal *24*, 1079-1091

Kilonsky D. J, Emr S. D (2000). Autophagy as a Regulated Pathway of Cellular Degradation. Science. *290*, 1717-1721

Kornak U, Kasper D, Bosl M. R, Kaiser E, Schweizer M, Schulz A, Friedrich W, Delling G, Jentsch T. J (2001). Loss of the ClC7 Chloride Channel Leads to Osteopetrosis in Mice and Man. Cell *104*, 205-215

Krock B. L, Bilotta J, Perkins B. D (2007). Noncell-autonomous photoreceptor degeneration in a zebrafish model of choroideremia. PNAS *104*, 4600-4605

Lange P. F, Wartosch L, Jentsch T. J, Fuhrmann J. C (2006). ClC7 requires Ostm1 as a B-subunit to support bone resorption and lysosomal function. Nature *440*, 220-223

Levine B, Kroemer G (2008). Autophagy in the Pathogenesis of Disease. Cell. *132*, 27-41

Liang C., Feng P, Ku, B, Dotan I, Canaani D, Oh B. H, Jung J. U (2006). UVRAG, A New Player in Autophagy and Tumor Cell Growth. Nat. Cell Bio. *8*, 688-699

Luca C, Kowalski T. J, Zhang Y, Elmquist J. K, Lee C, Killimann M. W, Ludwig T, Lui S, Chua S. C (2005). Complete rescue of obesity, diabetes, and infertility in db/db mice by neuron-specific LEPR-B transgenes. Jounral of Clinical Investigation *115*, 3484-3493

Maranda B, Chabot G, Decarie J-C, Pata M, Bouziane A, Moreau A, Vacher J (2008). Clinical and Cellular Manifestations of OSTM1-Related Infantile Osteopetrosis. Journal of Bone and Mineral Research *23*, 296-300

Marino G, Lopez-Otin C (2004). Autophagy: molecular mechanisms, physiological functions and relevance in human pathology. Cell. Mol. Life Sci. *61*, 1439-1454

Matsuoka Y, Picciano M, Malester B, LaFrancois J, Zehr C, Daeschner J. M, Olschowka J. A, Fonseca M. I, O'Banion M. K, Tenner A. J, Lemere C. A, Duff K (2001). Inflammatory Responses to Amyloidosis in a Transgenic Mouse Model of Alzheimer's Disease. American Journal of Pathology *158*, 1345-1353

Messing A, Brenner M (2003). GFAP: Functional Implications Gleaned From Studies of Genetically Engineered Mice. Glia *43*, 87-90

McInnes R. R, Michaud J. L (2007)Lissencephaly and LIS1: insights into the molecular mechanisms of neuronal migration and development Clin. Genet. *72*, 296-304

Mizushima N (2007). Autophagy: process and function. Genes and Development *21*, 2861-2873
Mizushima N, Hara T (2006). Intracellular Quality Control by Autophagy. Autophagy *2*, 302-304

Mizushima N, Ohsumi Y, Yoshimori T (2002). Autophagosome Formation in Mammalian Cells. Cell Structure and Function. *27*, 421-429

Mole S (2004). Neuronal ceroid lipofuscinoses (NCL). Eur. J. Pediatric Neurol. *8*, 101-103

Nicklin P, Bergman P, Zhang B, Triantafellow E, Wang H, Nyfeler B, Yang H, Hild M, Kung C, Wilson C, Myer V. E. MacKeigan J. P, Porter J. A, Wang Y, Cantley L. C, Finan P. M, Murphy L. O (2009). Bidirectional Transport of Amino Acids Regulates mTOR and Autophagy. Cell *136*, 521-534

Nixon R. A (2007). Autophagy, amyloidogenesis and Alzheimer disease. Journal of Cell Science. *120*, 4081-4091

Noctor S. C , Flint A. C, Weissman T. A , Dammerman R. S, Kriegstein A. R (2001). Neurons derived from radial glial cells establish radial units in neocortex. Nature *409*, 714-720

Ortega N, Behonick D. J, Werb Z (2004) Matrix remodeling during endochondral ossification. Trends in Cell Biology*, 14*, 86-93

Palm L, Hagerstrand I, Kristoffersson U, Blennow G, Brun A, Jorgenson C (1986). Nephrosis and disturbances of neuronal migration in male siblings-a new hereditary disorder? Arch. Dis. Child *61,* 545-548

Pangrazio A, Poliani P. L, Megarbane A, Lefranc G, Lanino E, Di Rocco M, Rucci F, Lucchini F, Ravanini M, Facchetti F, Abinun M, Vezzoni P, Villa A, Frattini A (2006). Mutations in OSTM1 (Grey Lethal) Define a Particularly Severe Form of Autosomal Recessive Osteopetrosis With Neural Involvement. Journal of Bone and Mineral Research *21*, 1098-1105

Pata M, Heraud C, Vacher J (2008) OSTM1 Bone Defect Reveals an Intercellular Hematopoietic Crosstalk. Journal of Biological Chemistry *283*, 30522-30530

Pekny M, Wilhelmsson U, Bogestal Y. R. Pekna M (2007). The role of astrocytes and complement system in neural plasticity. Int Rev. Neurobiol. *82*, 95-111

Pickford F, Masliah E, Britschgi M, Lucin K, Narasimhan R, Jaeger P. A, Small S, Spencer B, Rockenstein E, Levine B, Wyss-Coray T (2008). The autophagy-related protein beclin 1 shows reduced expression in early Alzheimer disease and regulates amyloid b accumulation in mice. The Journal of Clinical Investigation *118*, 2190-2198

Piper K, Boyde A, Jones J (1992). The relationship between the number of nuclei of an osteoclast and its resorptive capability in vitro. Anatomy and embryology *186,* 291-299

Prinetti A, Rocchetta F, Costantino E, Frattini A, Caldana E, Rucci F, Bettiga A, Poliani P. L, Chigorno V, Sonnino S (2008). Brain lipid composition in grey-lethal mutant mouse characterized by severe malignant osteopetrosis. Glycoconj. J. *26*, 623-633

Quarello P, Forni M, Barberis L, Defilippi C, Campagnoli M. F, Silvestro L, Frattini A, Chalhoub N, Vacher J, Ramenghi U (2004). Severe Malignant Osteopetrosis Caused by a GL Gene Mutation. Journal of Bone and Mineral Research *19*, 1194-1198

Rajapurohitman V, Chalhoub N, Benachenhou N, Neff L, Baron R, Vacher J (2001) The Mouse Osteopetrotic Grey-Lethal Mutation Induces a Defect in Osteoclast Maturation/Function. Bone *28*, 513-523

Ramírez A, Faupel J, Goebel I, Stiller A, Beyer S, Stöckle C, Hasan C, Bode U, Kornak U, Kubisch C (2004). Identification of a novel mutation in the coding region of the grey-lethal gene OSTM1 in human malignant infantile osteopetrosis. Hum Mutat. *5*, 471-476.

Rekate H. L (2009). A contemporary definition and classification of hydrocephalus. Semin. Pediatr. Neurol. *16*, 9-15.

Ritter M. R, Banin E, Moreno S. K, Aguilar E, Dorrel M. I, Friedlander M (2006). Myeloid progenitors differentiate into microglia and promote vascular repair in a model of ischemic retinopathy. Journal of Clinical Investigation *116,* 3266–3276

Rodriguez J. J, Olabarria M, Chvatal A, Verkhratsky A (2009). Astroglia in dementia and Alzheimer's disease. Cell Death and Differentiation *16*, 378-385

Roth P, Stanley ER (1992). The biology of CSF-1 and its receptor. Curr. Top. Microbiol. Immunol. *181*, 141-167

Rouach N, Koulakoff A, Abudara V, Willecke K, Giaume C (2008). Astroglial Metabolic Networks Sustain Hippocampal Synaptic Transmission. Science *322*, 1551-1554

Rubinsztein D. C (2006). The roles of intracellular protein-degradation pathways in neurodegeneration. Nature *443*, 780-786

Saura J (2007). Microglial cells in astroglial cultures: a cautionary note Journal of Neuroinflammation. *4*, 26

Schinke T, Schillin AF, Baranowsky A, Huebner A, Schulz A, Zustin J, Gebauer M, Priemel M, Villa A, Teti A, Amling M (2008). Rachitic defects in tcirg1-dependant osteopetrosis are caused by impaired gastric acidification. J. Bone Miner. Res. *21*, Suppl 1 (Abstract 1201)

Schoch S, Cibelli G, Thiel G (1996). Neuron-specific Gene Expression of Synapsin I. The Journal of Biological Chemistry *271*, 3317-3323

Schoppet M, Preissner K. T, Hofbauer L. C (2002) RANK Ligand and Osteoprotegerin: Paracrine Regulators of Bone Metabolism and Vascular Function. Arterioscler. Thromb. Vasc. Biol. *22*, 549-553

Scimeca J. C, Quincey D, Parrinello H, Romatet D, Grosgeorge J, Gaudray P, Philip N, Fischer A, Carle G. F (2003). Novel Mutations in the TCIRG1 Gene Encoding the a3 Subunit of the Vacuolar Proton Pump in Patients Affected by Infantile Malignant Osteopetrosis. Human Mutation *21*, 151-157

Segovia-Silvestre T, Neutzsky-Wulff A. V, Sorensen M. G, Christiansen C, Bollerslev J, Karsdal M. A, Henriksen K (2008). Advances in osteoclast biology resulting from the study of osteopetrotic mutations. Human Genetics *124*, 561-577

Settembre C, Arteaga-Solis, McKee M. D (2009). Proteoglycan desulfation determines the efficiency of chondrocyte autophagy and the extent of FGF signaling during endochondral ossification. Genes Dev. *22*, 2645-2650

Shacka J. J, Roth K. A, Zhang J (2008). The autophagy-lysosomal degradation pathway: role in neurodegenerative disease and therapy. Frontiers in Bioscience *13*, 718-736

Shapiro F (2008). Bone Development and its Relation to Fracture Repair. The Role of Mesenchymal Osteoblasts and Surface Osteoblasts. European Cells and Materials *15*, 53-76

Simnonsen A, Stenmark H (2008). Self-eating from an ER-associated cup. J. Cell Biol. *182*, 621-622

Simonsen A, Tooze S. A (2009). Coordination of membrane events during autophagy by multiple class PI3-kinase complexes. J. Cell Biol. *186*, 773-782

Sobacchi C, Frattini A, Guerrini M. M, Abinun M, Pangrazio A, susani L, Bredius R, Mancini G, Cant A, Bishop N, Grabowski P, Del Fattore A, Messina C, Errigo G, Coxon F. P, Scott D. I, Teti A, Rogers M. J, Vezzoni P, Villa A, Helfrich M. H (2007). Osteoclast-poor human osteopetrosis due to mutations in the gene encoding RANKL. Nautre genetics *8*, 960-962

Sobacchi C, Frattini A, Orchard P, Porras O, Tezcan I, Andolina M, Bbul-Hirji R, Baric I, Canham N, Chitayat D, Dupuis-Girod S, Ellis I, Etzioni A, Fasth A, Fisher A, Gerritsen B, gulino V, Horwitz E, Klamroth V, Lanino E, Mirolo M, Musio A, Matthijs G, Nonomaya S, Notarangelo L. D, Ochs H. D, Furga A, Valiaho J, van Hove J. L. K, Vihinen M, Vujic D, Vezzoni P, Villa A (2001). The mutational spectrum of human malignant autosomal recessive osteopetrosis. Human Molecular Genetics *10*, 1767-1773

Stark Z, Savarirayan R Osteopetrosis (2009). Orphanet Journal of Rare Diseases *4*,5

Steward C. G, (2003). Neurological aspects of osteopetrosis. Neuropathology and Applied Neurobiology *29*, 87-97

Street K. A, Xu G, Hall K. L, Intano G. W, McCarrey J. R, Herbert D. C, Kilimann M. W, Walter C. A (2005). Rat Synapsin 1 Promoter Mediated Transgene Expression in Testicular Cell Types. DNA and Cell Biology *24*, 133-140

Su M, Hu H, Lee Y, Azzo A, Messing A, Brenner M (2004). Expression Specificity of GFAP Transgenes. Neurochemical Research *29*, 2075-2093

Tamaki S. J, Jacobs Y, Dohse M, Capela A, Cooper J. D, Reitsma M, He D, Tushinski R, Belichenko P. V, Salehi A, Mobley W, Gage F. H, Huhn S, Tsukamoto A. S, Weissman I. L, Uchida N (2009). Neuroprotection of Host Cells by Human Central Nervous System Stem Cells in a Mouse Model of Infantile Neuronal Ceroid Lipofuscinosis. Cell *5*, 310-319

Tang C, Lee J, Galvez M. G, Robillard L, Mole S. E, Chapman H. A (2006). Murine Cathepsin F Deficiency Causes Neuronal Lipofuscinosis and Late-Onset Neurological Disease. Mol. Cell. Biol. *26*, 2309-2316

Tang G, Yue Z, Talloczy Y. Z, Hagemann T, Cho W, Messing A, Sulzer D. L, Goldman J. E (2008). Autophagy induced by Alexander disease-mutant GFAP accumulation is regulated by p38/MAPK and mTOR signaling pathways. Human Molecular Genetics *17*, 1540-1555

Teitelbaum SL, Ross FP (2003). Genetic regulation of osteoclast development and function. Nat. Rev. Genet. *4*, 638-649

Thiel G, Greengard P, Sudhof T. C (1991). Characterization of tissue-specific transcription by the human synapsin I gene promoter. Prac. Natl. Acad. Sci. USA *88*, 3431-3435

Tolar J, Teitelbaum S. L, Orchard P. L (2006). Osteopetrosis. The New England Journal of Medicine *351*, 2829-2849

Tolmachova T, Anders R, Abrink M, Bugeon L, Dallman M. J, Futter C. E, Ramalho J. S, Tonagel F, Tanimoto N, Seeliger M. W, Huxley C, Seabra M. C (2006). Independent degeneration of photoreceptors and retinal pigment epithelium in conditional knockout mouse models of choroideremia. Journal of Clinical Investigation *116*, 386-394

Tondravi M. M, McKercher S. R, Anderson K (1997). Osteopetrosis in mice lacking hematopoietic transcription factor PU.1. Nature *386* 81-84

Vacher J, Tilghman S. M (1990). Dominant Negative Regulation of the Mouse □-Fetoprotein Gene in Adult Liver. Science *250*,1732-1735

Vargas M. R, Johnson D. A, Sirkis D. W, Messing A, Johnson J. A (2008). Nrf2 Activation in Astrocytes Protects against Neurodegeneration in Mouse Models of Familial Amyotrophic Lateral Sclerosis. Journal of Neuroscience *28*, 13574-13581

Walker D. G, (1975). Bone resorption restored in osteopetrotic mice by transplants of normal bone marrow and spleen cells. Science *190*, 784-785

Wang J, Wang C, Orr A, Tydlacka S, Li S, Li X (2008). Impaired ubiquitin–proteasome system activity in the synapses of Huntington's disease mice. The Journal of Cell Biology *180*, 1177-1189

Wiktor-Jedrzejczak W, Bartocci A, Ferrante AW (1991). Total absence of colony stimulating factor 1 in the macrophage deficient osteopetrotic (op/op) mouse. Proc. Natl. Acad. Sci. *87*, 4828-4832

Wilson C, Vellodi A, (2000) Autosomal recessive osteopetrosis: diagnosis, management, and outcome. Arch. Dis. Child *83*, 449-452

Yamanaka K, Chun S. J, Boillee S, Fujimori-Tonou N, Yamashita H, Gutmann D. H, Takahashi R, Misawa H, Cleveland D. W (2008). Astrocytes as determinants of disease progression in inherited amyotrophic lateral sclerosis. Nature Neuroscience *11*, 251-253

Yilmazer-Hanke D. M (1998). Pathogenesis of Alzheimer-related neuritic plaques: AT8 immunoreactive dystrophic neurites precede argyrophilic neurites in plaques of the entorhinal region, hippocampal formation and amygdale. Clin. Neuropathol. *17,*194-198

Yoshida H, Hayashi S, Kinisada T, Ogawa M, Nishikawa S, Okamura H, Sudo T, Shultz L. D, Nishikawa S (1990). The murine mutation osteopetrosis is in the coding region of the macrophage colony stimulating factor gene. Nature *345*, 442-444

Yu W. H, Cuervo A. M, Kumar A, Peterhoff C. M, Schmidt S. D, Lee J, Mohan P. S, Mercken M, Farmery M. R, Tjernberg L. O, Duff K, Uchiyama Y, Naslund J, Mathews P. M, Cataldo A. M, Nixon R. A (2005). Marcoautophagy- a novel □-amyloid peptide-generating pathway activated in Alzheimer's disease. Journal of Cell Biology *171*, 87-98

Yue Z, Wang Q. J, Komatsu M (2008). Neuronal Autophagy. Autophagy *4*, 94-96

Zaidi M (2007). Skeletal remodeling in health and disease. Nature Medicine *13*, 791-801